Development of Mid-IR Laser

By

Varsha

A thesis submitted to the Faculty of Graduate Studies
Lakehead University
In partial fulfillment of the requirements for the degree of
Doctor of Philosophy
Chemistry and Material Science

Department of Physics
Lakehead University

Abstract

We proposed and demonstrated a mid-IR fiber laser at 1925 nm using a thulium-doped fiber as the gain medium. The designed laser needs lower pump power compared to that previously reported. The developed laser is compact and cost-effective to manufacture. We have presented the potential application of the laser in sensing gases responsible for climate change. We have developed a high-power pulsed laser at 1570 nm, which was used as the pump source for the thulium-doped fiber laser. Further, we have developed a pulsed laser at 1533 nm, which will be used as a pump source for generating a molecular gas laser using acetylene as a gain medium.

We have also introduced and demonstrated for the first time the use of an aqueous solution of gold nanorods and polyvinyl alcohol as a saturable absorber to produce pulsed and tunable pulsed lasers in the mid-IR region of the electromagnetic spectrum. We accomplished several important milestones, shaping future research endeavours in developing mid-IR lasers. **Chapter 8** summarizes our research accomplishments.

Publication and Contributions

Journal Publications

1. V. Varsha and G. Das, “Q-switched Er-Doped fiber laser using an aqueous solution of gold nanorods and polyvinyl alcohol,” Optical fiber technology, 83, 103672, 2024.

2. V. Varsha and G. Das, “Generation of wavelength-switchable nanosecond mode-locked pulses in Erbium/Ytterbium co-doped fiber laser cavity,” Results in Optics, 16, 100723, 2024.

3. V. Varsha and G. Das, “Tunable nanosecond mode-locked laser at 1570 nm and applications”, Optical fiber technology, Volume 90, http://doi.org/10.1016/j.yofte.2024.104083, 2025.

4. V. Varsha, and G. Das, “In-band pumped, high peak power gain-switched mode-locked thulium-doped fiber laser at 1925 nm”, Optics Continuum, Volume 4, Issue 1, pp. 30-36, 2025.

5. V. Varsha, and G. Das, “High-power self Q-switched mode-locked erbium-ytterbium doped fiber laser,” Optical Fiber Technology, Revised manuscript under review, April 2025.

Proceedings Publications

1. V. Varsha and G. Das, “Nanosecond mode-locked laser using an artificial saturable absorber,” Optica Laser Congress 2023, USA.

2. V. Varsha and G. Das, “Tunable passively Q-switched and Mode-locked fiber laser at 1.9 μm region using a mixture of GNRs and PVA as a saturable absorber”, Optica LAOP 2024, Mexico.

3. V. Varsha, J.O. Trevisanutto and G. Das, “Detection of Gases at the Molecular Level,” Optica LAOP 2024, Mexico.

4. N. Kaur, V. Varsha, and G. Das, “Surface-Enhanced Raman Spectroscopy (SERS) for the detection of Rhodamine 6G and Crystal Violet”, Optica Biophotonics Congress: Optics in the Life Sciences, April 2023, Canada.

Abstract Publications

1. V. Varsha and Gautam Das, “Passively Q-Switched fiber laser using an aqueous solution of gold nanorods and polyvinyl alcohol as a saturable absorber,” CAP Congress 2023. **(Received 3rd prize in oral competition)**

Acknowledgment

First of all, I would like to thank my supervisor, Prof. Gautam Das, for giving me an opportunity to work with him. His constant guidance and unconditional support motivated me each day to work better throughout this journey. I want to express my gratitude to committee members Dr. Mark Gallagher and Dr. Baoqiang Liao for their valuable time and suggestions whenever it was needed, despite their busy schedules. Also, I would like to thank other faculty and staff members for providing a good research environment.

Without a team, it's not possible to go far with the same momentum all the time. I really appreciate the support I received from all the members of the Photonic research group at Lakehead University. I would like to mention Dr. Joshua O. Trevisanutto for helping me with the laboratory activities when I started working in the lab and Dr. Jyothis Thomas for having meaningful discussions. As an international student far from home, I was fortunate to meet Tithi Das, who treated me like her family.

I would like to recognize my family members for their constant support, especially my husband, Dr. Puneet Chaudhary, who stayed far away most of the time but motivated me continuously. A special thanks to my sister Asha, who was always available for me whenever I needed emotional support. Last but not least, I like to mention our son

Arjun Singh, who came into our life towards the end of this journey and motivated me to achieve my goal.

Table of Contents

List of Figures

List of Table

List of Abbreviations

mid-IR	Mid-infrared
QCL	Quantum-cascade lasers
HBR	Hydrogen Bromide
PCF	photonic crystal fibers
LASER	light amplification by stimulated emission of radiation
TDFL	thulium-doped fiber laser
CO	Carbon monoxide
TDF	thulium doped fiber
CW	continuous wave
SA	saturable absorber
GNRs	Gold nanorods
PVA	polyvinyl alcohol
FBG	fiber Bragg grating
TIR	total internal reflection
MFD	mode-field diameter
SMF	single-mode fiber
NA	Numerical Aperture
MMF	multi-mode fiber
Yb	Ytterbium
Er	Erbium
Tm	Thulium
EDF	erbium-doped fiber

EYDF	erbium-ytterbium co-doped fiber
DC	Double-clad
DC-EYDF	double-clad erbium ytterbium-doped fiber
ASA	artificial saturable absorbers
NPR	nonlinear polarization rotation
NALM	nonlinear amplifying loop mirror
NOLM	nonlinear optical loop mirror
SESAM	semiconductor saturable absorber mirrors
Q-factor	Quality factor
ML	mode–locked
SPM	Self-Phase Modulation
YDF	ytterbium-doped fiber
SPM	Surface Plasmon Resonance
LSPR	localized surface Plasmon resonance
NaCMC	sodium carboxymethyl cellulose
AR	aspect ratio
CTAB	cetyltrimethylammonium bromide
BDAC	benzyl dimethyl ammonium chloride
$HAuCl_4$	Chloroauric acid
$AgNo_3$	Silver Nitrate
$NaBH_4$	Sodium borohydride
AA	Ascorbic acid
TEM	Transmission Electron Microscope
NLR	nonlinear refraction
CIR	Circulators
WDM	Wavelength division multiplexing
ASE	Amplified spontaneous emission
FFC	Fused fiber coupler
QS	Q-switched
NIR	near-infrared

GIMF	graded index multimode fiber
PC	polarization controller
SNR	signal to noise ratio
SQS	self-Q-switching
SML	self-mode-locking
SQS-ML	self-Q-switching mode-locking
ESA	excited state absorption
SRS	stimulated Raman scattering
SBS	stimulated Brillouin scattering
OI	optical isolator
OSA	optical spectrum analyzer
PM-EDF	polarization maintaining erbium-doped fiber
SHB	spatial hole burning
FWHM	full-width half maximum
GHG	greenhouse gases
GS	gain-switched
LD	Laser diode
DSR	dissipative soliton resonance
BWD	backward direction
FWD	forward direction
RF	radio frequency
HC-PCF	hollow-core photonic crystal fiber
IC	Inhibited coupling
PBG	Photonic bandgap
BIC	bound states in continuum

Chapter 1

Introduction

The second half of the last century was characterized by technological development in all the fields of science. A lot of inventions have happened with the efforts of researchers and scientists all around the world. One vision gave direction to another such as the phenomenon of "stimulated emission", predicted by Albert Einstein, became the fundamental of laser science. He discovered that when an atom is in an excited state, and a photon of the same energy as the energy difference between the two energy states strikes it, these photons will be discharged simultaneously, having identical frequency and phase, known as stimulated emission. Later on, this concept of stimulated emission was used to create a laser [1].

After this, it took almost half a century for the first working prototype of a laser, demonstrated in 1960 by Dr. Theodore Harold Maiman [2]. Lasers are an incredible source of powerful, coherent electromagnetic radiation. The ability to produce highly collimated, monochromatic, and intense beams of light that can deliver a large amount of energy precisely in a confined region makes it a favorable tool for various applications.

Mid-infrared (mid-IR) laser sources operating at wavelength 2.0 - 3.5 μm spectral regions have become popular due to their applications in biomedicine, remote sensing, telecommunication, molecular detection, material processing, free space communication, and laser surgery [3-7].

Many hazardous pollutants and gases such as NO, NO_2, CO_2 and N_2O have absorption bands in the mid-IR region (For example, CO_2 has absorption in 1.9 micron region). A mid-IR fiber laser is a good choice for applications related to the detection of chemicals at molecular levels. Further, many gases have overtone or a combination of fundamental and overtone bands in the mid-IR regions. A silicon detector can still be used in this band, which makes this band much more attractive for detecting gases at molecular levels [8]. Moreover, mid-IR region is also important in protein analysis due to the ability to provide detailed insights into molecular vibrations, structural properties and functional analysis. For example, the vibrational modes of peptide bonds such as amide I and amide II are located in mid-IR region which helps to understand the secondary structure of proteins (alpha-helices, beta-sheets etc.) [9]. The potential applications of the laser at this band and the unavailability of a compact laser system make developing a mid-IR laser source more attractive. The availability of new pump laser sources, efficient doped fibers, and fiber based on new materials make progress in mid-IR research much more efficient.

There are multiple ways to generate a laser in the mid-IR wavelength region. Quantum-cascade lasers (QCL), rare-earth-doped fiber lasers, and gas lasers are all significant contributors [10-12]. Since the first experimental demonstration of QCL in 1994 [13], these lasers have undergone tremendous development and emerged as a

promising technology for developing watt-level mid-IR lasers. These lasers cover a broad spectral range of around 2.5-10 μm region, but face difficulties below 2.5 μm [14]. Also, they have thermal management challenges, so there is a need to improve heat dissipation for the current application of QCL technology [15;16]. These lasers do have the advantage of high power, but their limited wavelength, complicated development process, and heat dissipation challenges make them less popular.

Another way to generate mid-IR wavelength lasers is based on rare-earth doped fiber, which has the advantages of high operation efficiency, good beam quality, excellent heat dissipating capability, and compact structure [17]. Because of these qualities, rare-earth-doped fiber lasers has drawn the attention of researchers around the world. Rare-earth doped fibers can be used as the gain medium for developing lasers at different wavelengths based on the doping ion, such as ytterbium-doped fibers (1.1 μm band) [18;19], erbium-doped fibers (1.5 μm band) [20], thulium-doped fibers (2.0 μm band) [21], and ZBLAN (zirconium barium lanthanum aluminum sodium fluoride) fibers (3.0 μm band) [22]. Using these gain fibers, lasers can be developed at a specific wavelength.

In past years, molecular gas lasers also drew attention as a means to generate a wavelength in the mid-IR region. In molecular gas lasers, the lasing medium is made up of one or a mixture of gases, and laser transitions occur between the vibrational and rovibrational energy levels of molecules. In 1972, Bell Laboratories of the United States reported an optically pumped mid-infrared (mid-IR) gas laser for the first time. A CO_2 gas laser was developed at 10.6 μm using a gas discharge pulsed Hydrogen Bromide (HBR) chemical laser as a pump source [23]. Many gases (C_2H_2, HCN, CO, and N_2O) have absorption in the 1.55 μm band. It was demonstrated that when the gases are

pumped by a laser at 1.55 μm, they can produce a mid-IR laser. Thus, they can be used to develop molecular gas lasers as a gain medium. But again, there is the constraint of a suitable pump source. So, with the availability of a pump source at the desired wavelength, mid-IR molecular gas lasers can become more attractive compared to other lasers.

For molecular gas lasers, gases with different regions of absorption and emission can be used as a gain medium similar to rare-earth doped fibers. To develop a laser in a 2.0-3.0 micron region, any gas which has emissions in this region can be used as a gain medium such as acetylene, hydrogen cyanide, and carbon monoxide. For example, acetylene has absorption at 1.5 μm region and emission at 3.1 μm region; and carbon monoxide has absorption at 1.57 μm and emission at 2.1 μm [24]. These gases can be enclosed in gas cells. Previously, bulk gas cells and glass capillaries have been extensively used to develop the system. However, this type of configuration makes the system bulky. To overcome this issue, new methods were discovered to make the design more compact and efficient. In place of bulky gas cells, optical fibers were used to hold gas. These optical fibers are special fibers known as photonic crystal fibers (PCF). The advent of these PCFs gave a new direction to the field of fiber gas lasers. These fibers are designed in such a way that they have a hollow core, which provides the perfect environment for the interaction of pump light and gas. Lasers can be developed at different wavelengths based on the choice of gas as gain medium [25;26].

For the development of a laser, in addition to gain media, i.e. rare-earth doped fiber or gas, another essential component is an optical resonator and excitation mechanism. In the gain medium, incident light circulates and gets amplified for lasing

action with the help of stimulated emission. The excitation mechanism or pumping source helps in exciting atoms to higher energy states, and optical resonators reflect the laser beam through the gain medium and get amplified. In the following sections we have discussed the fundamentals of lasers.

1.1 Interaction of radiation and atomic systems

Light is a collection of photons that have energy and momentum. A photon can interact with an atom if it has energy similar to the energy difference between two energy levels, which leads to three fundamental processes of lasing action: absorption, spontaneous emission, and stimulated emission [27]. An atom sitting in the ground state can make a transition to a higher energy state, due to interaction with incoming radiation by absorbing a photon, this is known as absorption. The atom at the higher energy state will make a downward transition to the ground state emitting a photon. This process is known as spontaneous emission.

Another process is stimulated emission, which is responsible for lasing action and occurs when incident photons interact with the atom at the higher energy level, forcing it to make a transition to the ground state and emit a photon. The emitted photon has the same frequency, polarization and energy as the stimulating photon. The emitted photons make multiple reflections inside the cavity and induce more stimulated emission, and laser emission occurs. Thus, for stimulated emission to occur, more atoms are required in a higher energy state compared to a lower energy, which is known as population inversion as shown in Figure 1.1.

To build a Laser, a three level or four level system is needed. In a two level system, the atoms always tend to stay in the ground energy level (E1) and needs a strong pumping transitions to create population inversion between E1 and E2. In a three level system, the middle state (E2) has a long lifetime than higher state (E3), which helps in creating population inversion efficiently between energy state E1 and E2 and the lasing action occurs between these two energy levels. The collection of these emitted photons appears as a coherent, monochromatic, and intense beam of light known as LASER as shown in Figure 1.1 (c) [28;29].

LASER is an acronym that stands for light amplification by stimulated emission of radiation, coined by Gordon Gould [1]. At thermal equilibrium, the probability of stimulated emission is much lower than spontaneous emission. To get the condition of stimulated emission, one needs to create an environment where more atoms are in a higher energy state, which is known as population inversion (Figure 1.1 (b)) and can be attained with external pumping.

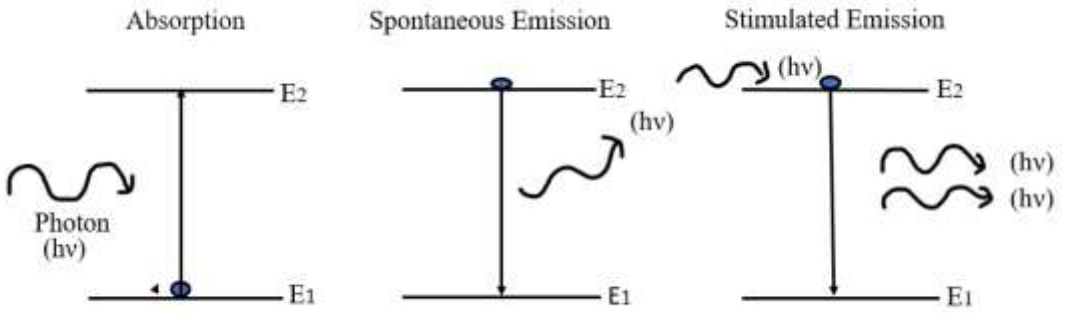

(a)

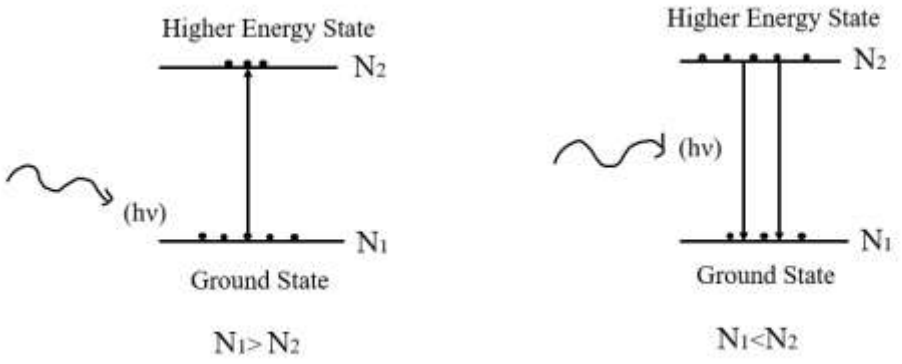

(b)

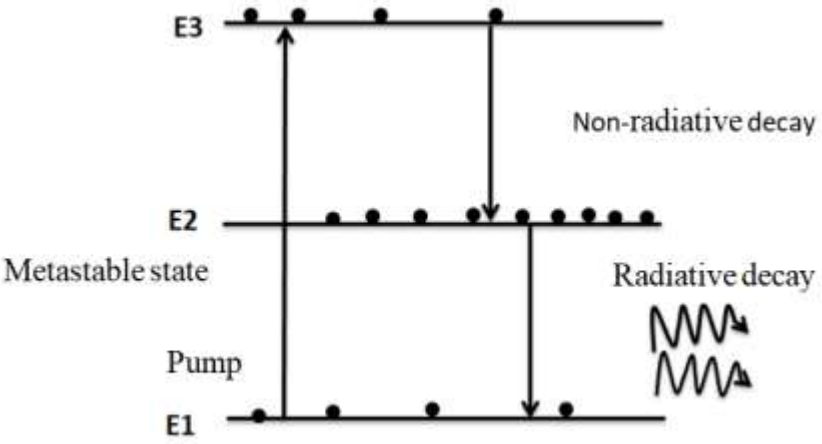

(c)

Figure 1.1: (a) Light matter interaction (b) Population inversion condition (c) Three level energy diagram of a Laser.

A laser comprises three main components: a resonator, a gain medium, and a pumping source (Figure 1.2). The resonator can be designed with the help of mirrors either in linear or ring configuration. A schematic of the laser is shown in Figure 1.2, which consists of two mirrors, one is highly reflecting and the second is partially

reflecting. Between these two mirrors a gain medium is placed to provide feedback, and the signal gets amplified in the gain medium. A laser is triggered with the help of a pumping system by achieving population inversion in the active medium or gain medium [30].

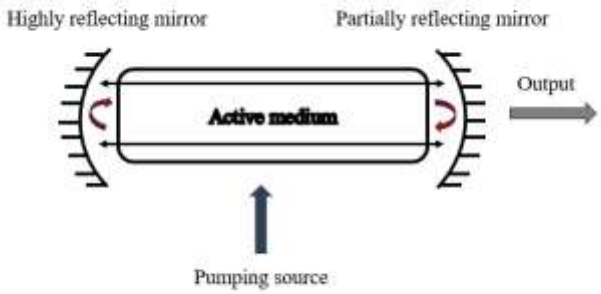

Figure 1.2: Schematic of the laser.

The objective of the research: The main objective of this research work was to develop a mid-IR laser, which was accomplished by developing a thulium-doped fiber laser (TDFL) at 1925 nm. The following chart shows the various steps of the research work.

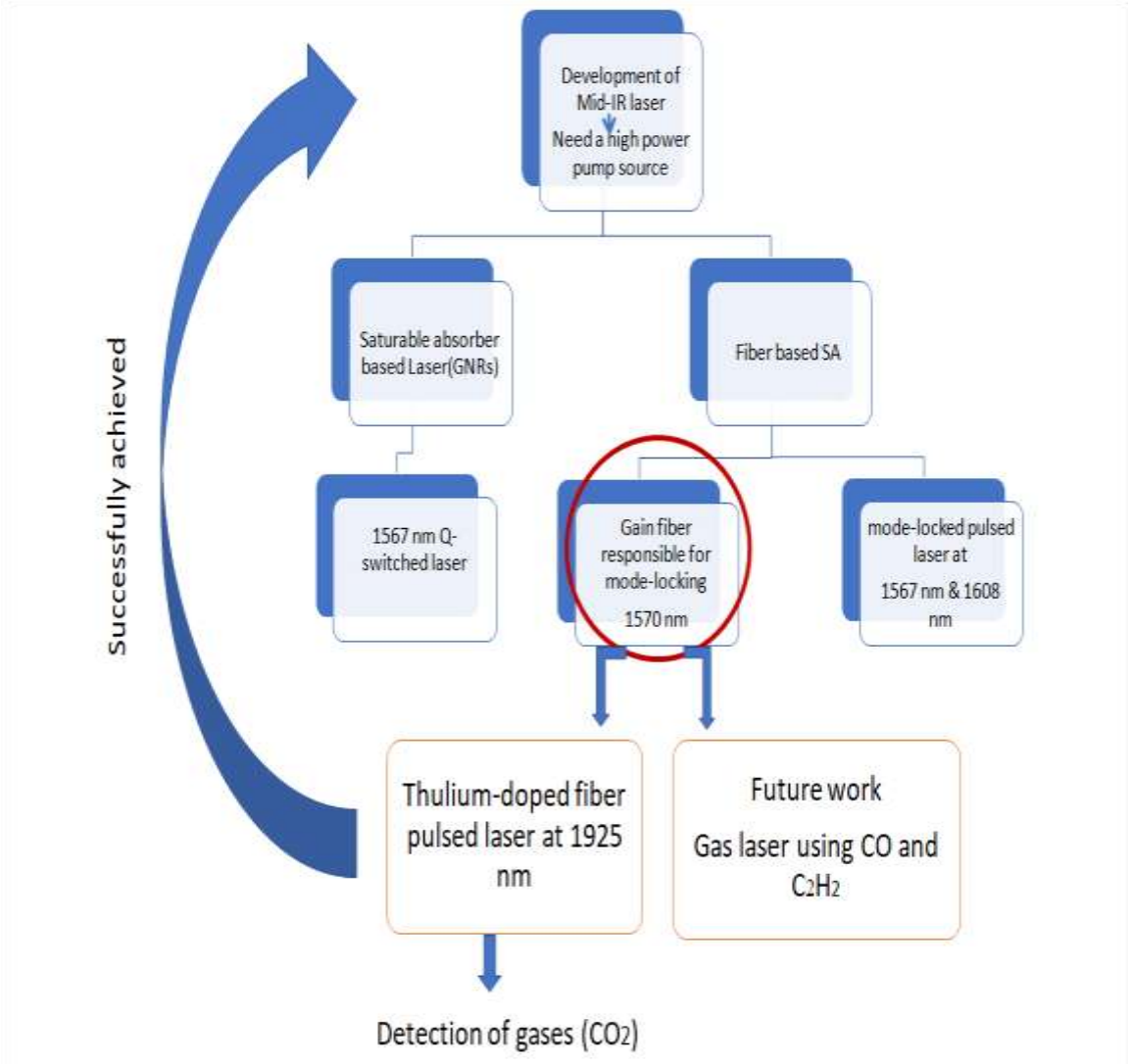

To achieve the research objective, we proposed two different directions **(i)** Based on a rare-earth doped fiber - thulium-doped fiber (TDF), and **(ii)** molecular gas laser – using acetylene (and CO) gas-filled Kagome fiber as the gain medium. A high-power

pump source is required to develop the proposed lasers. One can obtain the high power in two ways: (a) using a continuous wave (CW) laser and (b) a PULSED laser. It is always challenging to obtain high output power using a CW laser, as it needs cooling. Another option is to develop a pulsed laser, where one can change the peak power of the pulse by adjusting laser pulse parameters. We have developed several pulsed lasers in the 1.5 micron band, but the most important one was a pulsed laser at 1570 nm with pulse width, repetition rate and peak power of 340 ps, 6.57 MHz, and 72 W, respectively.

The pulsed laser at 1570 nm was chosen to be used as a pump source because thulium fiber has an absorption band in this wavelength region. In addition, thulium has an absorption band at 800 nm and 1100 nm. Pumping with a 1570 nm laser is called in-band pumping, as thulium also has emission in this band. Further, Carbon monoxide (CO) has absorption at 1570 nm and emits light at 2.36 μm, so the developed 1570 nm laser can also be used to develop the molecular gas laser based on carbon monoxide. We have also developed another pulsed laser at 1533 nm, which will be used to develop a molecular gas laser based on acetylene gas. Also, the laser at 1533 nm will be used together with acetylene to optimize the laser resonators before using CO.

Outline of the Thesis

A pulsed laser can be generated using several techniques. We have discussed the details of developing lasers using different methods in the following chapters.

Chapter 2 discusses the fundamentals of fiber optics and lasing, which includes a brief description of optical fiber, rare-earth doped fiber, Q-switching and mode-locking phenomenon, and the novelty of research work.

Chapter 3 discusses a Q-switched Pulsed Laser developed using a real saturable absorber (SA). An aqueous solution of Gold nanorods (GNRs) and polyvinyl alcohol (PVA) has been used as a saturable absorber (SA). The preparation and characterization of the SA is discussed briefly along with characteristics of the laser. Also the synthesis process of GNRs is discussed in the chapter.

> *The research work was published in - Optical Fiber Technology. Varsha and Gautam Das, "Q-switched Er - doped fiber laser using an aqueous solution of gold nanorods and polyvinyl alcohol", Optical Fiber Technology 83, 103672, 2024.*

Chapter 4 discusses the development of a dual-wavelength pulsed laser at 1568 nm and 1608 nm based on self-Q-switching and mode locking effect. The tunability of the laser was obtained using a tunable fiber Bragg grating (FBG), which has been described in detail. A detailed literature review and characteristics of the developed laser has been presented along with its advantages and disadvantages.

> *The research work was published in – Results in Optics. Varsha and Gautam Das, "Generation of wavelength-switchable nanosecond mode-locked pulses in an Erbium/Ytterbium co-doped fiber laser cavity", Results in Optics, Volume 16, 1000723, 2024.*

Chapter 5 discusses the development of a pulsed laser at 1570 nm. A high peak power was successfully achieved with development of this laser. It was based on self-Q-switching and mode locking in the gain fiber. The laser can be used as a pump source for developing a mid-IR laser using a thulium doped fiber, and carbon monoxide as a gain medium. Another pulsed laser at 1533 nm has been developed to use as a pump source for developing a molecular gas laser using acetylene as a gain medium.

Revised manuscript under review April 2025 – Varsha and Gautam Das, "Self Q-switched and mode-locked erbium - ytterbium co-doped fiber laser", Optical Fiber Technology.

Chapter 6 discusses the development of a thulium-doped fiber Laser at 1.925 μm based on a gain-switched mechanism. A complete review is presented about thulium-doped fiber laser and a gain-switched mechanism. This laser was tuned with the help of GNRs. Also, it was used for detection of CO_2 in real time.

Varsha and Gautam Das, "Tunable passively Q-switched mode locked fiber laser at 1.9 micrometer region using a mixture of gold nanorods and polyvinyl alcohol as a saturable absorber", 10-14 November, LAOP 2024, Mexico. (Proceedings)

Varsha, Joshua O. Trevisanutto and Gautam Das, "Detection of gases at the molecular level", 10-14 November, LAOP 2024, Mexico. (Proceedings)

Varsha and Gautam Das, "In-band pumped, high-peak power gain-switched mode-locked thulium doped fiber laser at 1925 nm", Optics Continuum, Volume 4, Issue 1, pp. 30-36, 2025.

Chapter 7 discusses the basics of molecular gas lasers. A brief description of photonic crystal fibers has been given, which includes a KAGOME fiber. Kagome fiber is a special class of PCF, which has a hollow core where gas and light can interact. The guidance mechanism of these fibers are different from simple optical fibers, it has been explained in detail.

Chapter 8 concludes the complete research work, and the future direction of this work.

Chapter 2

Fundamentals of Fiber Optics and Laser

In this chapter, we cover the fundamentals of fiber optics and fiber lasers. We have discussed different rare-earth doped fibers widely used in developing fiber lasers. We also discuss various techniques to build pulsed lasers, such as Q-switching and mode-locking, and their advantages and disadvantages.

2.1 Optical fiber

Optical fibers are cylindrical dielectric waveguides utilized for light transmission in telecommunications and developing active and passive optical devices [31].

The basic structure of the optical fiber is shown in Figure 2.1. An optical fiber consists of two co-axial dielectric cylinders called core and cladding. The core and cladding can be made of glass, plastic, or other materials. The cladding has a lower refractive index compared to the core. Further, the cladding is covered with a polymer jacket, which provides strength to the fiber and reduces the losses that may occur due to

bending of the fiber. The light propagates in the core of the fiber following total internal reflection (TIR) [32-34].

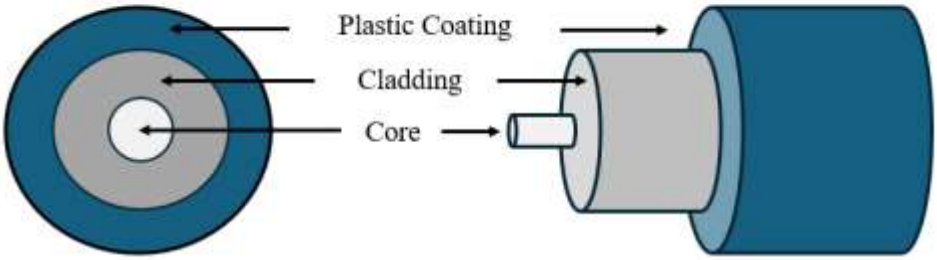

Figure 2.1: Structure of optical fiber.

An optical fiber can be classified into different types based on the refractive index profile, number of modes supported, dispersion properties, polarization-maintaining capabilities, and doping in the core [28;34]. The important characteristic parameters of an optical fiber are the V- parameter (or normalized propagation constant), mode-field diameter (MFD), Numerical Aperture (NA), and core diameter.

Fibers can be classified into two categories based on the core refractive index profile.

1. **Step-index fiber:** In a step-index fiber, the refractive index of the core is constant and there is an abrupt change in refractive index at the boundary of the core and cladding interface.

2. **Gradient-index fiber:** In a graded index fiber, the refractive index gradually changes from the maximum value at the center of the core to the core-cladding boundary.

Optical fiber can be divided into two categories based on the number of propagating modes.

1. **Single-mode fibers (SMF):** A single-mode fiber (SMF) has a small core diameter and can support only one mode that propagates through the fiber. For single-mode operation, the V number of the fiber should be ≤ 2.405. V parameter can be expressed as

$$V = \frac{2\pi a\, NA}{\lambda} \qquad [1]$$

Where a is the core radius, λ is the wavelength of light, and NA is the numerical aperture.

The numerical aperture (NA) is defined as

$$NA = \sqrt{\left(n_1^2 - n_2^2\right)} \qquad [2]$$

Where n_1 and n_2 are the core and cladding refractive indices.

The V parameter of a fiber is an important parameter as it tells the number of modes supported by the fiber [28]. In a multi-mode fiber (MMF) the V parameter relates to the number of modes (N) supported by the following equation:

$$N = \frac{V^2}{2} \qquad [3]$$

2. **Multimode fibers (MMF)**: A multimode fiber has a large core diameter compared to SMF and allows large number of modes to propagate in the core. The V number is greater than 2.405 for a fiber to be multimode.

Rare-earth-doped fibers can be obtained by doping a silica core fiber or chalcogenide glass fiber. These fibers are widely used in developing active optical components such as lasers, amplifiers, etc.

2.2 Rare-Earth Doped Fibers

The core of an optical fiber can be doped with rare-earth ions such as ytterbium (Yb), erbium (Er), and thulium (Tm). Rare earths are distinguished from other optically active ions because of some characteristics. They can absorb over narrow wavelengths and emit over long wavelength ranges, and these wavelengths are relatively independent of host material [35]. A fiber can be doped with multiple rare-earth ions, which enhances its efficiency in applications. Rare-earth doped fibers have emission bands over different regions of the electromagnetic spectrum, which helps in developing active components (e.g., Lasers and amplifiers) at a desired wavelength (e.g., 1100 nm, 1550 nm, and 2000

nm) for applications. In addition, various pump sources can be used according to the doping ion and laser wavelength required [36]. One of the requirements for designing lasers is to achieve an environment of population inversion, where more atoms can accumulate in an excited state compared to the ground states. The atoms at the excited state have a longer lifetime than the other excited states known as the metastable states. The atoms make a transition to the ground state following the spontaneous or stimulated emission process. In rare-earth doped fibers like erbium doped, the metastable state has a lifetime of 10 ms, which makes them favorable for designing lasers and amplifiers.

In this research, we have used three types of active fibers to develop pulsed lasers in 1.5 μm and 2.0 μm regions of the electromagnetic spectrum. More specifically, we have used erbium-doped fiber (EDF), erbium-ytterbium co-doped fiber (EYDF), and thulium-doped fiber (TDF) as a gain media.

2.2.1 Erbium-doped fiber (EDF)

Erbium-doped fiber is one of the most well-known and widely used rare-earth doped fibers, used in active components at the low-loss window of glass used in telecommunication. It is a three-level system with three different pump absorption bands at 800 nm, 980 nm, and 1480 nm, and emission occurs near 1.55 μm as shown in Figure 2.2. Each host material provides a slightly different environment for the doped ion to transitions. Oxide glass doped with Er ion has one metastable state $^4I_{13/2}$ with 10 ms lifetime which leads to gain at 1500 nm for the emission band $^4I_{13/2}$ to $^4I_{15/2}$. Pump wavelengths can be determined by the absorption bands of the gain fiber. Further, non-radiative transition occurs in 6 ms between $^4I_{11/2}$ and $^4I_{13/2}$. The 980 nm is advantageous

amongst the three because it shows more gain and better noise performance, also high power laser diodes are readily available at this wavelength [37].

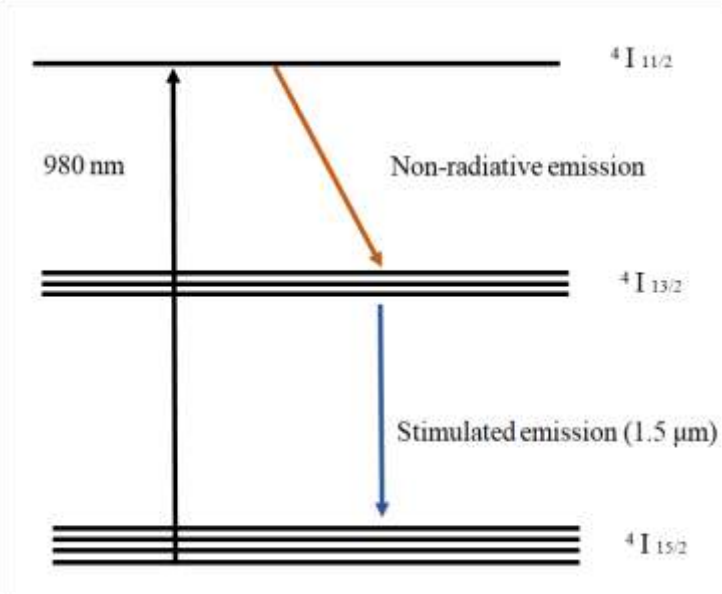

Figure 2.2: Energy level diagram for erbium-doped fiber [38].

2.2.2 Erbium-ytterbium co-doped fiber (EYDF)

A lot of work has been done on erbium-doped fibers, but to increase the efficiency, erbium-doped fibers can be co-doped with ytterbium ions (Yb). Since laser diode's operating wavelength depends on temperature, erbium absorption in silica is spectrally narrow for the $^4I_{11/2}$ – $^4I_{15/2}$. Any fluctuation in temperature directly impacts the performance of the laser diode, and thus the pump power conversion efficiency. To eliminate this problem, Yb ions can be co-doped in erbium fibers. Yb ions have larger absorption cross-sections and a broader absorption band than the erbium ions (Er). As

shown in Figure 2.3, Yb ions first absorb much of the pump light at 980 nm and make a transition to the $^2F_{5/2}$ state from the ground state $^2F_{7/2}$. These Yb ions in the excited states transfer their energy to the adjacent Er ions. After this energy transfer, Er ions are excited to $^4I_{11/2}$, and the Yb ions come back to the ground state $^2F_{7/2}$. At the time Yb starts its journey towards the ground state and before the energy transfers back to Yb, Er quickly goes to $^4I_{13/2}$ through a non-radiative transition, and creates population inversion between the $^4I_{13/2}$ and $^4I_{15/2}$ states and results in stimulated emission between these two states, initiated by spontaneous emission or input radiation [39].

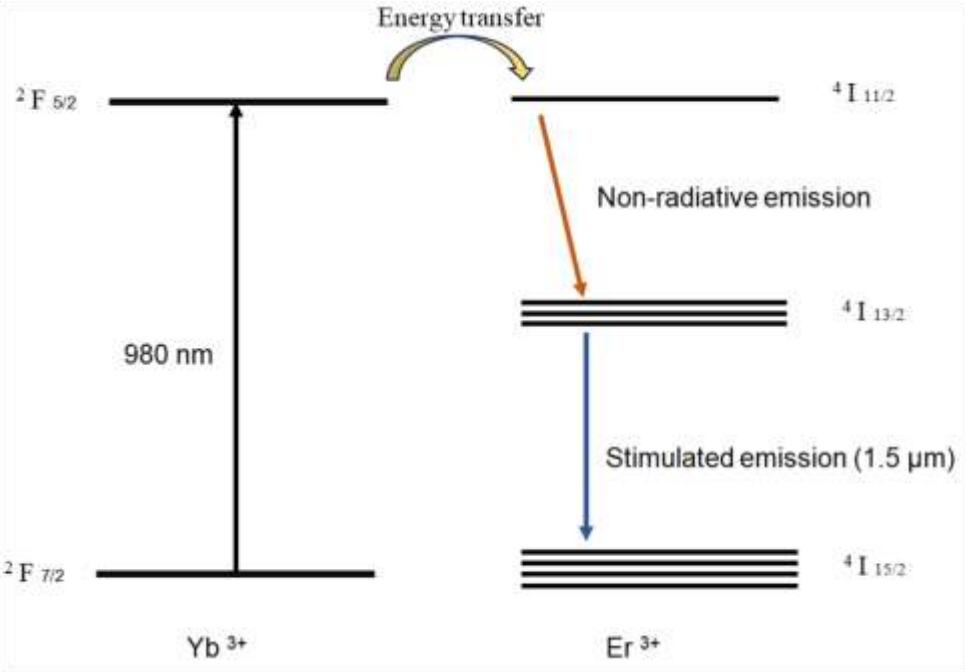

Figure 2.3: Energy levels for Erbium-Ytterbium co-doped fiber [40].

2.2.3 Thulium doped fiber (TDF)

As mentioned in the earlier section, we used TDF to generate a laser in the 2.0 μm region of the electromagnetic spectrum. In the periodic table, Thulium (Tm) lies next to erbium and mimics the same stable trivalent ionization level as erbium. It has three prominent absorption bands at 790 nm ($^3H_6$ – $^3H_4$), 1400 nm ($^3F_4$ – $^3H_4$), and 1600 nm ($^3H_6$ – $^3F_4$) [41]. Out of these three, 790 nm and 1600 nm bands are the most attractive. At 790 nm, several high-power laser diodes are commercially available, which makes this wavelength band important. Still, due to the low brightness of the diode pump source, double-clad fibers are widely used to increase the pump power absorption efficiency. The pumping band at 1600 nm matches the emission band of erbium-doped fibers, which makes it attractive as the field of EDF lasers is well explored and it is easy to modulate them as per the requirement of the pump source. Pumping with a laser in 1600 nm band is known as in-band pumping. In this case, electrons are directly pumped to the upper Stark levels (when an atom or electron exposed to an external field the energy levels can split into sub levels depending on the strength of the field, these sublevels are known as stark levels). This pumping region can achieve high pump power conversation efficiency [42]. The 2.0 μm region emission is across the transition ($^3F_4$ – $^3H_6$). An active component based on TDF is very attractive as it has 400 nm wide emission bands, from 1700 nm to 2100 nm. The wide emission band gives the opportunity of tunability in this region.

2.3 Double-clad (DC) doped fiber

Double-clad (DC) rare-earth doped fibers are great for high-power applications, as inexpensive high-power multimode laser diodes can be used as a pump source. The high pump power radiation can efficiently couple to the fiber which interacts with the rare-earth ions and increases laser output power.

A DC optical fiber is characterized by two concentric light-guiding regions, the core and inner cladding as shown in Figure 2.5. This fiber consists of three layers rather than two as in the case of standard fiber shown in Figure 2.4. All three layers are made of materials with different refractive indices. The signal light propagates along the core, and the two outer layers are claddings, which named these fibers "double-clad fiber." In an optical fiber, propagation of light is attained by total internal reflection at the core-cladding interface, but in the case of a double-clad fiber pump light undergoes total internal reflection at the boundary of inner cladding and outer cladding which is further guided around and through the core to excite the active ions, which are doped in the core region. These fibers are single-mode at lasing wavelength and multimode at the pump wavelength [38]. The shape of the cladding is important as the pump power is coupled to the cladding, so a large NA is required for efficient coupling of the pump laser. Further, the large surface area reduces the risk of damaging the fiber at high power. The shape of the cladding affects the light propagation through the core. It has been reported that in a double-clad circular fiber, pump absorption can be increased by offsetting the core and changing the shape of the cladding [43-45]. Different cladding shapes have been examined for enhancing absorption and splicing loss [46].

To generate a high-power laser in the 1.5 μm region, double-clad erbium ytterbium-doped fiber (DC-EYDF) is a suitable candidate as an active medium because the double-clad geometry of DC-EYDF allows high pump power radiation at 976 nm to be efficiently coupled to the fiber which supports high output power.

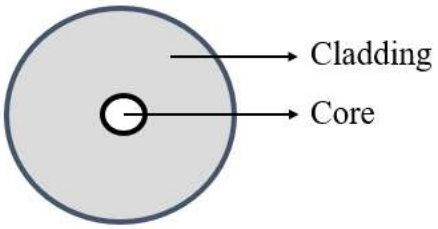

Figure 2.4: Schematic of Optical Fiber.

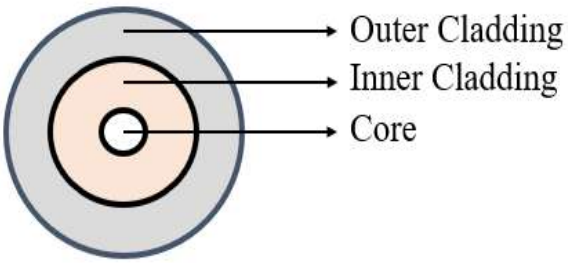

Figure 2.5: Schematic of Double-Clad Optical Fiber.

2.4 PULSED LASERS

A Laser can operate in a continuous wave (CW) or pulse regime. A few techniques convert the operating regime of a laser from continuous wave to pulse. It includes active

and passive techniques. The active mechanism includes an external modulator or switch to modulate light intensity, but light modulation is obtained passively in passive techniques. Q-switching and mode-locking are two well-known phenomena to generate pulses besides these self-Q-switching mode-locking and gain-switching are also important pulse generation techniques [47]. In this chapter, we will discuss briefly the Q-switching and mode-locking processes.

2.5 Principle of Q-switching

For generating pulses, internal loss of the lasing cavity needs to be controlled periodically so that the stored energy can be released in the form of pulses. As per the name Q-switching (Q factor), can do this task by modulating the total loss in the cavity. A laser cavity with a loss modulator is shown in Figure 2.6. Some standard Q-switching techniques include rotating mirror Q-switching, Electrooptic Q-switching, Acousto-optic Q-switching, and Passive saturable absorber (SA) Q-switching [29]. Further, Figures 2.6 (a) and (b) show Acousto-optic Q-switching and Passive saturable absorber Q-switching mechanisms.

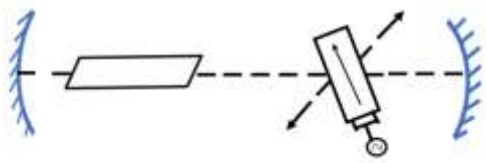

(a)

(b)

Figure 2.6: (a) Acousto-optic Q-Switching (b) Passive Saturable Absorber Q-Switching.

Before discussing Q-switching, it is important to describe the Quality factor (Q-factor) of a cavity because it plays a major role in Q switching. To build a laser cavity, optical resonators are important. A simple resonator consists of two mirrors that trap the multiple reflections and refocus the optical beam. Q-factor is a universal measure for this property of the resonator. It is defined as the ratio of energy stored in the cavity to the energy dissipated per cycle as shown in Equation 4.

$$Q = \varpi \frac{\text{Energy Stored by the Resonator}}{\text{Energy dissipated by the resonator}} \qquad [4]$$

The higher the quality factor, the lower the losses. For Q-switching, energy is stored in the amplifying medium with the help of pumping, while cavity Q is lowered to prevent the onset of laser emission. Low cavity Q means, the cavity losses are set to a high value, and during this time inversion and gain are pumped to a higher value as shown in Figure

2.7 (a) and (b). To build up the gain and increase the inversion, one of the mirrors can be blocked to stop the oscillation build-up. After this, the cavity losses are reduced instantaneously by suddenly introducing a high Q cavity as shown in Figure 2.7 (c). So that the beam evolve and extract the extra energy that has previously built in the upper laser level of the laser gain medium. This high value of gain causes the buildup of initial spontaneous emission at an unusually rapid rate, which initiates development of giant pulse of laser oscillation, as shown in Figure 2.7 (d) [29].

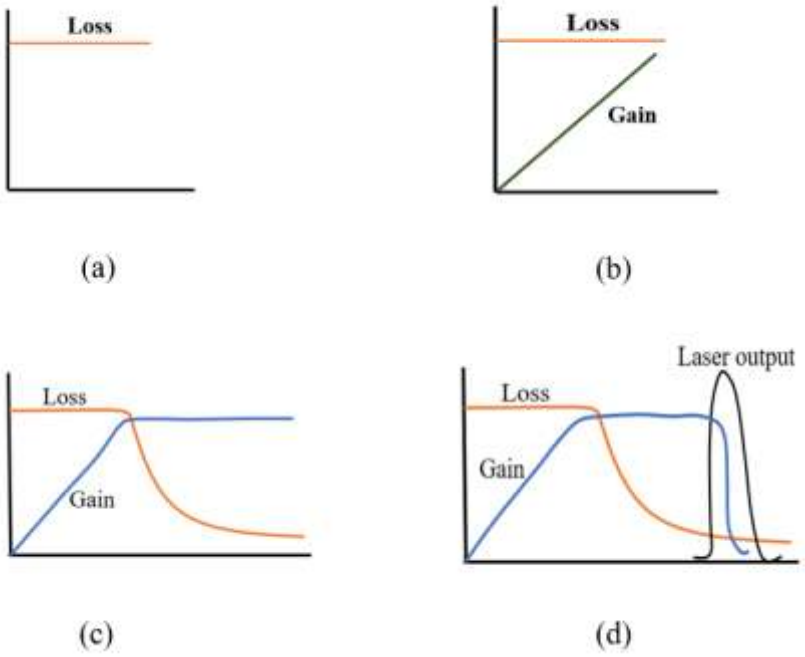

Figure 2.7: Laser Q-switching.

When a high cavity Q is restored, the stored energy is released as short pulses. For example, the increment of loss introduced in the cavity is more than the gain per round trip, which suppresses the lasing action, while the population inversion reaches its

maximum. Suddenly, this loss is removed and provides feedback to the cavity, which results in the form of pulses.

Several mechanisms have been used to introduce loss in a cavity. Initially, a Kerr cell was employed for this purpose by changing the polarization of light which introduces loss in the cavity. With increasing optical intensity there is a nonlinear change in the dielectric constant or refractive index of optical materials, this effect is known as the Kerr effect. In optical Kerr cells, applied voltage produces a refractive index change in a transparent but polarizable liquid placed between the electrodes. A degree of birefringence is induced by the Kerr effect, which is proportional to the square of the applied voltage [47]. Other mechanisms for Q-switching operation include mechanical shutters and electro-optic modulators [48;49].

An example of a component used for a passive Q-switching mechanism is known as a saturable absorber (SA), which can be artificial or real [50]. Real saturable absorbers are materials that exhibit an intrinsic nonlinear decrease in absorption when the intensity of light increases while artificial saturable absorbers (ASA) support intensity-dependent transmission [51;52]. Saturable absorption properties of ASA depends on the nonlinear effects happening inside the optical fibers based on the configurations used in the circuit such as nonlinear polarization rotation (NPR), nonlinear amplifying loop mirror (NALM), and nonlinear optical loop mirror (NOLM) [52].

Saturable absorption is a nonlinear effect that occurs due to a strong interaction of light with materials. Real saturable absorbers include semiconductor saturable absorber mirrors (SESAM), low dimensional nanomaterials and many other materials which possess nonlinear properties. These materials have the property of intensity-

dependent nonlinear absorption of light, which makes them suitable for behaving as a SA [53]. The absorption phenomenon in saturable absorbers can be explained with the help of Pauli's blocking principle, where a transition state or conduction band is fully occupied and no longer accepts electrons coming from the valence band [53]. These electrons make a transition once the incoming light interacts with the material and photons get absorbed by the electrons. In the case of low input intensity maximum photons are absorbed by electrons in the valance band, which results in less transmission. In contrast to this, when a high-intensity light interacts with the material, a large number of electrons transfer to the conduction band after absorbing photons leaving no space for more electrons or we can say that the conduction band gets saturated and does not accommodate more electrons which results in less absorption of photons and high transmission of signal in the form of pulses [53]. Besides material-based saturable absorbers, self-Q-switching is also an important way to generate pulses in which an unpumped section of the gain fiber itself acts as a SA at lower pump powers due to unsaturated ions [54].

2.6 Mode locking

Mode locking is a technique that produces extremely brief bursts of light. The word mode-locking describes the locking of multiple longitudinal modes in a laser cavity. The number of longitudinal modes in a cavity is determined by the length of the cavity. The mode locking employs diverse techniques to establish the appropriate phase correlation between the modes, resulting in consistent, constructive interference at regular intervals. Pulsed radiation can be produced by enforcing coherence between the phases of different

modes [55]. Mode locking has significantly transformed various scientific and technological domains. The pulses generated following this technique are called mode-locked (ML) pulses. The pulses are incredibly narrow, often in the femtosecond to nanosecond range, and have high peak power despite their low average power.

The evolution of mode locking has been characterized by significant advancements that have steadily improved its capabilities and expanded its range of application. Longitudinal modes in a laser are the distinct patterns of standing waves that can resonate within the laser cavity. A typical laser can support multiple longitudinal modes that oscillate independently. Mode-locking aligns their phases to generate coherent, high-intensity pulses. Each longitudinal mode corresponds to a unique frequency at which the light wave can propagate within the cavity. These modes are separated by a frequency interval that is determined by the inverse of the cavity round-trip time. For a laser to generate coherent pulses instead of CW light, it is necessary for the modes to not only cycle at their respective frequencies but also to preserve a precise phase connection. Mode-locking is a technique where the phases of all the longitudinal modes are synchronized in a way that they combine to produce strong interference at consistent intervals.

During propagation, the electromagnetic field oscillates spatially and temporally. In a laser oscillator, each mode oscillates independently, and the amplitude of the n^{th} mode can be written as [47]:

$$\mathrm{E}(\mathrm{t}) = \mathrm{E}_{\mathrm{n}}\, e^{i\left(\omega_{\mathrm{n}} t + \phi_{\mathrm{n}}\right)} \qquad [5]$$

Where ω_n is frequency and ϕ_n is phase of that mode. For mode-locking, if we assume that there is N modes with equal amplitude which oscillate in the cavity simultaneously, the combined amplitude can be written as:

$$E(t)=E_0\sum_{n=0}^{N-1}\left(e^{i(\omega_n t+\phi_n)}\right) \quad [6]$$

The difference between the frequency of adjacent modes is given by:

$$\omega_{n+1}-\omega_n = \Delta\omega = 2\pi\Delta\upsilon = \frac{2\pi c}{2\eta d} = \frac{\pi c}{\eta d} \quad [7]$$

Here, η is the refractive index, and d is the length of the cavity.

When these modes oscillate in a random fashion, the total intensity can be expressed as the square of the total amplitude of electric field, as shown in the following equation:

$$I(t)=|E(t)|^2=E_0^2\sum_{n=0}^{N-1}\left(e^{i(\omega_n t+\phi_n)}\, e^{-i(\omega_n t+\phi_n)}\right) \quad [8]$$

$$I(t)=NE_0^2 \quad [9]$$

From the above equation, it can be understood that the total intensity is N times the intensity of each mode. For mode-locking, all the modes should oscillate in phase which is $\Phi_n = \Phi_0$ for all 'n'. Total field amplitude can be expressed as:

$$E(t) = E_0 \sum_{n=0}^{N-1} \left(e^{i(\omega_n t + \phi_0)} \right) \quad [10]$$

$$E(t) = E_0 e^{i\phi_0} \sum_{n=0}^{N-1} \left(e^{i\omega_n t} \right) \quad [11]$$

The frequency of n^{th} mode can be expressed as:

$$\omega_n = (\omega_{N-1} - n\Delta\omega) \quad [12]$$

Equation 11 can be re-written as:

$$E(t) = E_0 e^{i\phi_0} \sum_{n=0}^{N-1} \left(e^{i(\omega_{N-1} - n\Delta\omega)t} \right) \quad [13]$$

Which upon expansion becomes:

$$E(t) = E_0 e^{i(\phi_0 + \omega_{N-1} t)} \left[1 + e^{-i\Delta\omega t} + e^{-2i\Delta\omega t} + ... + e^{-i(N-1)\Delta\omega t} \right] \quad [14]$$

The expression in brackets is a finite series that has value:

$$\frac{1 - e^{-iN\Delta\omega t}}{1 - e^{-i\Delta\omega t}} \quad [15]$$

After substituting this value in equation 14, the expression for E(t) becomes:

$$E(t) = E_0 e^{i(\phi_0 + \omega_{N-1} t)} \left[\frac{1 - e^{-iN\Delta\omega t}}{1 - e^{-i\Delta\omega t}} \right] \quad [16]$$

As we know, the total intensity is the square of the absolute amplitude, and it can be expressed as:

$$I(t)=E_0^2\left[\frac{1-e^{-i N\Delta\omega t}}{1-e^{-i\Delta\omega t}}\right]^2 \qquad [17]$$

Above expression can be re-written as:

$$I(t)=E_0^2\frac{\sin^2\left(\frac{N\Delta\omega t}{2}\right)}{\sin^2\left(\frac{\Delta\omega t}{2}\right)} \qquad [18]$$

This expression varies with t, but the maximum value occurs at:

$$\frac{\Delta\omega t}{2}=0,\pi,2\pi.....n\pi \qquad [19]$$

Difference between two maxima can be written as:

$$\Delta t_{sep}=\frac{1}{\Delta\upsilon_{sep}}=\frac{2\eta d}{c} \qquad [20]$$

Here, Δt_{sep} is the round trip time of the cavity. The maximum value of the intensity occurs when equation 18 satisfies the condition given in equation 19.

To make it simple, $\Delta\boldsymbol{\omega}t/2 = 0$ has been considered to solve the given equation:

$$I(t)_{lim}=\lim_{\frac{\Delta\omega t}{2}\to 0} E_0^2\frac{\sin^2\left(\frac{N\Delta\omega t}{2}\right)}{\sin^2\left(\frac{\Delta\omega t}{2}\right)} \qquad [21]$$

$$I(t) = E_0^2 \frac{N^2 \left(\frac{\Delta\omega t}{2}\right)^2}{\left(\frac{\Delta\omega t}{2}\right)^2} \qquad [22]$$

The maximum value of intensity is given by:

$$I(t) = N^2 E_0^2 \qquad [23]$$

From the above equation, it can be concluded that when modes are in phase their intensity is increased by a factor of N as compared to the case when modes were randomly matched. As shown in equation 20, the separation between two pulses is $2\eta d/c$ and pulse width is $1/\Delta\nu N$. Using these values, pulse duration can be expressed as:

$$\Delta t_p = \frac{2\eta d}{Nc} = \frac{2\pi}{\Delta\omega N} = \frac{1}{\Delta\upsilon N} = \frac{1}{\text{Gain Bandwidth}} \qquad [24]$$

From this equation, the pulse width of a pulse can be predicted based on gain bandwidth as they are inversely related [47].

To generate mode-locked pulses, synchronisation of modes can be achieved in two main ways, active and passive mode-locked technologies:

1. **Active Mode Locking:** Active mode locking is a technique that includes an external modulator, such as an electro-optic or acousto-optic device, to align the phases of the longitudinal modes within the laser cavity. Typically, this modulation is provided at a frequency that matches the round-trip duration of

the laser cavity. Electro-optic modulation involves the utilization of an electric field to alter the refractive index of a material within the laser cavity.

2. **Passive Mode Locking:** It is a method that achieves phase synchronization of the longitudinal modes without any external device. Instead, it depends on nonlinear optical characteristics of materials inside the cavity, such as a saturable absorber (SA) or Kerr nonlinearities, to trigger self-mode-locking behavior. It includes a SA, which absorbs incoming low-intensity light and transmits high-intensity light in the form of pulses. Kerr lens mode locking utilizes the self-focusing phenomenon caused by Kerr nonlinearity to achieve mode-locking. This method enables the production of highly narrow pulses without using any external modulation source. Passive mode locking is especially beneficial when small size, stability, and simplicity of use are of utmost importance, such as in portable laser systems, medical devices, and field applications.

2.7 Phenomenon involved in mode-locking

2.7.1 Self-Phase Modulation (SPM): A nonlinear optical phenomenon happens when a high-power pulse travels through a material that has a delayed reaction to the electric field. SPM involves a material with a refractive index that varies with the intensity of the light pulse, resulting in a phase shift that is directly proportional to the intensity [56]. As the pulse propagates through the material, the leading part encounters a greater refractive index than the trailing part causing a shift in pulse profile. The self-induced phase modulation causes the pulse width to widen by introducing distinct phase shifts to the

frequency components of the pulse. An intensity-dependent phase shift arises when a pulse passes through a medium with an intensity-dependent index of refraction (equation 25) and results in spectral broadening, known as SPM [38]. Where n_0 is a linear index, n_2 is a nonlinear index, and I(t) is pulse intensity.

$$n = n_0 + n_2 I(t) \qquad [25]$$

2.7.2 Optical Kerr Effect: The Kerr effect is caused by the interaction between the electric field of light and the electron cloud of the material [57]. It is a fundamental nonlinear optical phenomenon that occurs in materials, causing a change in refractive index in response to the intensity of light flowing through them.

In the presence of an electric field, the force associated with this field produces a distortion of the electron-charge cloud in the dielectric medium. If the applied field is strong enough, the polarization response of the medium becomes nonlinear. Hence, the Kerr effect plays a crucial role in mode locking and pulse creation in ultrafast laser systems by causing nonlinear phase modulation of the light pulse inside the laser cavity [57].

2.7.3 Nonlinear Amplifying Loop Mirror (NALM): It plays a significant role in passive mode-locking by exploiting nonlinear effects within an optical fiber loop to achieve pulse shaping and stabilization [58]. In a NALM configuration, the optical wave splits and propagates in two directions around a loop containing a nonlinear medium, typically an optical fiber. Due to the nonlinear Kerr effect, the phase difference in the counter-propagating waves depends on the radiation intensity. The counter-propagating waves

acquire different nonlinear phase shifts while completing a round trip inside the NALM, due to properties such as phase difference which vary along the pulse profile. It behaves similar to a SA when the NALM is adjusted such that the phase shift is close to 180 for the central intense part, this will be transmitted, and lower intensity parts of the pulse will be reflected. This phenomenon is like a SA where the central intense part is allowed to transmit, and the lower intensity gets absorbed.

2.7.4 Nonlinear Optical Loop Mirror (NOLM): It operates on a similar principle as NALM the only difference is there is no gain medium in the loop like a NALM. A nonlinear phase-shift is induced by self-phase modulation or cross-phase modulation. The input signal splits into two counter-propagating waves, after traveling the distance they return to the coupler and interfere. The optical path length experienced by two propagating fields is the same since they follow the same route but in opposite directions. The only disadvantage of a NOLM-based fiber laser is that one can only change the modulation depth like a NALM once we turn off the laser because the total length of the loop needs to be changed [59].

2.7.5 Nonlinear Polarization Rotation (NPR): It is also one of the essential methods for mode-locked fiber lasers based on intensity-dependent changes in polarization state when orthogonally polarized components of a single pulse propagate inside an optical fiber. The phenomenon involved in this process is the use of nonlinear birefringence of a single mode fiber, which is the same as the Kerr shutter. For this, one needs a polarizing component as a mode-locking element. In the configuration, a polarizer and analyzer are positioned appropriately inside the cavity to provoke polarization rotation of the light waves [60]. Hoffer et al. reported that the NPR effect is a self-sustaining mechanism for

generating ML lasers. Later, this technique was extensively used to produce short pulses [61].

After an extensive literature review, we found that researchers had proposed and demonstrated pulsed lasers in the 1.5 and 2.0-micron regions of the electromagnetic spectrum. The technologies spanned Q-switching, mode-locking, self-Q-switching mode-locking, and gain-switching. Initially, active and passive Q-switching were the main attractions for developing pulsed lasers. However, these methods had limitations. For example, in the case of passive techniques, lasers based on material-based saturable absorbers (SAs) faced difficulties in generating high-power lasers because of the low damage threshold of materials used for manufacturing SAs. On the other hand, an external modulator was needed for active techniques, which made the system complicated and expensive. Considering the above mentioned factors, self-Q-switched mode-locking (**Chapter 5**) and gain-switching (**Chapter 6**) attracted attention because of their efficiency and simple design.

Further, it was found that there were not enough available pump sources for developing lasers based on gain-switching. LDs were available to be used as pump sources, however it was difficult to modulate the output, which limited their use to generate gain-switched lasers. Further, researchers used amplifiers to enhance the output power of the pump laser to generate gain-switched lasers, but it made the laser design very complex and expensive.

In the thesis, we report lasers based on saturable absorber, self-Q-switched mode-locking and gain-switching. For a 2.0 micron laser, a homemade pulsed laser at 1570 nm was used as a pump source. The 1570 nm laser was developed based on self-Q-switched

mode-locking. No material-based SA was used, so output power was not limited based on the damage threshold of the material, as in the case of passively Q-switched lasers. The pump laser and main cavity designs for the 2.0-micron laser are simple and compact, making the overall system efficient and cost-effective. The power of the pump source was one obstacle in developing a laser in the 2.0-micron region. Researchers used amplifiers to obtain a high-pump power laser, making the system complicated and inefficient. However, there is no need for an amplifier in our laser because the laser at 1570 nm produced enough power (72 W peak power) to be used as a pump source, so it eliminated the need for amplifiers, giving it an advantage over other available lasers.

The 2-micron laser was used to detect carbon dioxide gas and can be used to detect other gases. Further, the tunability can be achieved by using FBGs or GNRs.

2.8 Conclusion

The objective of the thesis is to develop a pulsed laser in the 2.0 μm region of the electromagnetic spectrum. Silica core fibers doped with various rare-earth ions were used as gain media. To understand the development process, we have discussed the fundamentals of optical fibers, doped fibers, and the mechanism to develop a pulsed laser.

Chapter 3

Pulsed Laser based on aqueous Gold nanorods and Polyvinyl Alcohol solution as a Saturable Absorber

In this chapter, we discuss the development of an erbium-ytterbium co-doped fiber pulsed laser based on a saturable absorber (SA) at 1567 nm. An aqueous solution of gold nanorods (GNRs) and polyvinyl alcohol (PVA) was used as a SA. The laser was able to produce Q-switched pulses with a minimum pulse width of 9.6 μs having a repetition rate of 21.5 kHz, and a pulse energy of 0.15 μJ at a pump power of 2.195 W. We discuss the effect of GNRs and PVA concentration on pulse formation and explain briefly the characteristics of the pulsed laser based on a SA. We discuss in detail about the SA, as it is the key component in generating the pulsed laser. Further, we discuss the preparation of GNRs with a particular aspect ratio to obtain the desired wavelength of operation.

3.1 Introduction

As we have discussed earlier fiber lasers have drawn extensive attention due to their simplicity, compactness, and cost-effective nature. The majority of fiber lasers have been constructed using rare-earth doped fibers as a gain medium e.g., erbium-doped fiber

(EDF), ytterbium-doped fiber (YDF), and thulium-doped fiber (TDF). In **Chapter 2**, we discussed different mechanisms to develop a pulsed laser based on active and passive Q-switching and mode-locking techniques. The passive techniques based on a SA, were preferable to generate pulsed lasers due to easy integration into the cavity and easy fabrication compared to active techniques.

A key aspect of developing pulsed lasers is the exploitation of the SA. A SA can be real (material) or artificial (fiber nonlinearity based). The journey of saturable absorbers started with semiconductor saturable absorber mirrors (SESAMs) [62], but after that, a number of materials came into existence to be used as SAs. Each material has its advantages and disadvantages. For example, SESAMs were used for their stability and flexibility, but their application was limited due to their complicated manufacturing. Besides that, their high cost and narrow wavelength range also hindered their popularity [63]. Graphene, a 2D material, was also widely used as a saturable absorber, but due to its low modulation depth caused by its weak absorption, resulted in unstable performance [64]. Apart from these materials, many other emerging materials can be used as SAs, such as carbon nanotubes, black phosphorous, and other nanomaterials [65-67]. Amongst these materials, metal nanoparticles are favorable due to their ease of manufacture and tunable properties [68]. Metal nanoparticles such as gold nanorods are advantageous compared with other materials due to their high-order nonlinear optical properties, wide emission band, and tunability [69;70].

Gold nanoparticles have advantages over other materials due to their tunable Surface Plasmon Resonance (SPR), specifically a localized surface Plasmon resonance (LSPR) wavelength, which depends on the shape and size of the nanomaterials (e.g.,

GNRs). This LSPR effect arises when a small size particle interacts with light of a wavelength larger than the size of the GNR. The conduction carriers of the particle oscillate collectively in response to the electric field. This resonance phenomenon is known as LSPR [68]. Though this property helps in the tunability of these materials for many applications, a low damage threshold limited their popularity. Some methods have been proposed to increase the damage threshold of the nanoparticles, such as coating the nanoparticles with silica, mixing with polymers like Polyvinyl alcohol (PVA) [71] and sodium carboxymethyl cellulose (NaCMC) [71]. However, the integration method of SA is important in the case of direct integration between two fiber connectors, light illuminates directly on the surface of GNRs and damages them easily. Furthermore, other approaches were adapted to increase the damage threshold, such as increasing the interaction path for propagating light and GNRs. Tapered fibers and D-shaped fibers have been used to increase damage threshold by increasing the interaction path and decreasing instantaneous heating. For example, in a D-shaped fiber the instantaneous heating of GNRs is eliminated as the evanescent field interacts with the GNRs. In this process, GNRs are deposited on the surface of D-Shaped fiber where only the evanescent field interacts with GNRs elevating the damage threshold [72;73]. Similarly, In the case of tapered fibers, GNRs are deposited on the outer surface, and the evanescent field interacts with the GNRs and the interaction is much weaker compared with direct interaction which helps to increase the damage threshold of these GNRs [73]. We have adapted a new approach in this research to increase the damage threshold of the GNRs, where GNRs in aqueous form are used, so that heat can dissipate quickly without damaging the

nanorods at high pump power [74]. Also, to keep the GNRs from clustering the GNRs were mixed with PVA.

A lot of research work has been reported based on GNRs as a SA, initially nonlinear optical properties of the gold nanomaterial were explored but for the first time in 2012, Jiang et al. demonstrated a passive Q-Switched fiber laser at 1.5 μm using a gold nanocrystal (GNCs) based SA with 3.2 μs wide pulses at 30 mW pump power. These nanocrystals show an absorption peak at 523 nm but when mixed with NaCMC, it has a broadband absorption from 500 to 2000 nm. It was analyzed that by increasing the concentration of GNCs, both intensity and bandwidth can be increased [75]. However, GNRs show advantages over GNCs as they have two SPR peaks, the most important is the longitudinal surface plasmon resonance (LSPR) wavelength which can be tuned in wide range by varying the aspect ratio (AR=Length/width) [76]. Kang et al. reported a Q-Switched erbium-doped fiber laser based on gold nanorods as a SA (GNRs and NaCMC film) for the first time in 2013, where 4.8 μs pulses were obtained for a pump power of 275 mW at 1560 nm [77]. Similarly, mode-locked pulses were obtained using GNRs as a SA. However, the main focus of researchers was to increase the damage threshold. In 2014, Wang et al. reported microfiber-based gold nanorods as SA for pulse generation, in this research work with the help of geometric characteristics of the microfiber, the damage threshold was increased by employing the evanescent field interaction of propagating light with GNRs. Another advantage of using microfiber was increased saturable absorption as more GNRs were able to interact with the incident light so that narrow pulses could be generated [73]. But preparation of microfibers and depositing GNRs on their surface was a tedious task, which left a space for other methods

to increase the damage threshold. Another approach was adapted where silica encased gold nanorods were used as a SA for reducing optical damage. In 2016, Wang et al. reported a wavelength-switchable femtosecond pulse fiber laser based on silica-encased gold nanorods as a SA, they explained the process of developing a SA and anticipated it can be a good choice for increasing the damage threshold of GNRs [67]. In 2017, Jiang et al. reported a pulsed Er-doped fiber laser based on GNRs as a SA. They investigated tunable nonlinear SA behaviour of the GNRs with the help of an optical modulation method and altered the modulation depth. They were able to tune laser output in terms of pulse width and repetition rate with modulating light [78].

GNRs have advantages because of their wide tunability range over other SAs which make them accessible for development of a pulsed laser from the visible to mid - infrared region. In 2019, Luo et al. explored this via generating mid-infrared pulses in the 3 μm region. GNRs of aspect ratio 20 with an absorption band of 2.2-3 μm were used as a SA. Stable Q-switched pulses with pulse width 2.18 μs were generated at pump power of 307.2 mW. This work proved the capability of GNRs as a versatile SA for generating pulses in different wavelength regions [79]. In 2021, Lee et al. reported a Q-switched and mode locked Er-doped fiber laser using GNRs as a SA in the form of a film. They investigated the effect of number of films in the cavity on pulse generation and mentioned that the operating regime can be changed with a different number of film layers in the cavity [80]. In 2023, Shi et al. demonstrated a passively Q-switched erbium-doped solid-state laser using GNRs as a SA in 3 μm region. They mentioned that GNRs can be a promising material for 3 μm laser generation [81]. All these characteristics make a SA based on GNRs superior to others for developing pulsed lasers. In this research

work GNRs were used in aqueous form mixed with PVA for increasing the damage threshold. The GNRs structure was intact up to 2.9 W pump power. Also preparation of the SA was not complicated as reported in above mentioned articles [74].

3.2 Saturable Absorber (SA)

SA is a key component for pulsed laser generation. It is a typical nonlinear optical device that converts a continuous wave (CW) laser output into a short burst of energy known as a pulse laser. It is commonly used as a intensity-modulating device based on Pauli's blocking principle [82]. The saturation phenomenon occurs as more absorbing atoms or molecules within the SA medium are excited to an upper level by incident signal photons. As the signal intensity and upper state population increase, the probability of a photon interacting with an absorber in the ground state decreases, which leads to a reduced absorption coefficient within the medium. It transmits light at high excitation intensities with reduced optical loss when the initial states of the absorbing transition are empty, and the final states are fully occupied. SA induces a net loss on the low-intensity fluctuations that cannot saturate its absorption while allowing a net gain for those with a high enough intensity to cause saturation. After many round trips, the net loss leads to attenuation to low-intensity beats, while the highest-intensity beat is amplified into a pulse with high peak intensity [83].

The nonlinear absorption behavior of an SA depends on the intensity of incident light. Nonlinear absorption coefficient can be determined using following equation and experimental data can also be fitted using this equation to confirm the saturation effect [84].

$$\alpha = \alpha_{ns} + \frac{\alpha_s}{1 + \frac{I}{I_{sat}}} \qquad [26]$$

Where α is the intensity dependent absorption (optical loss), α_s and α_{ns} are saturable (modulation depth) and non-saturable absorption components, and I and I_{sat} are the light intensity and saturation intensity.

SA is a nonlinear optical modulator that means when the intensity of light is high, absorption is less, and further absorption is not possible which can be explained by Pauli blocking principle [82]. Absorption (optical loss) and intensity is inversely related to each other as shown in equation 26. Which indicates that by using this device in the laser cavity, the amplitude of the incident beam can be modified passively [85].

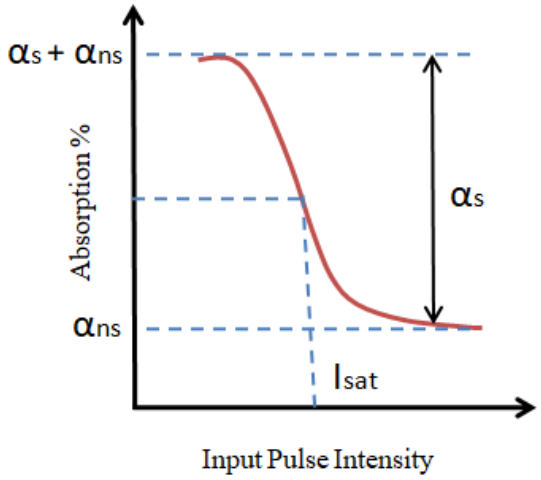

Figure 3.1: Example of saturable absorption curve.

A few parameters are important to understand the behavior of a SA, such as modulation depth, non-saturable loss, saturation intensity, and damage threshold of

material. Saturation intensity (I_{sat}) is defined as the signal intensity that reduces the absorption coefficient to half of its small signal value (absorption coefficient of the material when the input signal intensity is much lower than the saturation intensity). Modulation depth or transmission curvature near the peak is controlled by the optical pulse itself in which the absorption coefficient decreases when the light intensity increases. The modulation depth (α_s) is the difference between total background loss ($\alpha_s + \alpha_{ns}$) and non-saturable loss (α_{ns}), as shown in Figure 3.1 [85].

Noble metal nanoparticles due to their brilliant properties like SPR and size have advantages in many fields. These nanostructures are being used for early diagnosis of cancer, or in nanotherapeutic applications such as drug delivery agents [86]. Due to LSPR and nonlinear properties metal nanoparticles can be used as a SA to design pulsed lasers at different wavelengths. SAs are a key component in passive Q-switched or mode-locked lasers. LSPR is tunable by controlling the aspect ratio, so by using different size of GNRs as a SA, different pulse lasers can be designed in different regions [79;80].

3.3 Gold nanorods and synthesis

Metal nanoparticles show properties that are different from bulk materials such as SPR. Based on their characteristics and properties various methods have been discovered for synthesizing these nanoparticles. In the synthesis of nanoparticles, control over shape and size influences the optical, electronic, and catalytic properties. Amongst all the nanoparticles, GNRs are the most effective agents owing to their unique properties, i.e., longitudinal surface plasmon resonance (LSPR). For the synthesis of GNRs, uniformity of nanorods, size and shape, and chemical and thermal stability are highly desired.

Nanomaterial synthesis is extremely sensitive to all the factors involved in the process, i.e., experimental conditions, temperature, stirring rate, and even the cleanliness of glassware can be barrier in the path of producibility of GNRs. All the glassware should be washed with aqua regia (hydrochloric acid and nitric acid mixture) and then washed with deionized water for better results.

Several methods have been adapted for the production of GNRs, such as [87;88]:

1. Template method
2. Electrochemical methods
3. Seeded growth method
4. Seedless method

Out of these, the most conventional and widely used method to synthesize GNRs is the seeded growth method, but it has some limitations, i.e., Gold seeds need to be freshly prepared as they cannot be preserved for a long time. Analyzing the limitations of this method, researchers came up with a seedless method to synthesize GNRs which is the one step synthesis method [89]. The aspect ratio of GNRs impacts the properties, which makes it important to know the factors that control it while synthesizing.

3.3.1 Factors affecting the aspect ratio of GNRs

Many factors, such as chemicals, concentration, and amount of chemicals used during synthesis affect the AR of GNRs. Seed mediated methods provided a lot of information for changing the AR of GNRs. Nikhil R. Jana et al. reported GNRs with AR 18 and

explained the preparation of GNRs with different lengths using a seed mediated method [90]. Chen et al. reported a new approach for fabricating nanorods up to AR 70 by controlling the volume of the growth solution and synthesis process of fabricating GNRs up to AR 70 has been discussed briefly [91;92]. Further, the selection of surfactants is very important for the synthesis of long GNRs, experimental studies found that surfactants with longer chain lengths led to longer rods with higher yields as compared to shorter ones [93]. As in the case of cetyltrimethylammonium bromide (CTAB), the trimethylammonium head group can selectively bind to specific crystallographic facets of the seeds, while the tails of CTAB can form a bilayer structure with each other through interaction. The concept of binary surfactants was given by Nikoobakht and El-Sayed for long GNRs, though they gave this concept in respect to the seed-mediated method, it can be extended to seedless method too, but the ratio of CTAB and benzyl dimethyl ammonium chloride (BDAC) should be optimized [94]. Heptane is another chemical that can be used in the reaction to increase the length of GNRs. GNRs with different AR can be synthesized at different pH values and heptane concentrations [95]. Besides the chemicals, their concentration also plays an important role for the synthesis of GNRs. With varying concentrations, different GNRs of different shapes and sizes can be prepared. N.R. Jana reported that strong and weak reducing agent affects the growth process of GNRs. The process depends upon the critical nucleation rate for sodium borohydride and ascorbic acid. Strong reducing agent helps in nucleation and weak reducing agent helps the nanoparticles to grow. By controlling the ratio of ascorbic acid and $NaBH_4$, nucleation rate can be controlled which gives the opportunity to synthesize GNRs of different AR along with different shapes [96]. Overall, there is strong

experimental evidence that the uniformity, purity, and high yield of synthesized GNRs of the desired LSPR band depends upon the parameters such as molar concentrations, amount, pH, temperature, mixing process, etc. of the chemicals used in the reaction.

In this work, emphasis was on the Seedless method for the synthesis of GNRs. N.R. Jana first proposed the seedless method and discussed the major drawback of seed-mediated methods [96]. Primarily the experiment was done following the process given by El-Sayed et al. and modified accordingly for changing AR [88]. Chemicals used in the reaction were CTAB, Chloroauric acid ($HAuCl_4$), Silver Nitrate ($AgNo_3$), Ascorbic acid and Sodium borohydride ($NaBH_4$).

Chemicals	**Molar concentration**	**Amount used in exp**
Gold (III) Chloride solution ($HAuCl_4$)	1 mM	13 µl
CTAB	0.12 M	5 ml
Silver nitrate ($AgNO_3$)	4 mM	260 µl
Ascorbic Acid (AA)	78.8 mM	70 µl
Sodium borohydride ($NaBH_4$)	0.01 M	15 µl

Table 1: Table showing the chemicals, molar concentration and amount used in experiments to prepare GNRs with AR 10.

CTAB, Ascorbic Acid, $NaBH_4$, and $HAuCl_4$ (30 wt. % in dilute HCl) were purchased from Sigma-Aldrich. $AgNO_3$ was purchased from Thermo Fisher Scientific. All glass containers were cleaned with the aqua regia and nanopure water before the use. Aqua regia is a mixture of concentrated nitric acid and hydrochloric acid in a ratio of 1:3 by volume. Chemicals used in the reaction with their molar concentration and volume have been described in Table 1. Sartorius Microbalance was used for measuring chemicals.

3.3.2 Reaction mechanism for synthesis of GNRs

To synthesize GNRs, CTAB solution was prepared by mixing CTAB powder in nanopure water, keeping it on stirring Hot Plate [1](Model 2 10T from Fisher Scientific) at 60°C for approximately 20 minutes. Once the CTAB powder was mixed in water, the solution was brought to room temperature (25 - 30°C) by keeping it aside for an hour, no precipitation was observed. $NaBH_4$ solution was freshly prepared and kept in ice-cold water till the reaction took place. The $AgNO_3$ solution was stored in an amber glass bottle and kept in dark. 13 µl of $HAuCl_4$ (1mM) solution was added to 5ml of CTAB (0.12 M) solution. The solution turned yellowish without any precipitation after vigorously stirring for two minutes with a magnetic stirrer. Then, 260 µl of $AgNO_3$ (4 mM) was added in the solution and it turned opaque yellowish. Further, 70 µl of Ascorbic acid (78.8 mM) was added to the solution and stirred vigorously, the solution turned completely transparent.

[1] *Fisher Scientific Thermix Model 210T Stirring Hot Plate, Thermo Scientific, US.

It's worth mentioning that the solution turns transparent with the right amount of ascorbic acid which indicates successful completion of reaction until this step. Then, 15 µl of $NaBH_4$ (0.01 m) was added to the solution which gradually turned the solution to light brown. After adding $NaBH_4$, gradually the solution turned dark brownish from light brownish. Then the solution was kept undisturbed for about 5 hours and 30 minutes in a dark at room temperature and then with the help of the centrifugation process GNRs were segregated from the excess CTAB solution.

The characterization of the prepared GNRs was done with the help of Transmission Electron Microscope (TEM) images using JEOL (Model- JEM 2100PLUS) and absorption spectra using iHR550 spectrophotometer. To prepare the TEM sample 5 µl drop of GNRs solution was placed on a carbon-coated copper grid (TEM sample holder) and allowed to dry for a night. We were able to synthesis multiple shapes of gold nanoparticles in aqueous solution for example spheres, triangles and nanorods as shown in Figure 3.2.

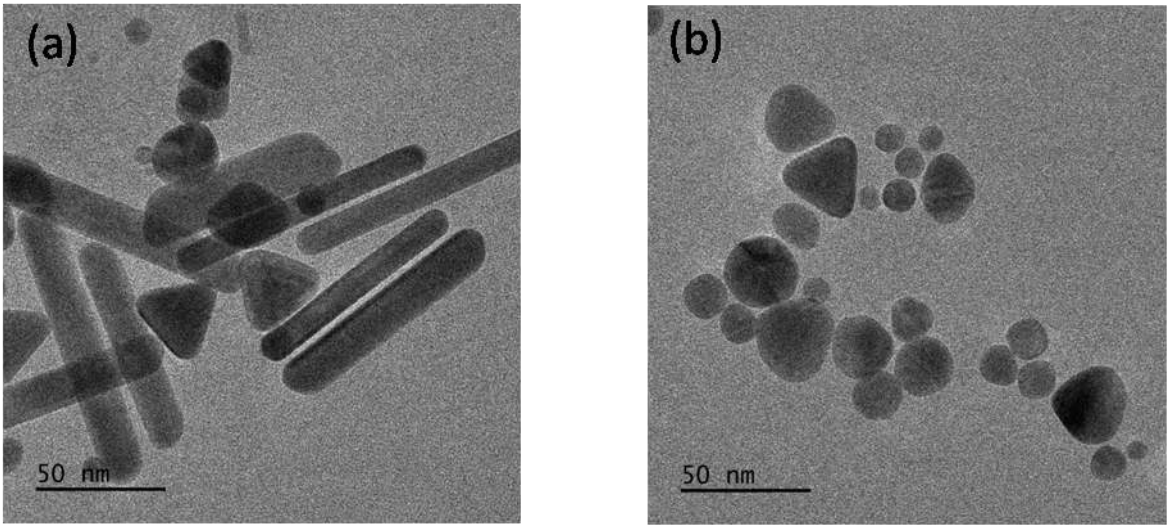

Figure 3.2: Multi shape nanoparticles.

Shape of the nanoparticles were changed by changing the concentration of chemicals as shown in Figure 3.3 [97]. The AR of GNRs was analyzed with the help of TEM images and the majority of them had an approximate AR of 10 as shown in Figure 3.3 (a), which corresponds with the LSPR peak observed by using iHR 550 spectrometer at 1400 nm (Figure 3.3 (b)). Two peaks are shown in the Figure 3.3 (b) one is at 765 nm which corresponds to width of the GNR and second is at 1470 nm which is due to length of the GNR.

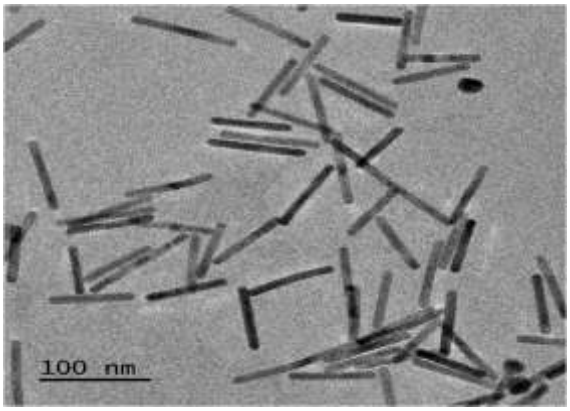

(a)

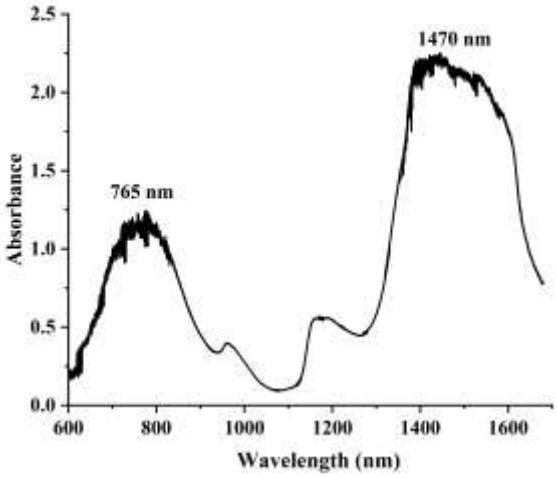

(b)

Figure 3.3: (a) GNRs with AR 10, and (b) Absorption spectra of prepared GNRs.

3.4 Preparation of Saturable absorber

GNRs can be used in different forms as a SA, for example by depositing directly on the fiber tip, or in the form of a film manufactured by mixing with polymer (e.g., PVA). In this research work, we used an aqueous solution of GNRs and PVA as a SA for increasing the damage threshold. GNRs alone can aggregate easily in solution, but a polymer can keep them segregated, which protects its properties and increases the damage threshold as PVA gives an extra layer of protection to the nanorods. When GNRs interact with light their temperature elevates which leads to shape deformation, but it can be controlled by changing the surroundings. It was found that the effective thermal conductance of GNR/Polymer is much higher than the GNR/CTAB, with this modification the damage threshold increases as heat will dissipate quickly towards the surroundings [98;99].

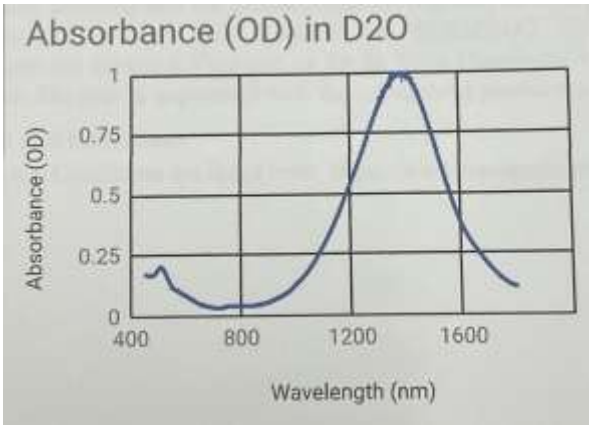

Figure 3.4: Absorption spectra of GNRs (Nanopartz, USA).

To prepare the SA, GNRs were purchased from Nanopartz Inc. USA with aspect ratio 10 (length and diameter 100 nm and 10 nm, respectively, and LSPR peak 1400 nm),

and PVA (Average molecular weight 85000-124000, 87-89% hydrolyzed) from Sigma Aldrich. GNRs with an AR 10 were chosen for the experiment because of the absorption in the 1.5 μm region, as shown in Figure 3.4.

The aqueous solution was prepared by mixing colloidal GNRs and PVA solution. PVA solution was prepared by mixing 2 g of PVA in 100 ml deionized water using a magnetic stirrer, keeping the temperature 70 – 80 degrees centigrade for approximately three hours, as shown in Figure 3.5 (a). After that, the solution was allowed to cool down at room temperature to observe any precipitation. Once the solution came to room temperature without any sedimentation, it was ready for further processing. To optimize the concentration of the PVA solution, the experiment was performed with different concentrations (i.e., from 1% to 10%). The best results were obtained when 2 g PVA was mixed in 100 ml deionized water. We set this 2% concentration throughout the work. Later, all the experiments were performed using the same amount of PVA (2%). Similarly, the volume of the GNRs solution was optimized, as absorption depended on the number of GNRs. Initially, an experiment was performed with the standard solution of GNRs, which produced much wider pulses. So, the concentration of GNRs was increased by taking more volume of solution and removing excess CTAB.

To increase the concentration of GNRs and remove excess CTAB from the standard GNRs solution, 200 μl of GNRs were centrifuged at 13500 rpm for 20 minutes, and 100 μl supernatant was taken out, as shown in Figure 3.5 (b). The remaining 100 μl GNRs solution was mixed with 100 μl PVA. It was mixed on a magnetic stirrer without heat for 40 minutes and ultrasonication was used for uniformity, as shown in Figure 3.5 (c).

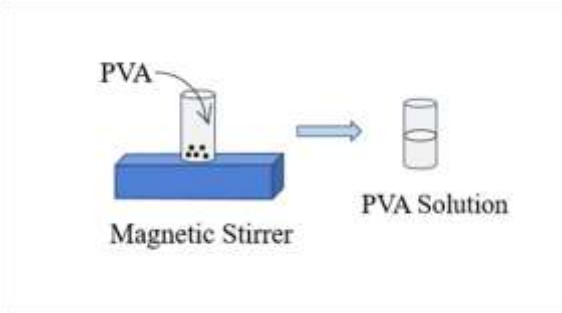

(a)

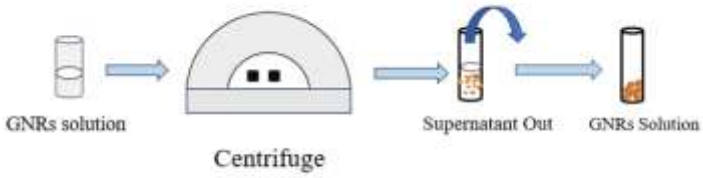

(b)

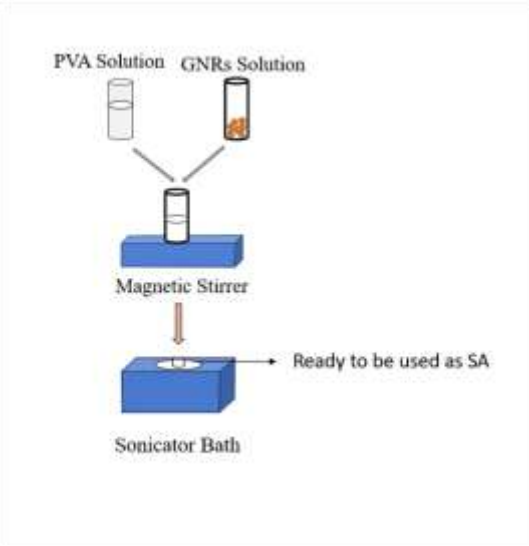

(c)

Figure 3.5: (a) Setup used to mix PVA powder in water (b) Setup for removing excess CTAB using a centrifuge (c) Preparation of SA by mixing PVA solution and GNRs solution.

The prepared solution was observed for 6 hours, and no precipitation was seen. This solution was used as a SA. Before using it in the circuit, its characterization was done by measuring its absorption and whether it was good to be used as a SA with the help of twin power detector measurements.

Figure 3.6 (a) and (b) show the (TEM) images of the GNRs at two different concentrations, indicating that to increase the density of GNRs, a larger volume of GNRs is required.

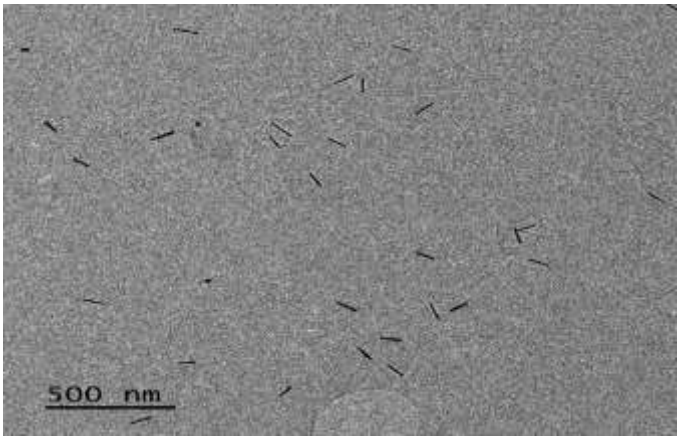

(a)

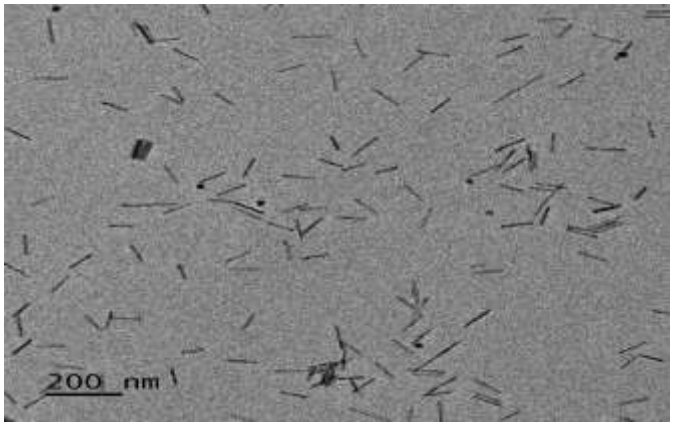

(b)

Figure 3.6: (a) TEM image of GNRs solution (200 µl) (b) TEM image of GNRs (300 µl)

3.5 Characterization of Saturable Absorber

Based on its nonlinear properties, a material can be used as a SA. These properties can be analyzed with the help of measuring nonlinear coefficients such as nonlinear absorption and nonlinear refraction (NLR) [100]. There are a few techniques to measure the nonlinear properties of materials, one is the Z-scan technique and another is twin power detector technology [101;102].

Using the Z-scan technique, changes in index and absorption can be determined easily. In this measurement setup, a lens focuses the beam to get a continuously variable laser intensity. Then, the sample is placed after the lens and moved in the z-direction as per the name of this technique, and light is collected after the lens using a detector. By recording the position of the sample, the transmission as a function of incident laser intensity can be determined. With the help of transmittance as a function of z-position, information about light-matter interaction can be extracted [53]. Another method is the twin power detector technology, which was used in this work to determine the nonlinear absorption of the SA.

3.6 Twin power detector technology

The nonlinear optical absorption of a SA can be characterized by using a power-dependent transmission technique based on a balanced twin detector measurement system.[102]. In this, the input intensity is divided into two parts, one is passed through the material and the other is transmitted directly to investigate the behavior of light

absorption in the material. When input intensity is weak, the absorption is linear, but with increasing input intensity, the absorption decreases gradually and saturates [103].

Figure 3.7 shows the homemade setup to characterize the saturable absorber. A mode-locked fiber laser with a pulse duration of 25 ns and a repetition rate of 7.812 MHz at 1570 nm was used to determine the SA's nonlinear properties. A variable attenuator was used to change the incident light on the SA, and a 50:50 coupler to split light equally. Figure 3.8 was obtained by comparing the results of the power meter (FOT-90A, resolution 0.01 dB, EXFO). By fitting the experimental data shown in Figure 3.8, we found a saturation intensity of 1.75 KW/cm^2, a non-saturable loss of 45.5%, and a modulation depth of 10.4%, which confirmed that the aqueous solution of GNRs and PVA can be used as a SA.

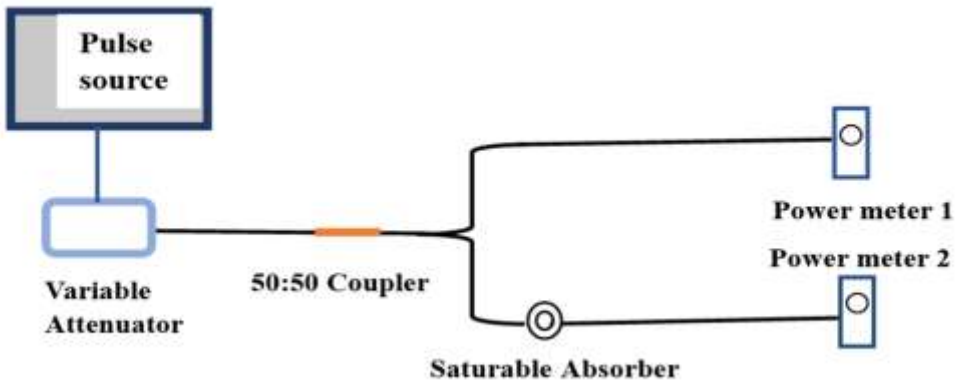

Figure 3.7: Schematic diagram of the twin power detector technology to obtain nonlinear absorption characteristics.

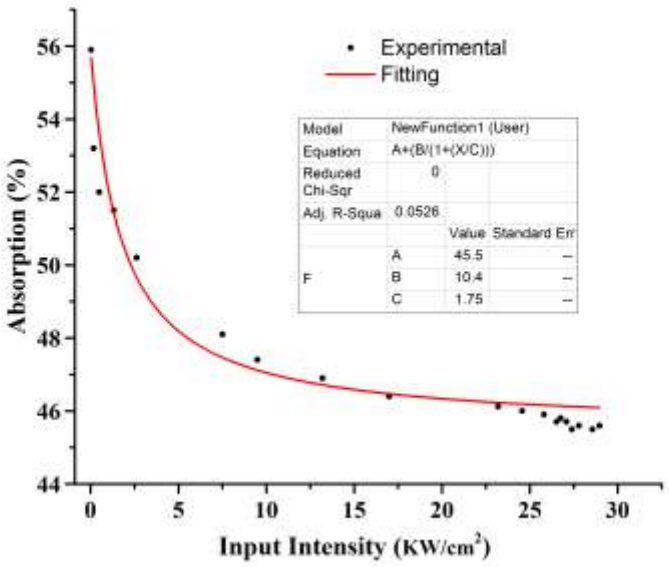

Figure 3.8: Nonlinear absorption of SA.

3.7 Experimental Setup

Figure 3.9 (a) shows the schematic of the laser. It is a linear cavity formed by two polarization-independent optical circulators (CIR). The signal passes through the gain medium twice for each round trip and thus enhances the output power level. A double-clad erbium-ytterbium co-doped fiber (DC-EYDF, absorption at 915 nm 1.7 dB/m) of 6 m has been used as the gain medium. The total cavity length was approximately 18 m. A 976 nm pigtailed multimode laser diode with a maximum output power of 9 W was used as a pump. A multimode fused fiber coupler (6x1,1) acted as a wavelength division multiplexing (WDM) coupler (to combine pump and signal wavelengths). A polarization-independent circulator (CIR) was used as a broadband reflector, reflecting the backward propagating amplified spontaneous emission (ASE). The second polarization-independent

circulator (CIR) formed a unidirectional ring cavity. Two circulators together formed a Fabry-Perot cavity. The output from Port 3 of the CIR enters the SA. Figure 3.9 (b) shows the schematic of the cell containing the aqueous solution of GNRs and PVA, which acts as a SA. Figure 3.9 (c) shows the cell with two FC/PC connectors and a ceramic split mating sleeve forming a microcell to hold the aqueous solution. To make the microcell, a pigtailed FC/PC connector was connected to the ceramic split mating sleeve and secured with epoxy to develop the cell. The tube was filled with 10 µl solution and a second pigtailed connector was inserted at the other end. The thickness of the GNRs and PVA solution held between two ferrules was 390 µm (measured using a traveling microscope with a vernier constant of 10 µm). The laser output was monitored using a 10% fused fiber coupler (FFC) connected to an Oscilloscope (TDS 7104, 1 GHz) through a high-speed photodetector (DET08CFC/M, 5 GHz InGaAs Photodiode with rise time 70 ps and fall time 110 ps, Thorlabs), and average power was measured using a power meter.

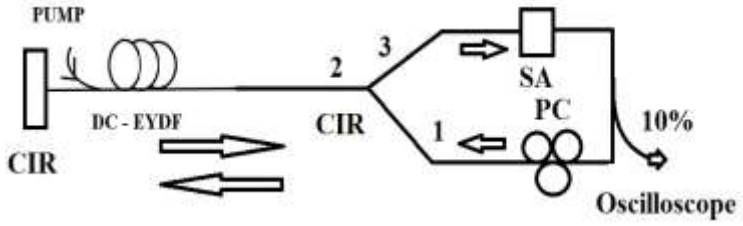

(a)

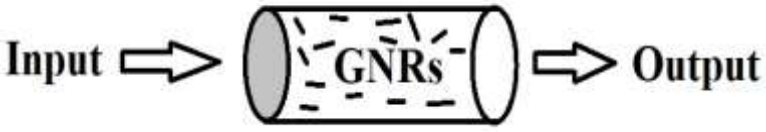

(b)

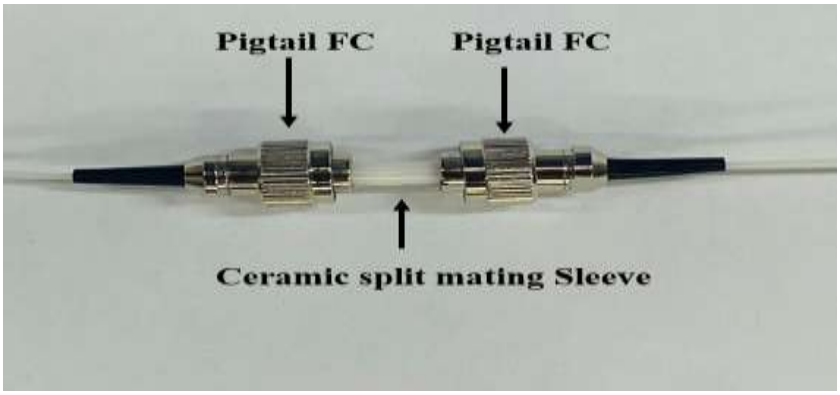

(c)

Figure 3.9: (a) Schematic of the laser; (b) Schematic of a tube filled with the aqueous solution of GNRs and PVA; and (c) Ceramic split mating sleeve connected between two FC connectors.

3.8 Results and Discussion

Laser output was characterized by using an optical spectrum analyzer and oscilloscope. Figure 3.10 shows the output of the laser at 1567 nm. This wavelength lies in the absorption region of GNRs, used as a SA. This configuration produced only Q-switched pulses as no mode-locking was observed at different orientations of polarization controller plates, and a different amount of SA solution was tried. Q-switched pulses were generated at a pump power of 1.1 W. With increasing input pump power the repetition rate was increased and pulse width decreased as shown in Figure 3.11, which confirmed the Q-switched behavior of pulses.

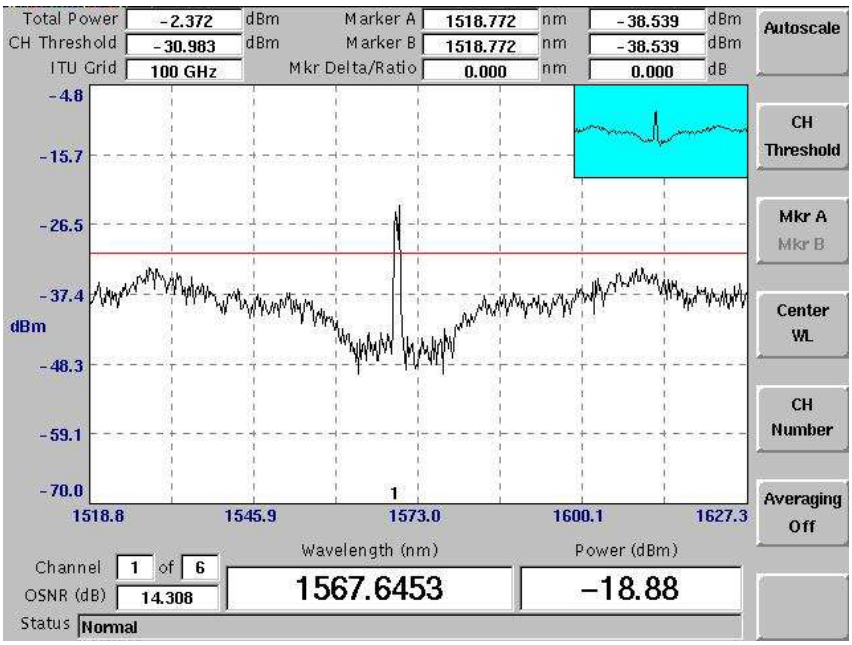

Figure 3.10: OSA Output at 2.8 A (1.85 W) pump current.

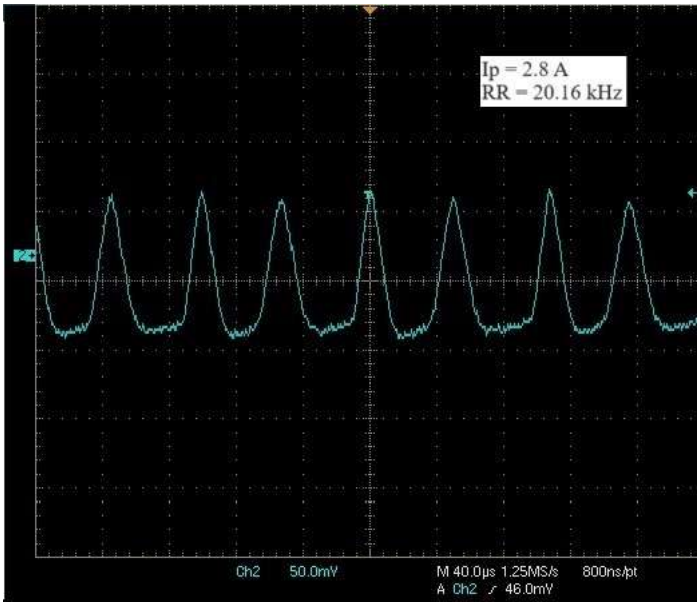

(a)

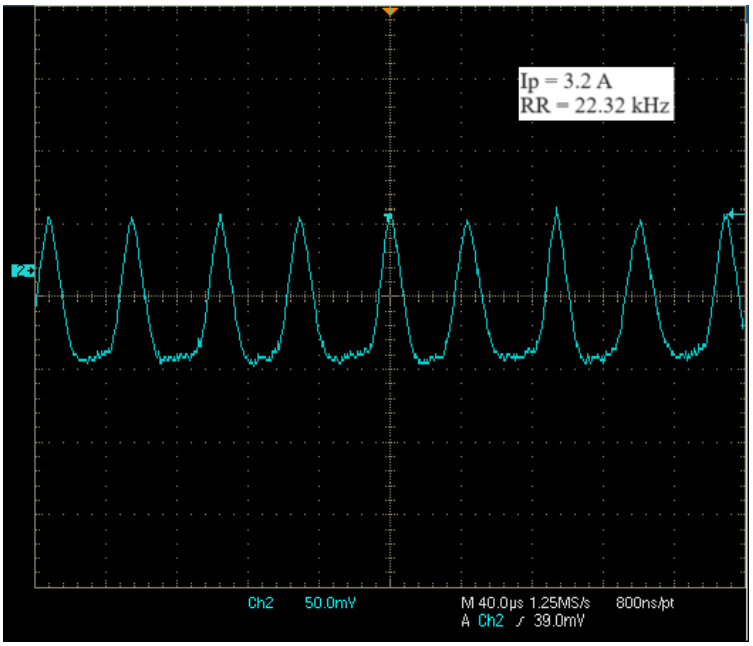

(b)

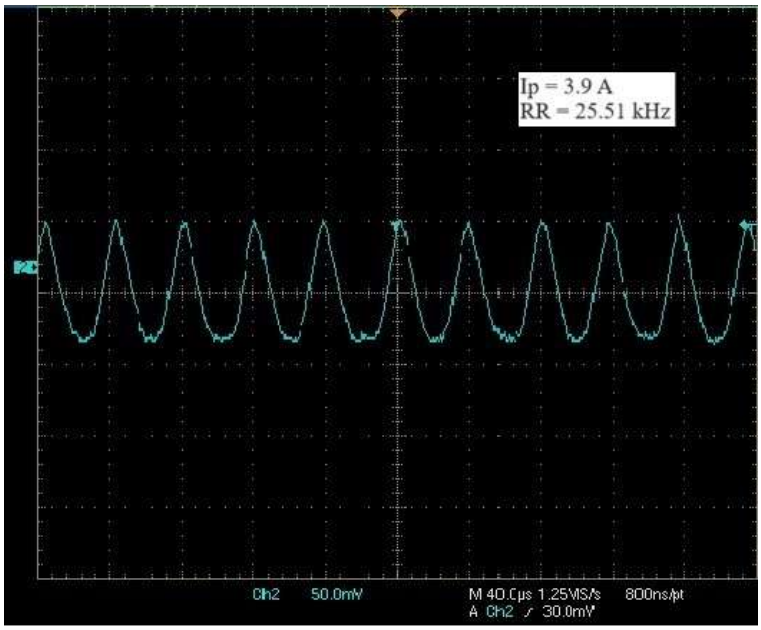

(c)

Figure 3.11: (a) Q-Switched pulses obtained at 2.8 A (1.85 W), (b) At 3.2 A (2.25 W), and (c) At 3.9 A (2.8 W) pump current.

The pulse width continuously decreased until the pump power reached 2.9 W and became unstable beyond this power. However, once the pump power was reduced pulses became stable which means the SA was not damaged up to and including that power level. Also, the pulses were observed for 4 hours and were stable. It was observed that the output of laser did not change after repeated operation with the same GNRs solution over a long period, which shows the stability of the structure of the GNRs (relative humidity in the lab was 20%). Further, the lifetime of SA is an essential factor for real applications. We performed experiments over two months with the prepared SA and each time the same results were produced (threshold power, center wavelength, and pulse duration). Figure 3.12 (a) shows the variation of average power with pump power, and Figure 3.12 (b) shows the variation of pulse width and repetition rate with input pump power.

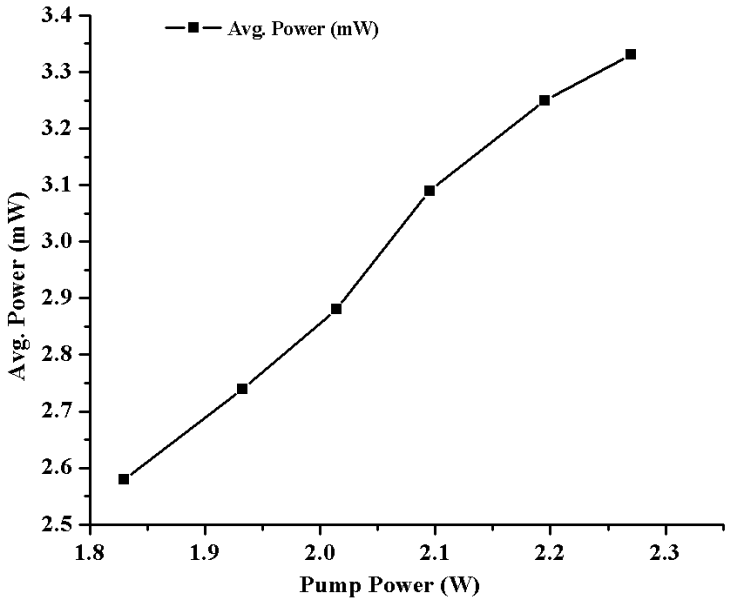

(a)

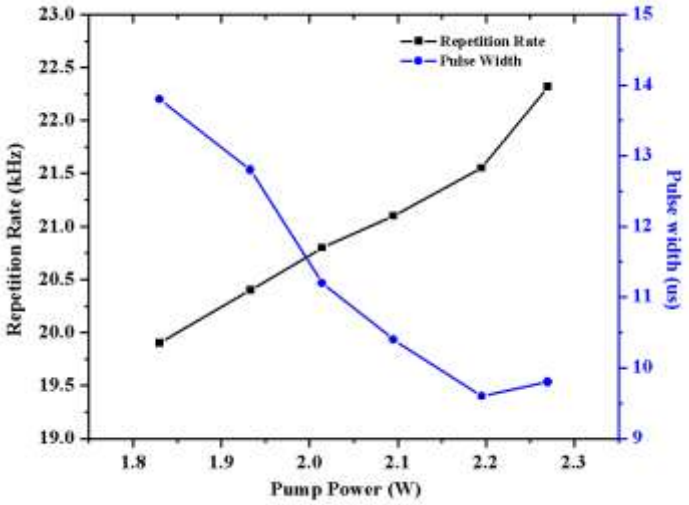

(b)

Figure 3.12: (a) Average power versus Pump Power and (b) Variation of the Pulse width and Repetition Rate with Pump power.

3.9 Background of the experiment

In the beginning, the experiment was performed with standard GNRs solution, which was added to the tip of the ferrule of a connector and used in the laser cavity once dried. It was observed that multiple drops were required to produce Q-switched pulses, but their width was much broader because of a smaller number of GNRs on the tip of the ferrule. The increase in modulation depth generally decreases the pulse width, as the pulse width is inversely related to the modulation depth shown in Equation 27. After repeated experiments, we concluded that a denser solution of GNRs is required, which is capable

of increasing light absorption, thus increasing the modulation depth. In a Q-switched fiber laser, pulse width and modulation depth are related according to equation 27 [104].

$$\tau_p = \frac{3.52\, T_r}{\Delta\alpha} \qquad [27]$$

Where τ_p is the pulse width, Tr is the cavity round trip time, and $\Delta\alpha$ is the modulation depth.

To determine the optimum concentration of the PVA solution, five concentrations were tested to obtain the pulsed laser with the desired width. The best results were obtained when 2 mg PVA was mixed with 100 µL deionized water. The viscosity of the PVA solution was very high at higher concentrations, so when the GNRs were mixed, they could not align with the incident beam of light.

The experiment was performed without using a SA in the cavity and with only a PVA solution, but no pulse was obtained, which confirms that the aqueous solution of GNRs and PVA is effective as an SA. Q-switched pulses appeared at 1567 nm once the SA was introduced in the cavity. Although the LSPR wavelength of the GNRs was 1400 nm, the GNRs solution had a wide absorption bandwidth (~ 380 nm @ 0.5 absorbance), as shown in Figure 3.4. One of the advantages of the aqueous solution of GNRs and PVA as a SA is that one can obtain a desired wavelength by adjusting the AR of GNRs, which is not possible for the generation of Q-switched pulses based on alcohol, deionized water, and pure water.

3.10 Conclusion

We have used GNRs with AR 10 as a SA to develop a laser at 1567 nm. The GNRs were mixed with PVA to increase their damage threshold and for uniform distribution. **The main contribution of this research work is using an aqueous solution of GNRs and PVA mixture as the SA**. Different concentrations of GNRs and PVA were used and optimized with experimentation.

We verified experimentally that the aqueous solution of GNRs and PVA can be used as a SA. Q-Switching operation was achieved with a minimum pulse width of 9.6 μs, maximum average power of 3.25 mW, and repetition rate of 21.5 kHz at 2.195 W pump power. The GNRs in the aqueous solution used as the SA were not damaged till 2.9 W of pump power. Stable laser operation was examined for four hours, indicating that the aqueous solution of GNRs and PVA could act as a SA.

The developed pulse laser can be used in gas spectroscopy, as this region is significant for many gases because their overtone and combination of overtone bands lie in this region. Also, this laser has potential application as a pump source to develop another laser in the 2.0-micron region because TDF has an absorption band in the 1550 nm region. Though this laser has low output power, but it can be enhanced using an amplifier.

Chapter 4

A dual-wavelength mode-locked fiber laser

In this chapter, we describe the development of a dual-wavelength mode-locked (ML) fiber laser at 1568 nm and 1608 nm. The laser wavelength was tuned by incorporating a fiber Bragg grating (FBG) in the cavity. We will discuss the pulse formation mechanism and how we achieve tunability. Depending on the cavity length and losses, the laser could generate Q-switched (QS) and mode-locked (ML) pulses at different wavelengths. Characteristics of QS and ML pulses based on pump power, cavity length, and losses were explored. The QS pulses were generated with a repetition rate of 22.73 kHz and a pulse width of 12.2 µs at a pump power of 3.1 W at 1608 nm for a 30 m long cavity. The laser produced 520 ns ML pulses at 1568 nm with a repetition rate of 877 kHz with an additional 200 m of single-mode fiber (SMF). Further, FBGs were used to tune the wavelength of the ML pulses from 1572 nm to 1578 nm.

4.1 Introduction

Precisely tunable fiber lasers operating in the pulsed regime in the near-infrared (NIR) and mid-infrared (mid-IR) regions of the electromagnetic spectrum, have applications in sensing, spectroscopy, optical communication, and biomedical research [105-107]. NIR lasers based on erbium-doped fiber (EDF) have been developed for applications in detecting trace gases, where the emission spectrum of EDF matches with the overtone rovibrational transition bands of gases of interest [108;109]. Moreover, the unique absorption properties of C_2H_2, CO, N_2O, and HCN gases can be utilized as a gain medium for developing mid-IR molecular gas lasers, where a NIR laser is used as a pump source [110;111].

A fiber laser is compact, cost-effective in manufacturing and most importantly, one can have an all-fiber design where alignment is not required. One can use active or passive Q-switching (QS) or mode-locking (ML) to produce a pulsed laser. Further, passive QS or ML can be achieved using a SA, which can be natural or artificial. Artificial saturable absorbers (ASA) attracted attention due to the lack of natural materials and the complicated manufacturing process of these materials. ASAs are not wavelength specific, have a high damage threshold, and can be used for extended periods [52]. Further, natural SAs have low damage threshold, which limits their use in practical implementation. However, they provide low cavity loss and can produce high-quality pulses.

Several ASA have been proposed and demonstrated to produce pulsed lasers, such as a mode-locked erbium-doped fiber laser using an air-gap etalon in the cavity [112] and

Er/Yb co-doped double-clad CW and ML fiber lasers above 1.6 μm based on linear loss control in the cavity [113]. Several mechanisms based on fiber nonlinearity and different configurations have been reported for generating QS and ML pulses, such as a nonlinear optical loop mirror (NOLM) [114] and nonlinear polarization rotation (NPR) [115]; Anjum et al. presented a reflection mode SA based on nonlinear multimode interference in a graded index multimode fiber to develop a laser at 1905 nm with stable mode-locked pulses [116]; Alamgir et al. reported a thulium-doped ML laser based on nonlinear polarization rotation [117]; and Li et al. reported a mode-locked Er-doped fiber laser based on nonlinear multimode interference using a single-mode fiber-graded index multimode fiber-single mode fiber (SMF-GIMF-SMF) structure as a saturable absorber [118]. So, by using different methods without incorporating any material based SA, QS or ML pulses can be generated.

In addition to the discussed mechanism, other reliable techniques for generating pulses are self-Q-switching and self-mode-locking, based on heavily doped active fiber which acts simultaneously as a gain medium and SA [119-121]. Zhang et al. reported a self-Q-switching and mode-locking in an all-fiber Er/Yb co-doped fiber ring laser. A section of un-pumped Er/Yb co-doped fiber was used as a SA. The laser was operating in a Q-switched regime at lower pump power and by incorporating the Mach-Zehnder interferometer the laser was made to operate in continuous wave mode-locking at high pump power [54]. Several reports have been published to generate ML pulses where a longer length of SMF was incorporated in the laser cavity. Zulkipli et al. reported generation of Q-switched pulses with the help of Eu_2O_3 as a SA. Still, no mode-locking was observed as cavity dispersion and nonlinearity need to be optimized for mode-

locking. Adding a SMF increases nonlinearity and enables the generation of stable mode-locked pulses [122]. Similarly, Najm et al. reported that Q-switched pulses were generated by incorporating a SA (8-HQCdCl$_2$H$_2$O-PVA thin film), but mode-locking was achieved with an additional 200 m SMF, which optimized the nonlinearity and cavity dispersion [123].

Several techniques have been proposed and demonstrated for developing tunable pulsed a lasers using a bandpass filter [124], chirped fiber Bragg grating [125], long-period fiber grating [126], Sagnac filters [127], and tunable fiber Bragg grating [128]. However, a tunable fiber Bragg grating (FBG) filter is attractive as it is compact and has low insertion loss.

This research work generated Q-switched pulses using the Er/Yb co-doped fiber as a gain medium. At lower pump power, the unpumped section of the gain medium acted as a SA, which was reflected in the pulse shape. The laser switched to ML regime once a SMF with 200 m length was incorporated in the cavity. Behavior of ML pulses with three different lengths of SMFs were examined. The gain medium, an extended length of SMF, and high pump power produced the necessary balance between non-linear phase shift and dispersion. The laser cavity contains a free-space (air gap) module formed by two collimators that switch the wavelength operation. Further, the laser was tuned by incorporating a FBG in the cavity.

4.2 Experimental setup

The schematic of the laser is shown in Figure 4.1 (a). A double-clad Erbium/ytterbium co-doped fiber (EYDF: DC-EY-12/130, CorActive, absorption 22.2 dB/m at 976 nm) of

length, NA, and core/cladding diameter of 6m, 0.21 and 11.86/130 μm, respectively, with hexagonal cladding structure was used as the gain medium. A pigtailed multimode laser diode which can produce a maximum output power of 9 W at 976 nm, was used as a pump source for the gain fiber through a multimode fused fiber coupler (6+1x1). The multimode fused fiber coupler acted as a 976/1550 nm wavelength division multiplexing (WDM) coupler. A Fabry-Perot cavity was formed with the help of two polarization-independent circulators (CIR). CIR1 acts as a broadband reflector. CIR 2 forms a ring cavity consisting of a free space module made of two collimators mounted on three axes translational stages, single mode fiber (SMF), an all-fiber polarization controller (PC), and a 10% fused fiber coupler (FFC) to obtain the output of the laser. The 10% output was fed into a 2% FFC, and output was monitored using an optical spectrum analyzer (OSA, Anritsu MS9740 A) with a resolution of 0.03 nm and a power meter (FOT-90A) and 98% port was connected to a digital oscilloscope (TDS 7104, 1 GHz) through a high-speed photodetector (5 GHz InGaAs Photodiode, DET08CFC/M, Thorlabs). Initial experiments were performed without SMF, and the cavity length was approximately 30 m.

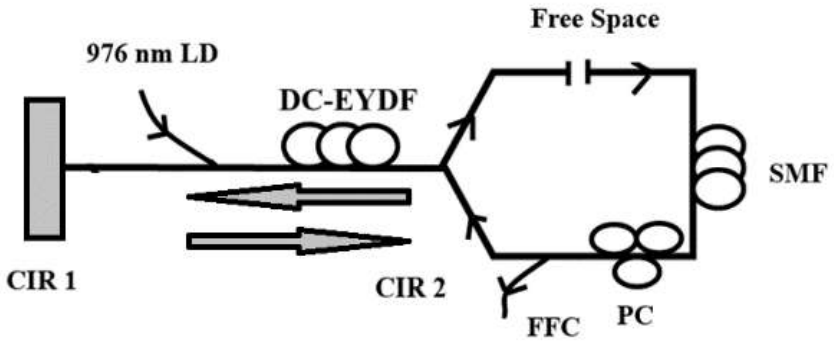

(a)

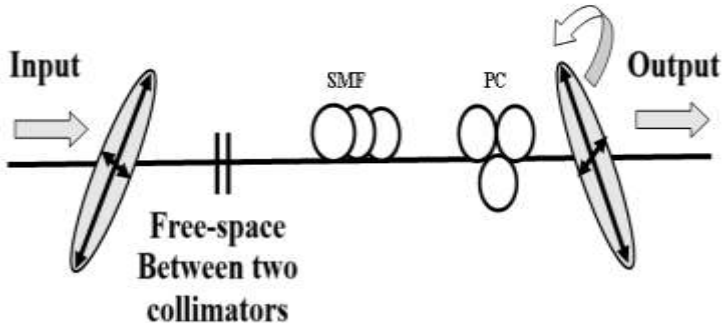

(b)

Figure 4.1: (a) Schematic of the Laser, where CIR1 and CIR 2 – Polarization-independent circulators, PC – Polarization controller, EYDF – Erbium-Ytterbium co-doped fiber, SMF – Single-mode fiber, FFC – 10% fused fiber coupler, and (b) optical components in the ring cavity formed by CIR 2.

Figure 4.1 (b) shows the components inside the ring cavity formed by CIR 2. A PC in the laser cavity was used to control the polarization state of light. Most notably, with proper adjustment of PC plates, one can obtain intensity-dependent cavity losses that favor the switchability of wavelength and help in self-started mode-locking [129]. In this configuration, the PC inside the cavity can change the ellipticity and rotate the polarization state of light when PC plates are adjusted. Further, elliptically polarized light enters the free space module via CIR 2, propagates through the SMF and passes through the PC.

4.3 Results and Discussion

Initially, the experiment was performed without additional SMF when the cavity length was approximately 30 m, which produced laser light at 1568 nm and 1608 nm. Figure 4.2

(a) shows the laser at 1608 nm when the cavity loss was minimum (maximum alignment of free space module), and with higher losses the cavity produced laser at 1568 nm (Figure 4.2 (b)). We could generate both wavelengths when the cavity loss was balanced, as shown in Figure 4.2 (c). We could switch wavelengths from 1568 nm to 1608 nm with the help of a free space module or by adjusting the cavity losses [113].

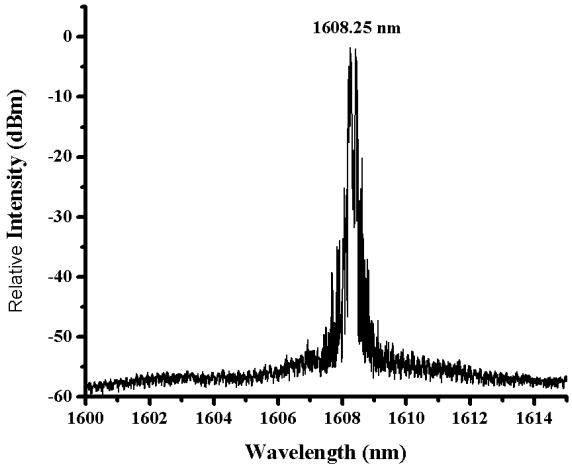

(a)

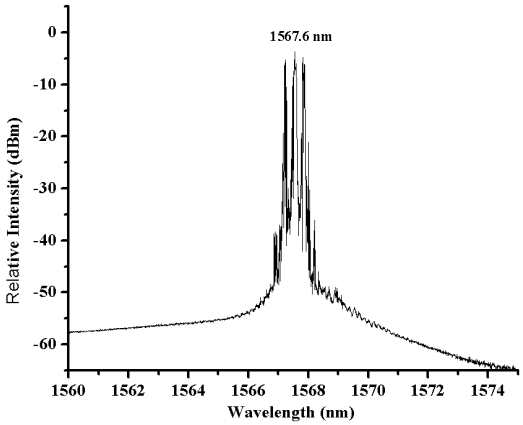

(b)

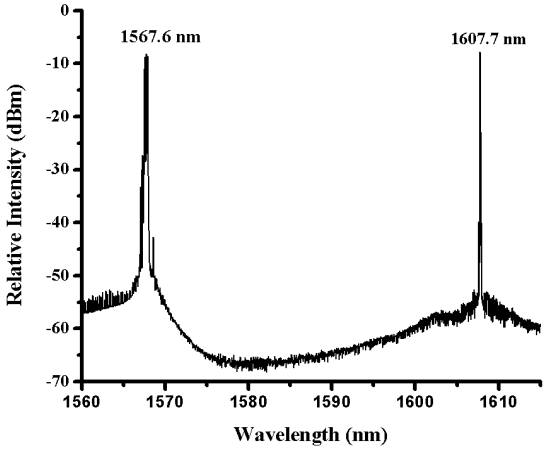

(c)

Figure 4.2: The output of laser obtained with an OSA, (a) at 1608 nm, (b) at 1568 nm, and (c) at both wavelengths 1568 and 1608 nm.

The laser could generate QS pulses at 1608 nm, but getting them at 1568 nm was impossible. These pulses had a pulse width of 12.2 μs and a repetition rate of 22.73 kHz and were generated at 3.1 W pump power. It was observed that pulse characteristics changed with pump power but for stability the loss was adjusted at each level. Because of that, we couldn't get the exact behavior of pulses. QS pulses stayed up to a pump power of 5 W, but no mode-locked operation was obtained even when the PC plates were adjusted in each possible manner. In addition, the free space module was adjusted from minimum to maximum alignment, but no mode-locking was observed. Figure 4.3 shows the generated QS pulses at 3.1 W without SMF at 1608 nm.

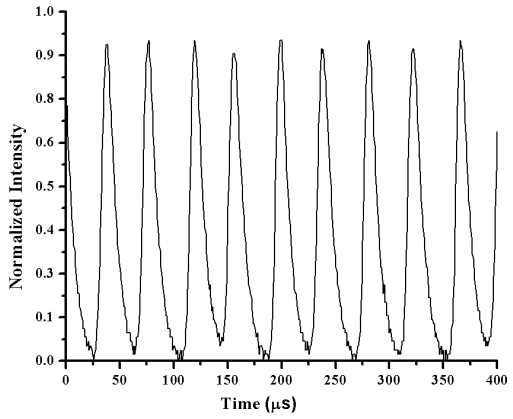

Figure 4.3: Q-switched pulses at 1608 nm at 3.1 W pump power.

With this configuration, it was not possible to generate mode-locked pulses, so a segment of SMF was added in the cavity as it was already proven that an extended length of SMF provides nonlinearity, which initiates the SPM required for the mode-locking phenomenon [130;131]. We examined this configuration with 50 m, 100 m, and 200 m SMF.

With 50 m SMF, Q-switched pulses were produced at 1608 nm with a pulse width of 24.4 μs and repetition rate of 12.76 kHz as shown in Figure 4.4 (a) but in this case mode-locked pulses were also obtained at 1568 nm with lots of adjustment in PC plates and free space module (Figure 4.4 (b)). Although, the quality of ML pulses was not very good, it still signifies that with the proper length of SMF good mode-locked pulses can be generated. Generated mode-locked pulses had a pulse width of 184 ns and repetition rate of 2.51 MHz (Figure 4.4 (b)).

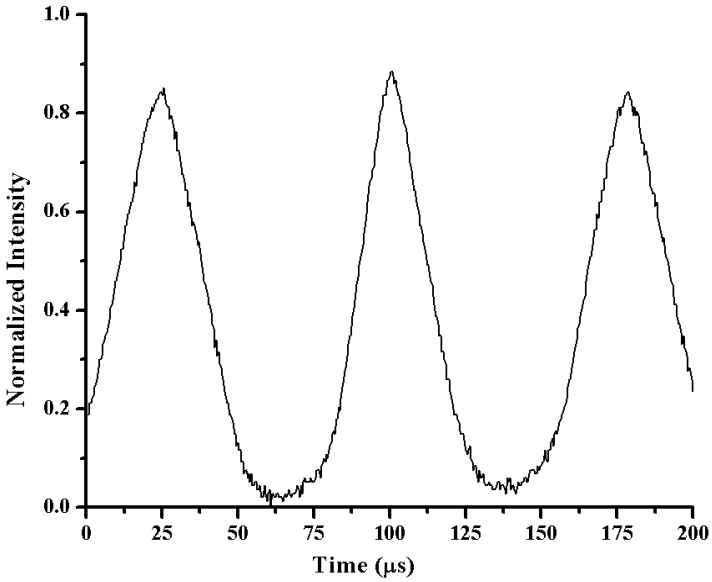

(a)

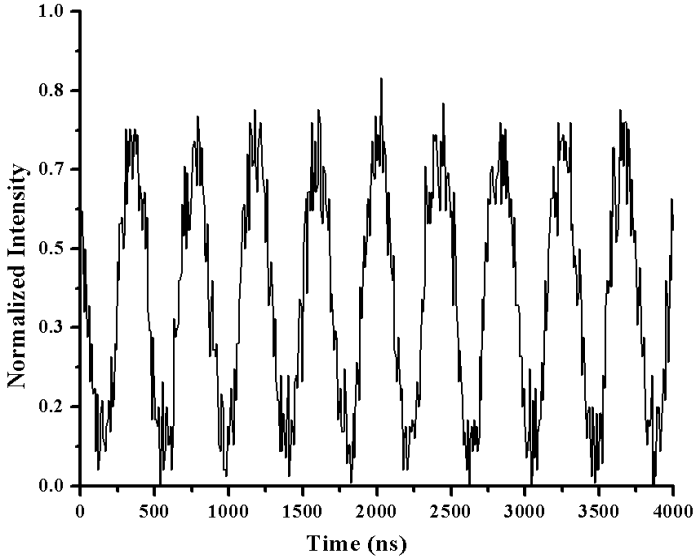

(b)

Figure 4.4: Output of the laser at 3.1 W pump power (a) QS Pulses at 1608 nm and (b) ML Pulses at 1568 nm.

With 100 m SMF, Q-switched pulses were produced at 1608 nm with a pulse width of 24.8 μs and repetition rate of 12.38 kHz as shown in Figure 4.5 (a). It was not like the case in no SMF, where Q-switched pulses were obtained by themselves without adjusting PC plates and the free space module, here we needed to adjust these parameters for the stability of pulses. Also, mode-locked pulses were generated at 1568 nm which were more stable than the previous case (50 m SMF). Pulses had a pulse width of 310 ns and a repetition rate of 1.613 MHz, as shown in Figure 4.5 (b). The QS pulses were always generated at 1608 nm when loss in the cavity was minimal. The low loss in the cavity allows more 1550 nm band emission to propagate through the gain fiber, which after re-absorption produces emission at the L-band region. It is likely that not all erbium ions absorb the C-band light and emit in the L-band or we can say that some ions remain unsaturated and act as a SA. Further, the asymmetric shape of the QS pulses with fast rise time and slower decay time is also attributed to the saturable absorption phenomenon.

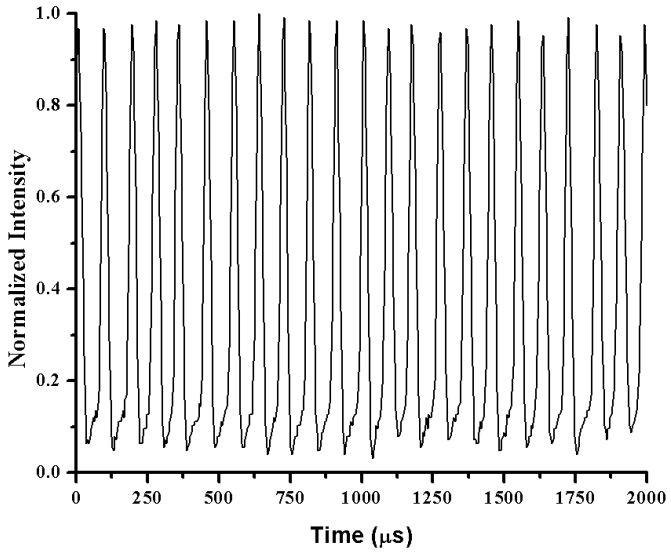

(a)

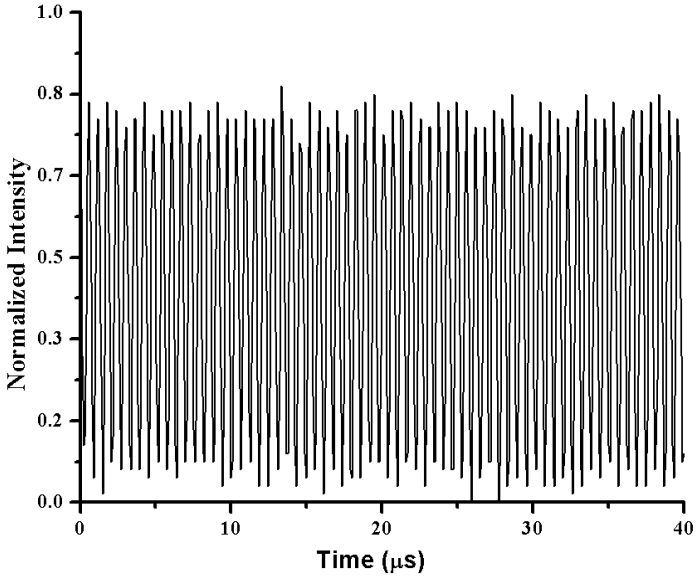

(b)

Figure 4.5: Output of laser at 3.0 W pump power (a) Q-switched pulses at 1608 nm (b) ML pulses at 1568 nm.

With 200 m SMF, mode-locked pulses were generated at both the 1568 nm and 1608 nm wavelengths. The threshold current for mode-locked pulses was 1.9 A (1.12 W). The stability of pulses was different at both wavelengths and dependent on pump power. Most stable ML pulses, as shown in Figure 4.6, were obtained at 1568 nm at 4 A (3.1 W) pump current with pulse width, repetition rate, average output power, and pulse energy of 520 ns, 877 kHz, 2.15 mW, and 2.45 nJ. The length of the laser cavity was approximately 230 m corresponding to longitudinal mode spacing of 893 kHz. There was some mismatch in the experimental value of central frequency and theoretical value, it may be due to a discrepancy in the measurement of the length of the fiber. With increasing cavity loss laser wavelength could switch from 1608 nm to 1568 nm.

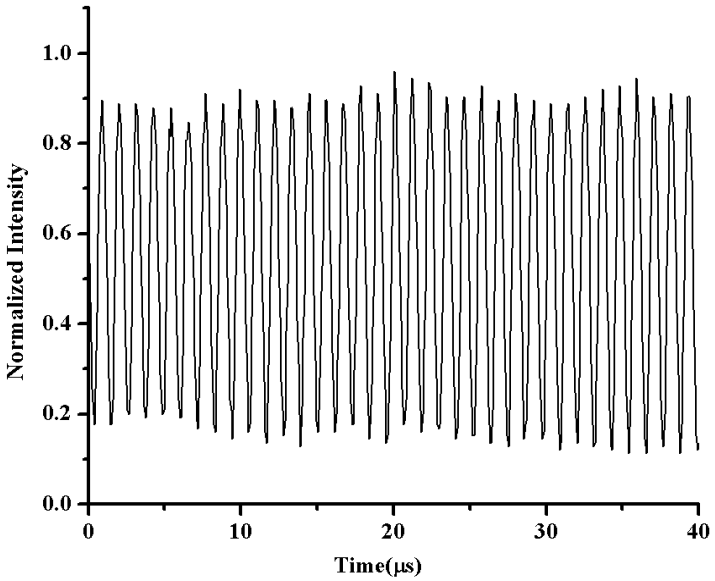

Figure 4.6: Mode-locked pulses at 1568 nm.

The stability of pulses was determined using an RF spectrum analyzer, and the temporal profile of pulses was observed on an oscilloscope. Figure 4.7 shows the RF spectrum of generated ML pulses with a signal-to-noise ratio (SNR) of 50 dB and a repetition rate of 877 kHz. It matched the repetition rate obtained using an oscilloscope. With these experiments, it was observed that an optimized length of SMF was needed to generate stable ML pulses. The stability of pulses changed with different lengths of SMF. Stable ML pulses were generated in the case of 200 m SMF, where the length of SMF was enough to generate nonlinearity, which initiates SPM to produce mode-locked pulses. The SPM arises due to Kerr nonlinearity. The total group velocity dispersion occurs in the laser cavity due to the gain fiber (23 ps/nm.km at 1550 nm) and the SMF (18 ps/nm.km at 1550 nm) that balances the nonlinear phase change in the cavity. Longer length of SMF increased the nonlinearity in the cavity.

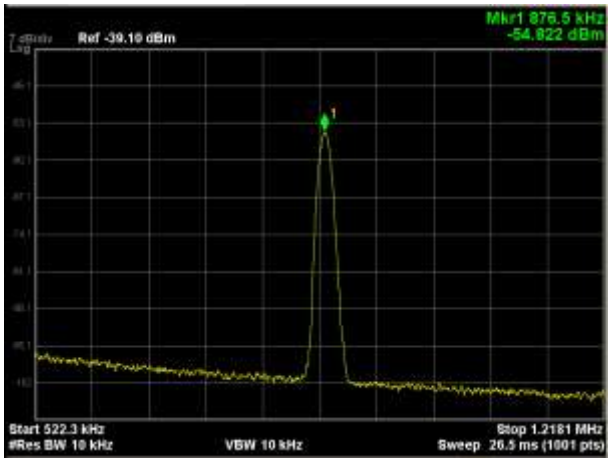

Figure 4.7: RF spectrum of laser obtained at pump current 4A (3.1 W).

Usually, a starting trigger is needed to initiate the formation of pulses, which includes active mode lockers or physical knocks [132;133], but in this work, that initial trigger was not required. The free space module was adjusted to switch the operation wavelength [55].

In this laser configuration, a free space module was used as a loss mechanism to confirm whether this loss was controlling the behavior of pulses. We replaced the free space module with a digital variable attenuator, where the attenuation varied from 0.857 dB to 3 dB, output was identical to the free space component. Another experiment was done by replacing the free space module with two FC/PC connectors connected by a sleeve, where the separation of the ferrule tips was adjusted to change the insertion loss. In both cases, it produced output identical to that of the free space module. We could operate the laser in QS or ML at 1608 nm or 1568 nm by adjusting the linear loss introduced by the free space module, attenuator, or FC/PC connectors and finely adjusting the polarization controller plates.

4.4 Wavelength Tunability

Another advantage of the developed laser is its tunability, where the peak wavelength of the laser can be tuned over a wide range using a fiber Bragg grating (FBG) as shown in Figure 4.8. The tunability was approximately 7 nm at the same pump power. The polarization controller was kept at the same position for studying wavelength tunability. Initially, the experiment was performed with tunable FBG with a center wavelength of 1570.027 nm, Reflectivity of 98.4%, and 3dB bandwidth of 0.220 nm) as a wavelength selector. The laser-produced ML pulses at different wavelengths are shown in Figure 4.9.

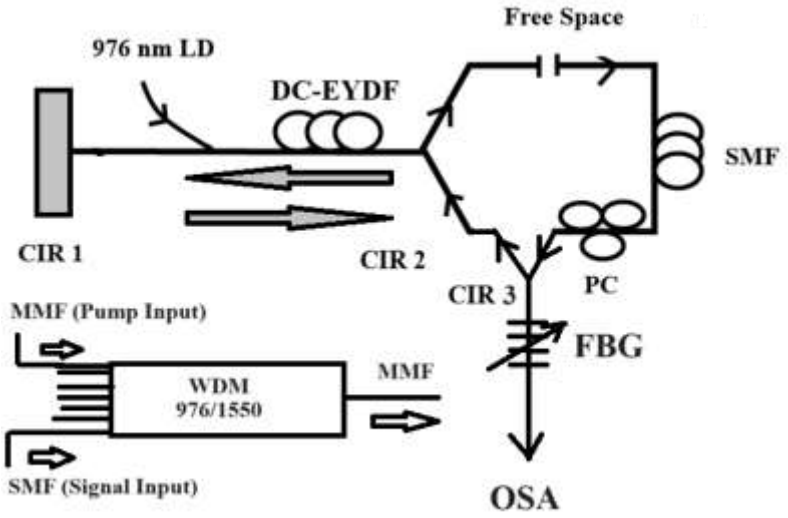

Figure 4.8: Schematic of experimental setup.

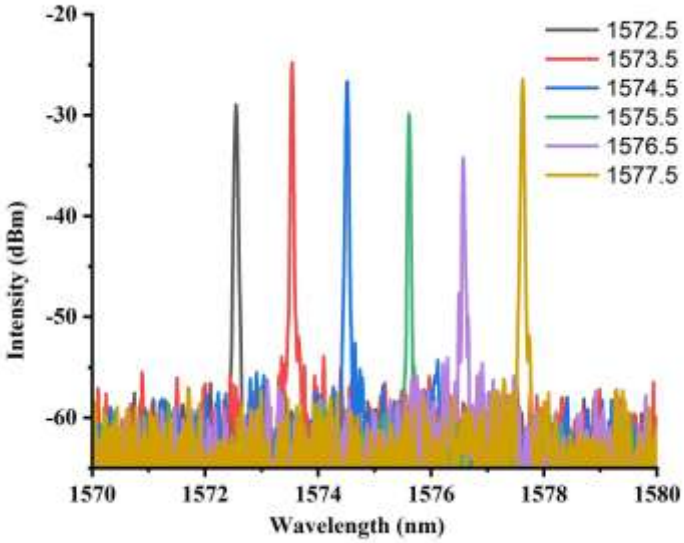

Figure 4.9: Output of tunable mode-locked laser obtained using an OSA at different wavelengths.

At each wavelength, the free space module was adjusted to improve the stability of pulses. This was also one reason behind the different output power at each wavelength. Besides this, the non-uniformity of the ASE spectrum of DC-EYDF was responsible for different average power at different wavelengths. In addition, ML pulses had different characteristics at each wavelength. Figure 4.10 shows ML pulses at 1572.5 nm with a pulse width of 464 ns and a repetition rate of 856.6 kHz (Figure 4.10 (a)) and at 1577.5 nm with a pulse width of 513 ns and a repetition rate of 856.8 kHz (Figure 4.10 (b)), respectively. The pulse width variation is due to higher group velocity dispersion at longer wavelengths. Also, the presence of an extended length of SMF induced nonlinear birefringence in the cavity and contributed in the formation of such large mode-locked pulses [123;130].

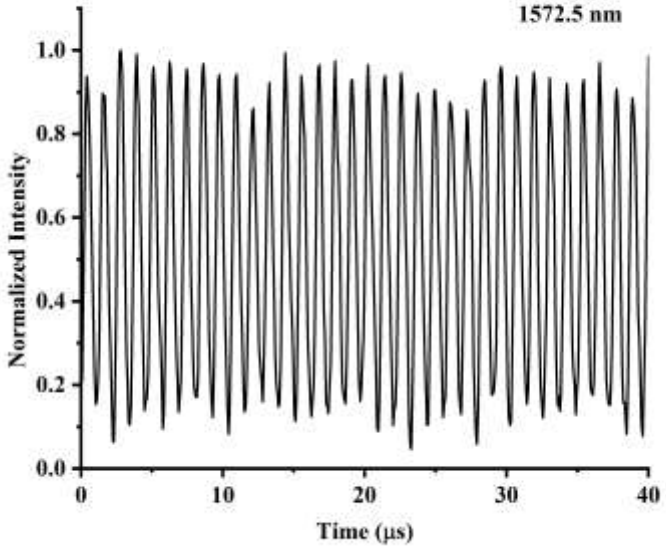

(a)

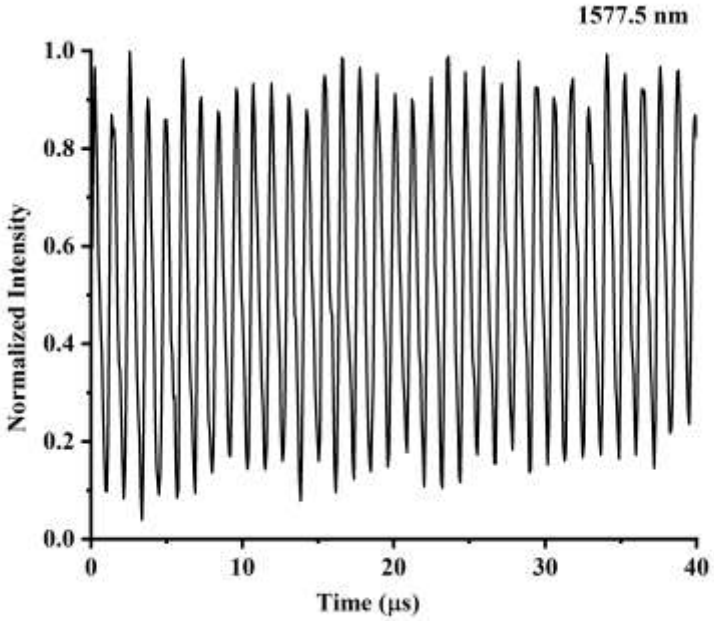

(b)

Figure 4.10: The temporal profile of mode-locked pulses measured by an oscilloscope (a) at 1572.5 nm and (b) at 1577.5 nm.

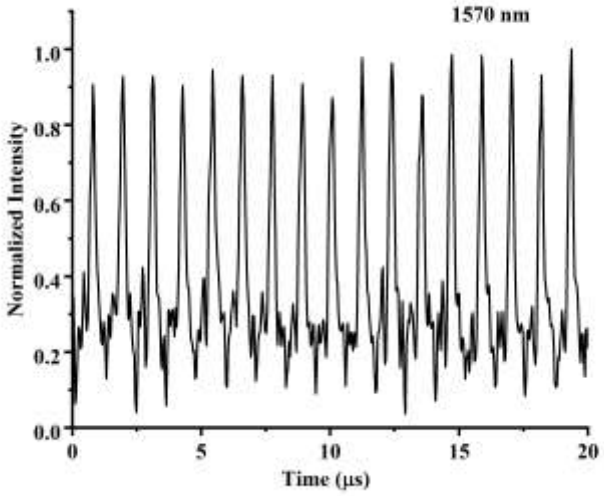

(a)

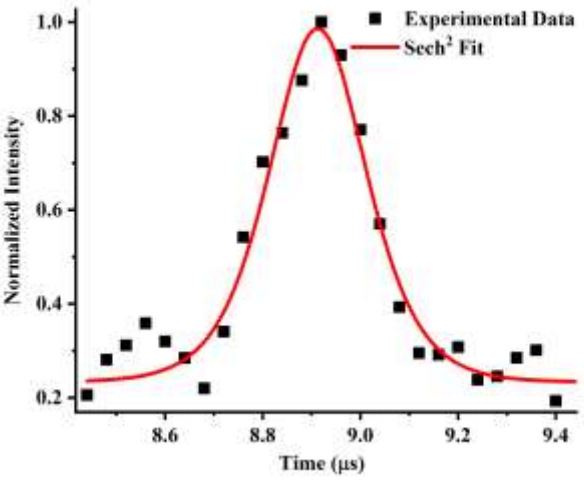

(b)

Figure 4.11: Temporal characteristics of mode-locked pulses obtained using an oscilloscope (a) 20 μs scale (b) single pulse profile.

However, the research objective was to generate a pulsed laser at 1570 nm for its possible application as a pump source for developing a mid-infrared laser (Mid-IR). The tunable FBG was replaced with single wavelength FBG with center wavelength,

reflectivity, and bandwidth of 1570 nm, 91.03%, and 0.172 nm, respectively. Figure 4.11 (a) shows the ML pulse train on 20 μs scale, and (b) shows the single pulse profile, experimental data is shown in black dots, and the red line shows hyperbolic secant fitted pulse output, which confirms that the generated pulses resemble optical solitons.

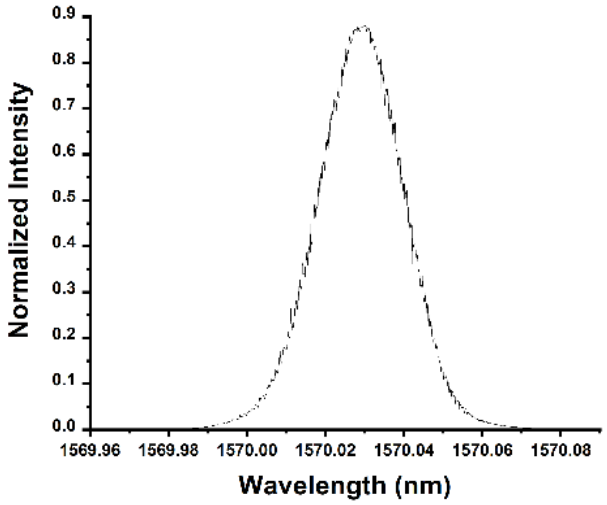

(a)

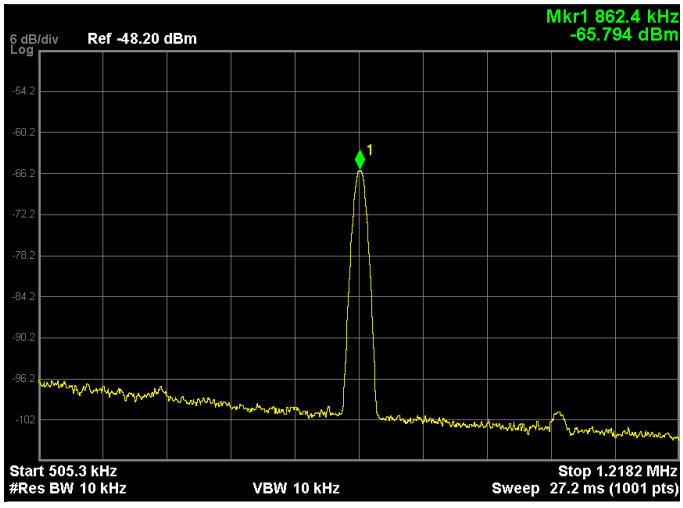

(b)

Figure 4.12: Output of the Laser obtained using an (a) OSA (b) RF Spectrum Analyzer.

Figure 4.12 (a) shows a spectrum of laser obtained with an OSA, and (b) shows the RF spectrum with a fundamental frequency of 862.4 kHz.

The generated pulses had pulse width, repetition rate, output power, and pulse energy of 240 ns, 862 kHz, 5.76 mW and 6.68 nJ at 3.5 W pump power. A signal-to-noise ratio (SNR) of approximately 40 dB was observed, indicating stable pulses. The fundamental frequency of 862.4 kHz was observed with a RF spectrum analyzer, matched with the repetition rate obtained using an oscilloscope, and the theoretical values obtained using the length of the laser cavity. Without FBG, the laser could generate ML pulses at 1568 and 1608 nm.

The novelty of the proposed design is **(1)** we could obtain a switchable dual-wavelength pulsed laser by varying the cavity loss using the free space module either in a Q-switched or mode-locked regime; **(2)** We could insert any natural saturable absorber (e.g., gold nanorods) in the free space to obtain a mode-locked laser at a desired wavelength, and **(3)** With the help of tunable FBG in the cavity, we could obtain mode-locked pulses at different wavelengths. It is to be noted that by removing the free space module, the output power can be increased, but no significant change was observed in the stability of laser.

4.5 Conclusion

A dual-wavelength pulsed laser at 1568 nm and 1608 nm was developed using gain fiber as a SA and SPM. Wavelength was switched with the losses provided using a free space module. Laser produced QS and ML pulses and the operating regime was switched with

the incorporation of SMF in the cavity. The quality of the QS pulses was good compared to ML pulses, as no element was included in the cavity that could improve pulse quality. The laser was tuned using FBG, and mode-locked pulses were generated at each wavelength. The output power of the laser was low, which is a disadvantage, as we need a high-power laser at 1570 nm to be used as a pump source for generating a mid-IR laser in the 1.8 μm to 2 μm region. The output power of the laser slightly increased when the free space module was removed by splicing SMFs, but it was not enough for our application, which led to the development of a modified cavity for the generation of a high-power pulsed laser.

Chapter 5

Generation of pulsed laser at 1570 nm and 1533 nm

This chapter presents a high-power self-Q-switched mode-locked fiber laser at 1570 nm. A double-clad Erbium-Ytterbium co-doped fiber (DC-EYDF) was used as a gain medium. The gain fiber acted as a saturable absorber (SA) and produced mode-locked pulses at high-pump power. The cavity design was optimized to increase the power and quality of pulses. Stable Q-switched pulses with a minimum width of 4.2 μs and maximum repetition rate of 25 kHz and mode-locked pulses with a minimum width of 340 ps and repetition rate of 6.57 MHz were obtained. The Mode-locked pulses had a pulse energy of 24 nJ and a peak power of 72 W. The developed laser was used as a pump source for developing a thulium-doped fiber laser. It can be used as the pump source for developing a molecular laser based on carbon monoxide.

Further, this chapter describes the development of a pulsed laser at 1533 nm, which will be used as the pump source for the molecular laser using acetylene gas as the gain medium.

5.1 Introduction

High-power pulsed lasers are in demand due to their applications in medicine, remote sensing, optical communications and mid-IR wavelength generation. As discussed in Sections 2.5 and 2.6, pulsed lasers can be developed following different techniques, such as Q-switching and mode-locking [69;134]. Besides these, other mechanisms have also been explored for generating pulses, such as self-Q-switching (SQS), self-mode-locking (SML), and self-Q-switching mode-locking (SQS-ML) [119;135-137]. Researchers often focus on finding the different phenomena responsible for generating pulses without incorporating any modulator in the cavity, which has several advantages such as no limitation on the damage threshold of the SA, and no need of alignment. A heavily doped silica fiber as a gain medium or an un-pumped section of a gain fiber have been identified and implemented to develop pulsed lasers (e.g., SQS, SQS-ML). It was found that gain fiber can act as a SA at lower pump power, due to the un-pumped portion of the doped fiber. The inhomogeneous absorption along the fiber arises due to a quenching effect (process of dissipating energy stored in excited state due to non-radiative process) between energy levels formed by active ion pairs or clusters, resonant-energy transfer between two ions at the close proximity and excited state absorption [138-140]. Further, it was reported that based on the pumping condition a heavily doped fiber has the ability to generate pulses in different regimes. For example, at low pump power, DC-EYDF can act as a SA and generate SQS pulses, which originate from the relaxation oscillation due to Er ion pairs in highly doped gain fibers. With increasing pump power, the gain along the length of active fiber becomes more uniform than that at lower pump power, which

eliminates relaxation oscillation and makes SQS pulses disappear at high pump power [136].

In 1993, Myslinski et al. reported Self-mode-locking in a Q-switched fiber laser, which is due to mode-beats between axial modes of the laser cavity at lower pump power, and with increasing pump-power SPM supports further mode coupling and sustain mode-locking. Further, longitudinal mode coupling occurs due to the broadening of pulses by SPM and forces SML operation [141].

In 2004, Cruz Vicente et al. reported a diode-pumped SQS erbium-doped all-fiber laser. They explained the physical mechanism of self-Q-switching based on excited-state absorption (ESA) in erbium-doped fiber, which resulted in a thermally induced nonlinear change in refractive index in the erbium-doped fiber [142].

In 2006, Zhang et al. reported a Self-Q-switching and mode-locking in an all-fiber Er/Yb co-doped fiber ring laser based on an un-pumped section of gain fiber as a SA. Different thresholds were observed for SQS and self-mode-locking. The laser was converted into a CW mode-locked laser by incorporating a Mach-Zehnder interferometer in the cavity [54].

In 2010, Upadhyaya et al. reported that self-pulsing can be initiated by relaxation oscillations and saturable absorption along a weakly pumped portion of the doped fiber at low pump power without getting affected by the length of the gain fiber. However, at high pump power, pulses are generated either because of stimulated Raman scattering (SRS) or stimulated Brillouin scattering (SBS) and also depends on the gain fiber length. They briefly describe the process of suppressing relaxation oscillations with the help of a

passive fiber and pump power [143]. After a thorough investigation, researchers found all the possible mechanisms responsible for generating SQS and SML pulses in rare earth doped fiber lasers.

In 2014, Liu et al. reported SML operation in a thulium-doped fiber laser, where ML pulses were generated without a mode-locker. The ML pulses were generated based on SPM and weak saturable absorption effect in a heavily doped TDF [144].

In 2018, Ibarra-Escamilla et al. reported a Self-Q-Switch and CW Operation of a Tunable Dual-Wavelength Er/Yb Double-Clad Fiber Laser based on saturation effect in a weakly pumped section of Er/Yb DCF due to formation of the Er ion pairs. The Laser was in SQS regime at low pump power and became CW at high pump power. They obtained dual-wavelength by adjusting intracavity losses using a fiber optical loop mirror with high birefringence fiber in the loop [145].

Although a lot of literature is available for understanding the mechanism of self-mode-locking, it was still limited to qualitative analysis only. In 2023, Zeng et al. quantitatively analyzed the generation and working principle of SML lasers. Their investigation focuses on the effect of gain saturation energy, polarization property of the circulating waves, and the effect of dispersion. They found, in the case of normal dispersion, the threshold is much lower as compared to the case of anomalous dispersion but more sensitive towards polarization properties. They briefly explained the effect of ion concentration on the operating regime and the quenching effect responsible for generating pulses [146].

Many fiber lasers have been reported based on single-clad erbium-doped fibers pumped with a single-mode diode laser in core pumping techniques. However, the output power of the laser was very low for practical applications where high power is required. For high power pulses, specifically high peak power pulses in the 1.55 μm region, DC-EYDF as a gain medium is preferred over EDF. DC-EYDF has high absorption at 976 nm, as Yb ions absorb the pump energy and transfer non-radioactively to Er ions [147;148]. Thus DC-EYDF became a good choice due to its excellent power scalability for generating high-power pulsed lasers. In Chapter 2 we discussed in detail the characteristics of DC-EYDF.

In this chapter, we presented a high-power ML laser at 1570 nm in a linear cavity configuration based on self-Q-switching and mode-locking techniques. The design is unique and novel as no mode-locker was required to develop the laser. A DC-EYDF was used as a gain medium. We investigated laser operating regimes and temporal characteristics of pulses at different pump power levels. We observed Q-switched mode-locked pulses at low pump power, and mode-locked pulses were generated when the pump power was 694 mW. However, the laser operated in a ML regime above this pump power, which is attributed to the weak saturable absorption and SPM effect. The developed laser will find many applications. We reported application of the laser as a pump source to develop a TDF laser at 1925 nm with lower threshold. We also showed the application of the developed 1925 nm laser for detecting carbon dioxide in the atmosphere.

5.2 Experimental setup

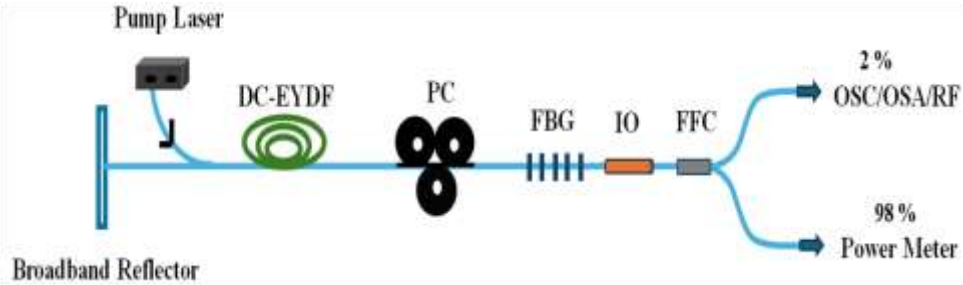

Figure 5.1: Schematic of the experimental setup.

Figure 5.1 is the schematic of the laser. A broadband reflector, which was formed using an all-fiber polarization-independent three port circulator (CIR), and a fiber Bragg grating (FBG), with Peak wavelength, reflectivity, and bandwidth of 1570.00 nm, 40%, and 0.2 nm, respectively, formed a Fabry-Perot cavity. The length of the cavity was approximately 15.5 m. A DC-EYDF (DC-EY-10/128-20-01, CorActive) of length, absorptions at 915 nm and 1535 nm, and NA of 4 m, 1.7 dB/m and 76.1 dB/m, and 0.2, respectively were used as a gain medium, which was pumped by a multimode diode laser at 976 nm through a multimode fused fiber coupler (6+1x1), that acted as a 1550/976 nm wavelength division multiplexing (WDM) coupler. The maximum output power of the pump laser was 2.6 W. An all-fiber polarization controller (PC) was used in the cavity to control the polarization state of the circulating wave. The laser output was connected to a polarization-independent optical isolator (IO), which eliminated any back reflection. A 2% fused fiber coupler (FFC) was used to monitor the output of the laser. The 2% output of the FFC was fed into a 10 GHz photodetector (818-BB-51F, rise time < 25 ps, Newport), and the temporal characteristics of the laser were obtained using a 10 GHz Oscilloscope (MS068B, Tektronix). The oscilloscope also provided the real-time RF

spectrum of the pulses. An Optical Spectrum Analyzer (OSA, MS9740S, Anritsu) was used to obtain the laser spectrum. The 98% output of the FFC was connected to a power meter (FOT 90A, EXFO) to obtain the output power.

5.3 Results and Discussion

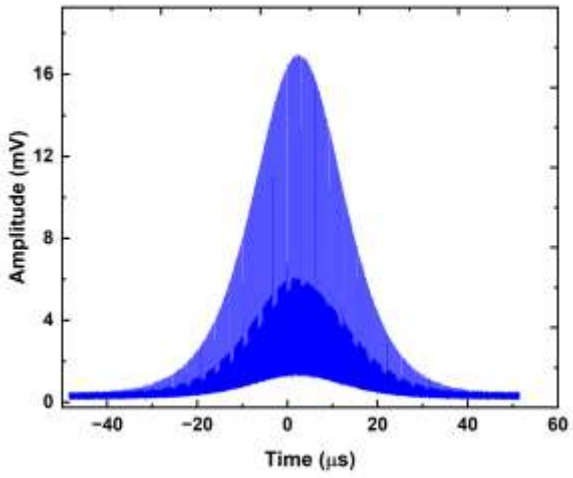

(a)

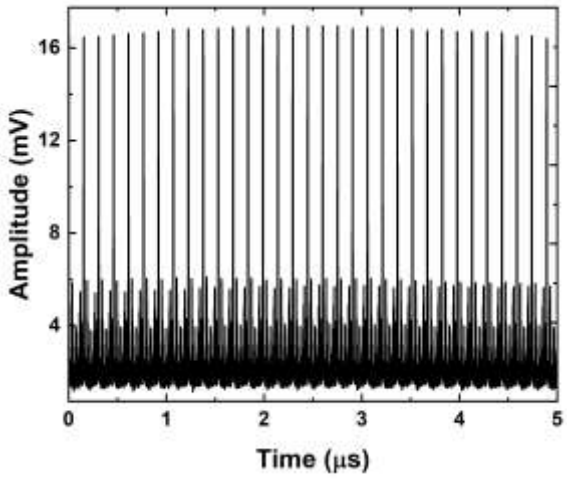

(b)

Figure 5.2: Temporal profile of (a) Single SQS and (b) SML pulses at threshold (205 mW).

Figure 5.2 shows a single SQS and SML pulse, when the pump power reaches the threshold value of 205 mW. We observed the SQS and SML pulses simultaneously at low pump power, where SML pulses were visible inside the SQS envelope. At threshold, the SQS pulse repetition rate and width were 3.25 kHz and 29.8 μs, respectively (Figure 5.2 (a)). Figure 5.2 (b) shows the ML pulses (zoomed portion from Figure 5.2 (a)) with a pulse width of 1.6 ns and a repetition rate of 6.57 MHz, which matched the fundamental frequency supported by the cavity. At high pump power (~ 695 mW), the SQS pulses disappeared, and the laser operated in the SML regime.

Figure 5.3 shows the laser output at different pump power till 695 mW, beyond this power the laser switched to a ML laser. Further, the pulse width decreases, and the repetition rate increases with increasing pump power. We varied the pump power from 281 mW to 694 mW, and the corresponding repetition rate changed from 7.86 kHz to 24.42 kHz, and the pulse width decreased from 11.7 μs to 4.61 μs. Once the pump power reached 695 mW, the pulse profile started changing, as shown in Figure 5.3 (c), and completely switched to a mode-locked regime beyond this pump power level.

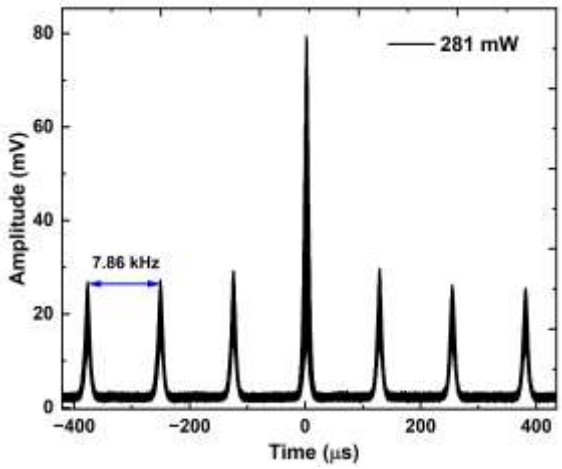

(a)

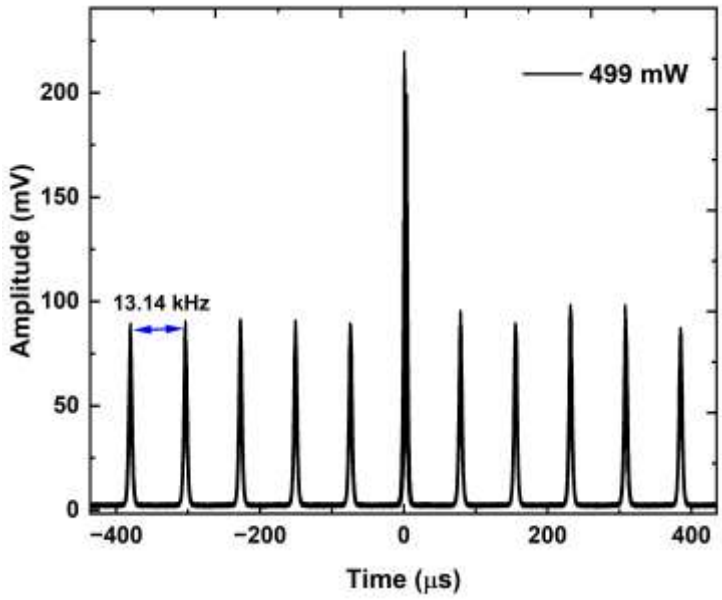

(b)

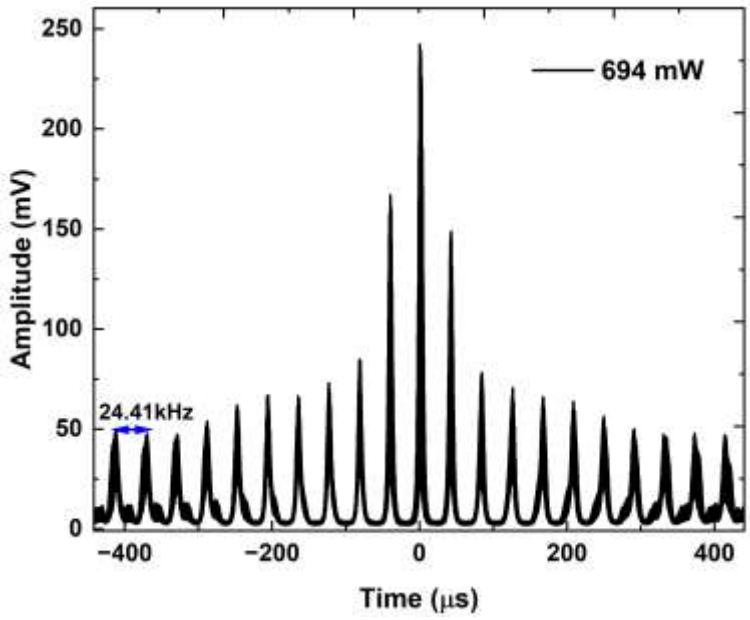

(c)

Figure 5.3: Temporal profile of SQS pulses obtained at different pump powers obtained with an Oscilloscope (a) at 281 mW, (b) at 499 mW, (c) at 694 mW.

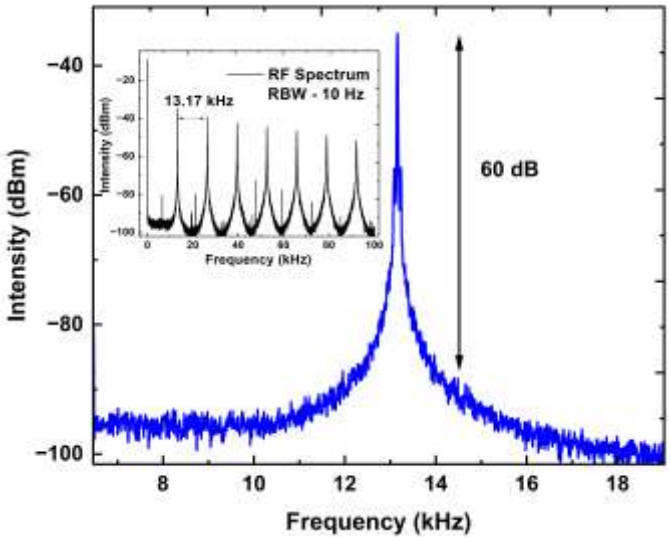

Figure 5.4: RF spectra at 499 mW pump power.

Figure 5.4 shows the RF spectra of SQS pulses. The Inset shows the spectra observed for SQS pulses over the 100 kHz range with a frequency spacing of 13.17 kHz, obtained with a resolution bandwidth of 10 Hz for the RF analyzer at 499 mW pump power. The SNR was approximately 60 dB, confirming the high stability of the pulses. The frequency spacing matched that obtained from the oscilloscope data, as shown in Figure 5.3 (b).

Figure 5.5 shows the SML pulses at a pump power of 2.4 W. Figure 5.5 (a) shows the ML pulses in a 4 μs time scale. Pulses were highly stable and the amplitude was almost uniform**.** The repetition rate was 6.57 MHz and remained constant throughout the experiment. Figure 5.5 (b) shows a single-pulse profile of SML pulses obtained using an oscilloscope, and the pulse width was 340 ps**.** However, based on the theoretical calculation, it seems pulse width is in the femtosecond order [135]. Figure 5.5 (c) shows

the RF spectra of SML pulses with SNR more than 60 dB for a resolution bandwidth of 500 Hz in a range of 500 MHz, confirming the high stability of laser.

ML pulses were obtained up to a maximum available pump power of 2.6 W. Stability was same at each pump power.

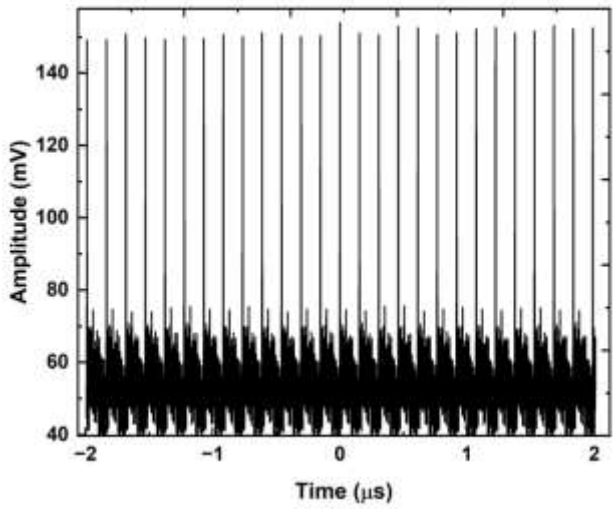

(a)

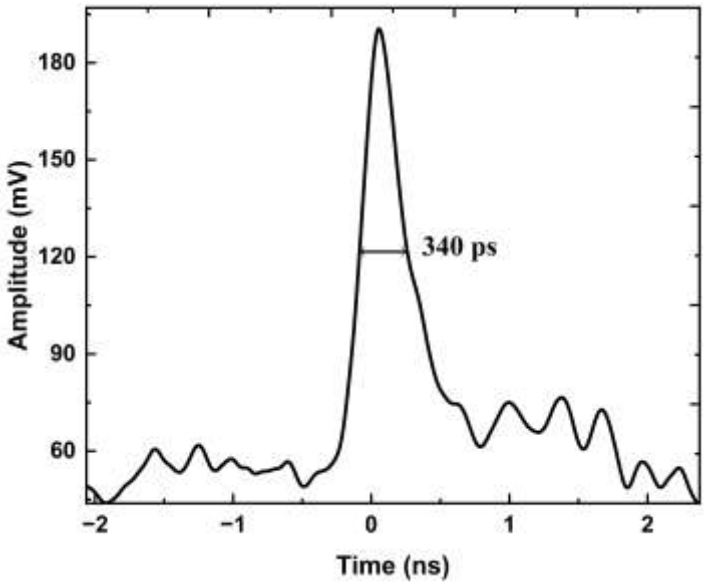

(b)

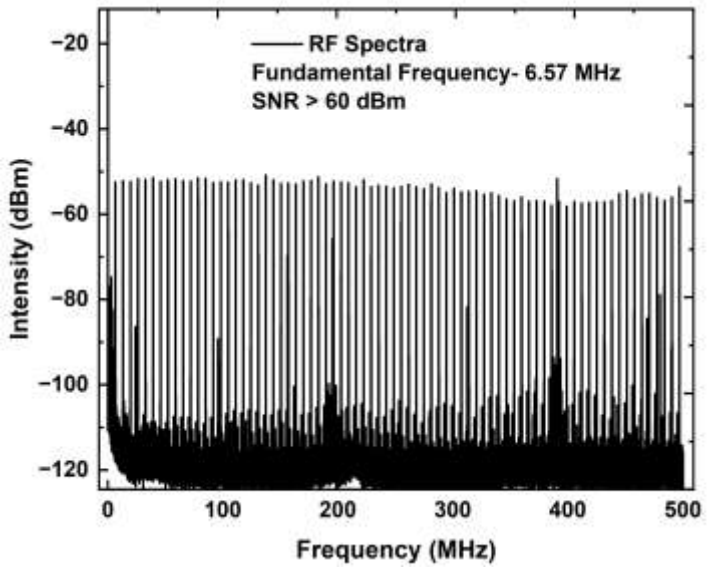

(c)

Figure 5.5: The temporal profile of mode-locked pulses and corresponding RF spectra at a pump power of 2.4 W using an oscilloscope (a) single pulse profile (500 ps/div), (b) mode-locked pulses with 4 μs scale and (c) RF spectra.

Figure 5.6 (a) shows the average output power of the laser increases linearly with pump power. The threshold pump power was 205 mW. The laser switched to the SML pulse regime when the pump power increased to 695 mW.

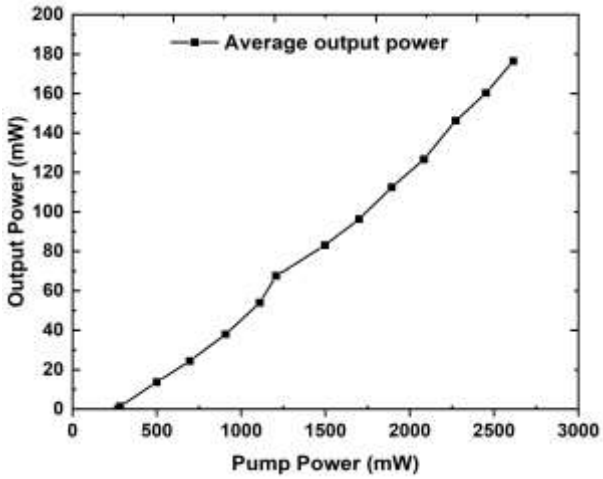

(a)

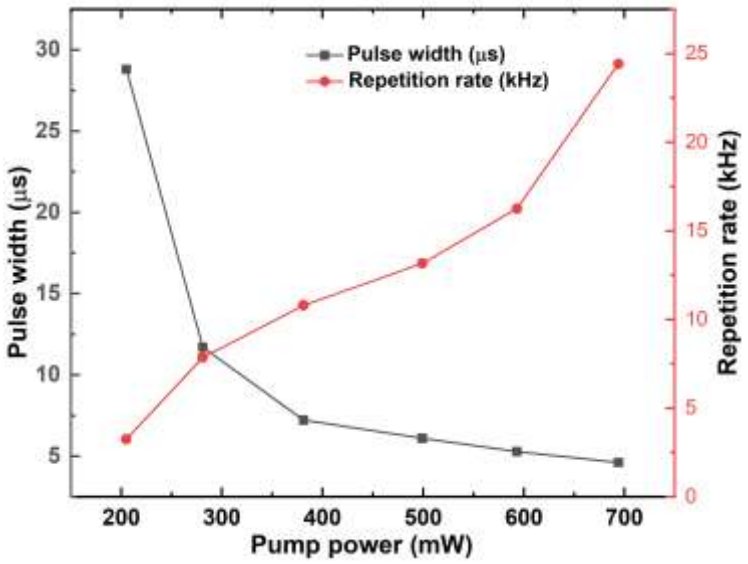

(b)

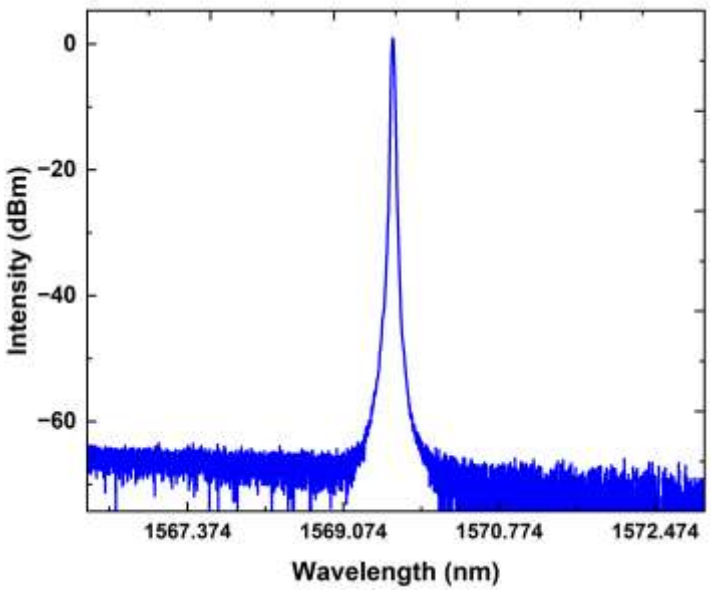

(c)

Figure 5.6: (a) Average output power with pump power; (b) Variation of pulse width and repetition rate with pump power, and (c) Output spectra of laser obtained with an OSA.

Figure 5.6 (b) shows the variation in pulse width and repetition rate of SQS pulses with pump power. The repetition rate was linearly increasing and the pulse width

decreased with increasing pump power, which also confirms the typical behaviour of SQS pulsed laser, and Figure 5.6 (c) shows the OSA spectrum of the laser at 1570 nm.

5.4 Applications

As we discussed previously, pulses with narrow widths and high peak power are helpful for many applications, including laser surgery, material processing, and mid-IR wavelength generation. In this research work, we used the laser as a pump source to develop a mid-IR laser. We obtained ML pulses with 2 W peak power at 1925 nm by pumping a TDF with the generated pulses at 1570 nm with 72 W peak power. Finally, we have developed a carbon dioxide gas sensor using the developed laser as a pump source for TDF. Chapter 6 discusses the characteristics of the developed thulium-doped fiber laser (TDFL) at 1925 nm using a 1570 nm pulsed laser as a pump source. Further, the developed laser at 1570 nm can be used as a pump source to develop a gas laser using CO gas as a gain medium because CO has absorption at 1570 nm.

5.5 Pulsed Laser at 1533 nm

Figure 5.7 is the schematic of the laser. An elliptical core (3.8x14.8 μm) polarization-maintaining erbium-doped fiber (PM-EDF) with absorption and NA of 7.2 dB/m at 980 and 0.15, respectively, was used as the gain medium. A 980 nm diode laser with a maximum pump power of 500 mW was used to pump the gain fiber through a 980/1550 nm wavelength division multiplexer (WDM). Two polarization-independent optical isolators (OI) were used inside the cavity for unidirectional wave propagation to prevent

the spatial hole burning (SHB) effect. To improve stability, the polarization state of light was adjusted with the help of all-fiber polarization controller plates. A small piece of erbium-doped fiber was used as a SA. The FBG used for the selection of peak wavelength had a center wavelength of 1533 nm, peak reflectivity of 95.61%, and a FWHM (full-width half maximum) of 0.392 nm. The SA and FBG together formed a transient grating resulting from the standing wave pattern formed in the SA segment that helped in improving the system's stability. The laser operated in CW mode at lower pump power but switched to ML laser at higher pump power. An additional 200 m SMF was incorporated in the cavity for balancing nonlinearity and dispersion in the cavity. The operating principle of SA has been discussed in detail in Chapter 2 and 3.

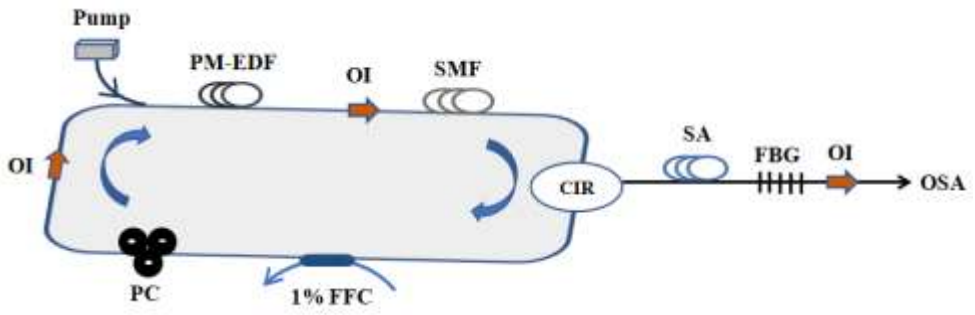

Figure 5.7: Schematic of experimental setup.

5.6 Results and Discussion

The ML pulses were obtained once the pump power crossed the threshold power of 30 mW. The repetition rate of the laser remained constant for all pump powers. However, the pulse width decreased with the increase in pump power. We obtained highly stable pulses as shown in Figure 5.8. Further, Figure 5.8 shows ML pulses at different pump powers.

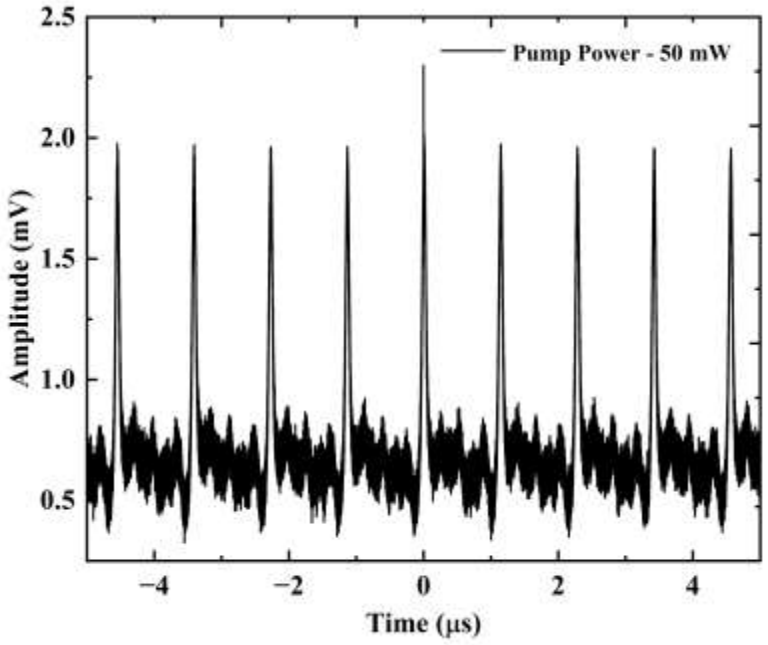

(a)

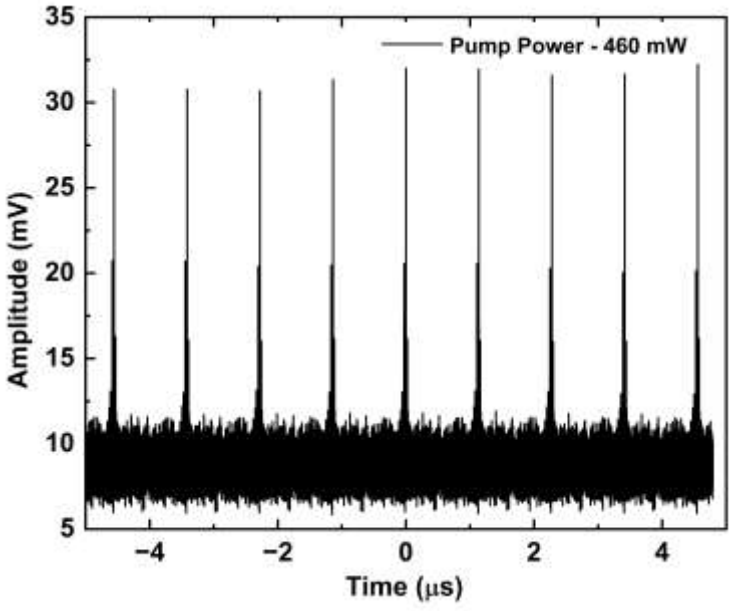

(b)

Figure 5.8: Mode-locked pulses at different pump powers (a) at 50 mW and (b) at 460 mW.

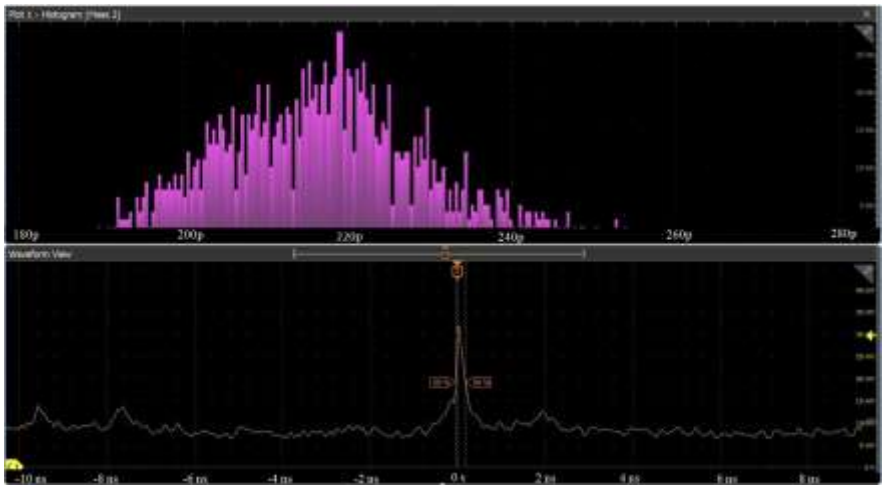

Figure 5.9: Temporal profile of single pulse and histogram view obtained using an oscilloscope.

Figure 5.9 shows the mode-locked pulses at 410 mW pump power. The histogram shows that most of the pulses had a width of 220 ps. The histogram option gives us the measurement of pulse width and is verified by using the software Origin. The histogram view gives pulse width of the maximum number of pulses and in waveform view the single pulse profile can be seen.

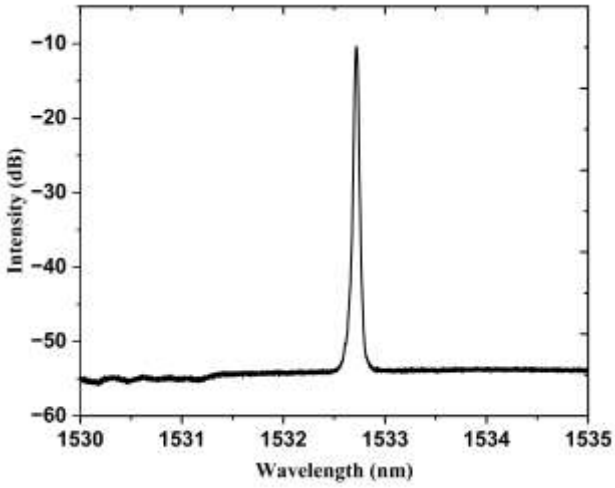

(a)

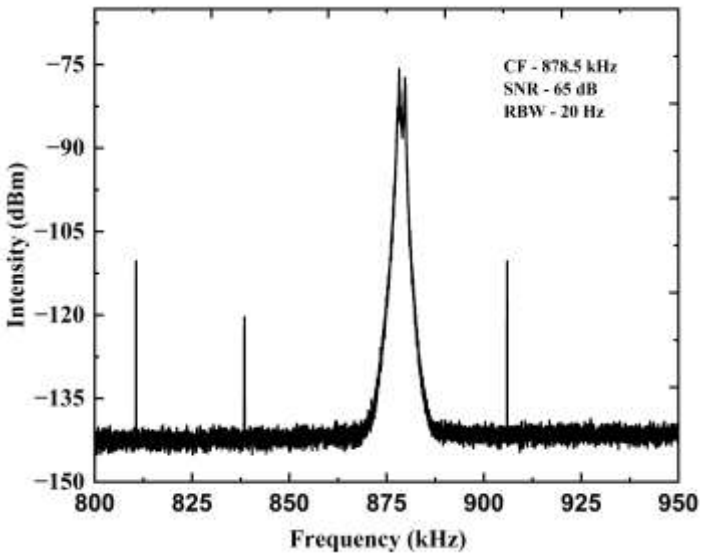

(b)

Figure 5.10: (a) Output spectra of laser obtained with an OSA**,** and (b) RF spectra.

Figure 5.10 (a) shows the output spectra of the laser obtained using OSA, and (b) shows the corresponding RF spectra of the pulses. The fundamental frequency was 878.5 kHz, which matched the obtained repetition rate with the help of an oscilloscope. The SNR of the pulse was 65 dB obtained with a resolution bandwidth of 20 Hz, which confirmed the stability of the pulses. The small peaks on the side of the central peak were noise from the instrument, which was confirmed when no signal was sent to the oscilloscope.

5.7 Conclusion

A pulsed laser at 1570 nm was demonstrated, which produced SQS and SML pulses at low pump power and purely SML laser at high power. The laser produced SQS pulses

with a minimum width of 4.61 μs and a maximum repetition rate of 24.41 kHz. Further, the laser produced SML pulses with a minimum width of 340 ps and a repetition rate of 6.57 MHz. At pump power 2.4 W, the average output power, pulse energy, and peak power were 160 mW, 24.46 nJ, and 72 W, respectively. The experiment was repeated with FBG at different reflectivity and no change was observed in the temporal characteristics of the laser, only the output power. A tunable FBG can produce SML at different wavelengths as per requirement. The developed laser was used as a pump source to produce a gain-switched mode-locked thulium-doped fiber laser at 1925 nm **(Chapter 6)**. The developed laser can also be used as the pump for the development of molecular gas lasers **(Chapter 7)**.

Further, the developed ML laser at 1533 nm is highly stable, confirmed with the SNR observed on the RF spectrum analyzer. The temporal characteristics of pulses were observed on an oscilloscope for more than three hours, in that time span pulses were uniform and stable. This laser has potential application in developing a molecular laser using acetylene gas as a gain medium. Acetylene gas has a vibrational rotational energy level having absorption at 1533 nm and can be selected to attain population inversion for emitting laser in a 3 μm region **(Chapter 7)**.

Chapter 6

Mid-IR Pulsed Laser using Thulium-doped Fiber as the Gain Medium and Applications

This Chapter describes the development of an environmentally stable and compact thulium-doped fiber (TDF) laser and its application. We discuss the operating principle and output characteristics of the laser, which include pulse duration, repetition rate, and wavelength tunability. The laser was developed based on the gain-switching principle in a doped fiber. The designed laser generates mode-locked (ML) pulses at 1925 nm with a minimum width of 105 ps and repetition rate of 20 MHz inside the envelope of gain-switched pulse. Further, the average power, pulse energy, and peak power of the ML pulses are 4.9 mW, 0.24 nJ, and 2 W, respectively, for a pump power of 160 mW at 1570 nm. The tunable property of the laser was obtained using gold nanorods (GNRs). The laser resonator was modified by using a FBG to verify the stability of the laser and to study the feasibility of tunability of the laser using the FBG. In addition, we have developed an Intra Cavity Absorption Spectroscopy (ICAS) system when the laser operated close to the threshold. We present our preliminary data based on atmospheric carbon dioxide (CO_2).

6.1 Introduction

A Laser in the mid-IR region has attracted attention due to its applications in spectroscopy, medicine, pollution monitoring, and material processing [149-152]. A pulsed laser source in the 1.8 to 2.0 μm region is an area of interest because this is an eye-safe region. Amongst other doped fiber lasers, such as erbium-doped fiber (EDF), lasers based on TDF have been a hotspot for the research groups as TDF supports emission in a broad range of approximately 400 nm [153]. Further, TDF has absorption in three different regions of wavelengths around 800 nm, 1100 nm, and 1600 nm, so any of these bands can be used as a pump source, also it has emission in different bands as shown in Figure 6.1. The $^3F_4$ – $^3H_6$ transition covers a broad emission band of approximately 1700 nm to 2100 nm, an attractive feature of this fiber [154]. The development of highly efficient TDF and the availability of the pump sources, which match the absorption band of the fiber, made researchers choose the fiber as the gain medium to generate lasers in the mid-IR region of the electromagnetic spectrum.

Thulium is a rare-earth element in the lanthanide group next to erbium on the periodic table, having an atomic number of 69. In a periodic table, the lanthanide group comprises Cerium to Lutetium elements. These elements exist as a trivalent cation (3^+) because this is the most stable ionization level [155].

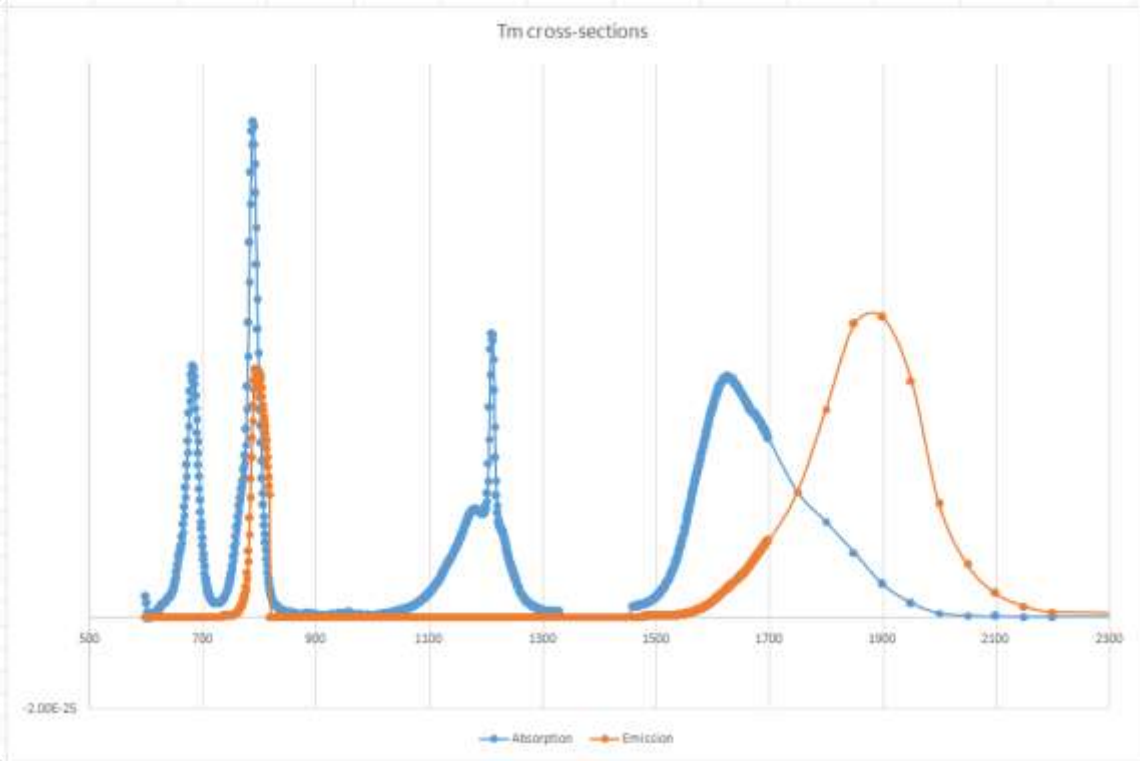

Figure 6.1: Absorption and emission spectrum of Tm doped fiber (CorActive).

Although a laser in the 2.0-micron band has been developed for applications in medicine, little progress has been made in gas spectroscopy, where greenhouse gases (GHG) such as carbon dioxide, nitrous oxide, and methane have high absorption [156]. One of the advantages of the above band is that a detector operating at normal temperature can be used – no cooling is required. Another advantage is that water has high absorption at this band, so it can be used in laser ablation applications, such as in laser lithotripsy, the kidney stones undergo fragmentation and breaks into small pieces and passes out of the body through the urinary tract because of thermal expansion and vaporization due to heat from the absorption of radiation by water [157]. In addition, a

laser at 2.0-micron can be used for generating high-power nonlinear optical parametric oscillators and pump sources for other mid-IR lasers, such as Holmium Lasers [158;159].

Q-switched (QS) and mode-locked (ML) techniques have been extensively used to generate pulses. Further, one can use active or passive methods to generate QS and ML pulses. An active technique involves an external controller to provide modulation in the laser cavity. However, these bulky components are not the choice of researchers as they create barriers to the portability and robustness of the laser. Passive techniques involve fiber nonlinear properties or any other nonlinear phenomenon, such as intensity-dependent nonlinear devices known as SA for generating pulses. These are more compact and cost-effective and can be grouped under artificial or real SAs [21;52]. Artificial SAs, such as nonlinear polarization rotation (NPR) [160], nonlinear amplifying loop mirror (NALM) [161], and nonlinear optical loop mirror (NOLM) [162], are widely used, but their stability is more dependent on environmental fluctuations. Thus, a real SA, which is based on material that is transparent to high-intensity light and becomes a loss element for lower intensity, is easy to implement. They have the ability to self-start and are easy to incorporate into the laser resonators [163]. Various types of SA material have been explored, such as semiconductor saturable absorbers (SESAM), metal nanomaterials (e.g., GNRs), carbon nanotubes, and graphene [164-167]. However, as discussed in **Chapter 3**, material-based SAs have some limitations, such as complicated fabrication processes and low damage thresholds.

A lot of research has been done on TDF lasers using SAs, since the first tunable Q-Switched TDF laser was demonstrated in 1993 [168]. Besides Q-switching and mode-locking, gain switching is another technique to generate narrow pulses where a pulsed

laser was used as the pump source. The pulsed laser causes the population inversion and gain to increase considerably above threshold before the laser oscillation has time to build up from the initial noise level in the cavity, which leads to the emission of a giant spike [29]. A laser based on a gain-switched (GS) technique is compact, cost-effective, and easy to develop as shown in Figure 6.2.

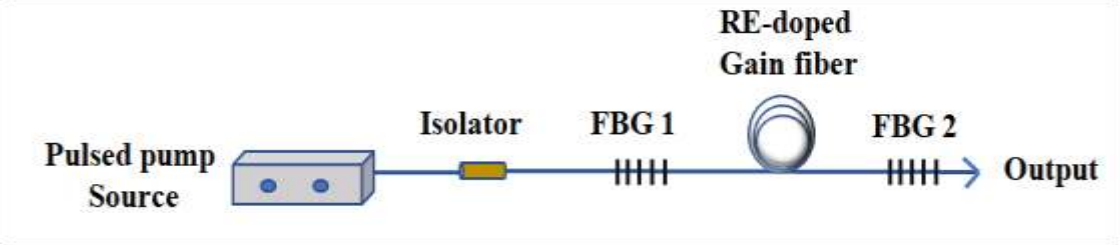

Figure 6.2: Setup of a gain-switched fiber laser.

Stuart D. Jackson and T. A. King reported the first 2.0 µm GS fiber laser in 1998. They realized that the output of the laser was limited by the pump excited state absorption (ESA) process; due to the ESA mechanism the majority of the excited population was driven towards other energetic states. However, it can be suppressed with the right selection of pump wavelength and optimized configuration of the cavity [169]. After this, a lot of reports have been published on 2.0 µm gain switched fiber lasers using different pump sources. Initially, Laser diodes (LDs) or ML fiber lasers were used to achieve gain-switching. ML lasers are preferable over LDs, because LDs have relatively narrow modulation bandwidth, which limits the pulse duration and repetition rate. In gain-switching, output pulses appeared in the form of relaxation spikes, so different

pumping bands were used, and the advantages and disadvantages of each pumping band were analyzed.

In 2005, Zhang et al. reported a GS Tm-doped double-clad silica fiber laser pumped by a 1064 nm laser from a Nd: YAG laser, but output pulses were built up by a series of relaxation oscillations [170].

To improve the efficiency and suppress these relaxation spikes, further research was done using other pumping sources. In 2007, Jiang et al. reported a GS TDF laser with a pulse width of 10 ns and repetition rate of up to 500 kHz based on a modulated 1550 nm LD as a pump source. They demonstrated that fast gain switching can eliminate the relaxation spikes and generate stable output pulses [171]. In 2011, Simakov et al. reported an efficient, polarised, gain-switched operation of a TDF laser. Pulses with width 25 ns and repetition rate up to 300 kHz were achieved using a pump source at 1.55 μm. A two-stage amplifier was used to enhance the output power, which made the design complicated [172]. In 2012, Zhou et al. reported an all-fiber GS TDF laser pumped by a 1.558 μm laser with a minimum pulse width of 29 ns at a 10 kHz repetition rate. They studied the relationship between cavity length and pulse built up time, they were able to eliminate relaxation spikes with cavity optimization and 1.558 μm pumping wavelength [173]. In 2014, Jiao Z. et al. reported an efficient all-fiber GS TDF laser at 1926.7 nm using a pulsed laser at 1.55 μm as a pump source. The reported laser configuration was much simpler and more compact. However, the threshold was 254.5 mW. Further, the relaxation spikes didn't appear in this case, which confirmed that this pumping wavelength is a good choice for generating stable output pulses [174]. In 2017, Chowdhary et al. reported a TDF laser having a pulse width of 256 ns and a repetition

rate of 750 kHz using a 1.56 μm dissipative soliton resonance (DSR) ML erbium/ytterbium co-doped fiber laser as a pumping source. It was concluded that a DSR ML seed laser generates high power compared to a traditional mode-locked laser, which reduces the need of an amplifier to amplify the power [175].

In 2019, Swiderski et al. reported a mode-locking and self-mode-locking-like operation in a resonantly pumped GS TDF laser. A repetition rate of 50 kHz and 111 MHz was reported for GS and ML sub-pulses. In a GS laser, self-starting mode-locked resembling pulses were reported with a pulse width of 110 ps for the first time [120].

In 2021, Duran-Sanchez et al. reported a GS 2.0 μm laser based on a double-clad TDF as a gain medium pumped by a 793 nm pulsed laser. They found that even though pumping at 793 nm exhibits a series of relaxation spikes, with optimization of pump power level and pump laser pulse parameters, instability of the laser can be suppressed [176]. In recent years, self-pulsing effects in fiber lasers also attracted attention to use as a pump source for the development of GS fiber lasers because of cost-effectiveness and compactness as it eliminated the need for any external device in both the configurations, pump source, and gain-switched fiber laser design [177;178].

In 2024, Ma et al. reported a GS 2.0 μm fiber laser pumped by a QS mode-locking self-pulsing EDF laser for the first time, which generated 366.2 ns wide pulses with a repetition rate of 37-73 kHz at a threshold pump power of 205 mW. The pump pulses were amplified to develop a GS fiber laser [179]. They demonstrated the advantages and potential of self-pulsing fiber lasers as a pump source.

We mentioned earlier, three pump wavelength bands can be used in a TDF laser based on their absorption bands at 790 nm, 1064 nm, and 1550 nm as shown in Figure 6.1 [173]. Several reports have been published using these pumping bands, and the advantages and disadvantages of each band have been realized. In 2000, Dickinson et al. reported a GS TDF laser pumped at 790 nm [180]. When pumping is done at 790 nm, output pulses are in the form of relaxation oscillation spikes because of the cross-relaxation effect. As from $^3H_6$ to $^3F_4$ energy level, population relaxation time is longer, so it is difficult to achieve population inversion of the $^3F_4$ level, which results in spikes of relaxation oscillations [173]. Another approach for pumping is using a 1064 nm band, but it also gives output in a series of relaxation spikes. In 1998, Jackson et al. reported gain switched fiber laser using Nd: YAG laser as a pump source [169]. Due to the pump ESA mechanism, the laser output appeared as relaxation spikes, even when pumping was done at 1064 nm.

Among these three pumping schemes, a 1550 nm pump band is considered to be efficient in achieving high beam quality, narrow pulse width, and high pulse energy [174]. Also, the pump source at the 1550 nm band allows resonant pumping with significantly reduced quantum defect and absence of an ESA effect and eliminates cross-relaxation processes, producing stable pulses [181;182].

We designed, for the first time, a 1570 nm self-Q-switched mode-locked double-clad erbium-ytterbium doped fiber laser, which was used as the pump source for developing a mid-IR laser in the 2.0 μm band using the principle of resonance gain-switching in a TDF laser. The threshold power was 53 mW which is

much lower than the previously reported lasers. In addition, the designed laser resonator was compact and simple. The details of the laser are described in **Chapter 5**.

The advantages of the GS fiber lasers are as follows [183]:

Simple configuration: An all-fiber, compact GS fiber laser can be developed without using a mode locker in the cavity, as in Q-switching and mode-locking.

High pulse energy: In gain switching, pulse energy is not limited by the low damage thresholds of cavity components, such as material-based SAs.

Wide spectral coverage and narrow bandwidth: Gain-switching has been realized for almost all the rare-earth-doped, such as Nd, Er, Yb, and Tm fibers. So, a GS fiber laser can be developed from the NIR to mid-IR regions of the electromagnetic spectrum. Generating narrow bandwidth lasers is another advantage of gain-switched fiber lasers. Less than 1 nm wide spectral bandwidth has been achieved with the help of a FBG.

In the current research project, we primarily focused on developing a tuneable thulium-doped fiber laser (TDFL) and explored its application for gas spectroscopy. We have developed the laser based on the principle of gain-switching. The main advantages and uniqueness of the developed laser are: **(i)** low threshold, **(ii)** high stability, **(iii)** generation of ML pulses with 105 ps width and 2 W peak power, and **(iv)** tunability using GNRs. The stability of the laser was verified by comparing the output of the laser with that based on a FBG at 1925 nm. We have pulses which closely resemble Q-switching, as GNRs can act as a SA. We presented the experimental results based on carbon dioxide gas, which show the application of the laser as a real-time gas sensor [184].

6.2 Laser Design - Experimental Setup

Figure 6.3 is the schematic of the Gain-switched thulium-doped fiber laser (GS-TDFL). The laser resonator was a quasi-ring resonator with a total length of 10.2 m and it is comprises of **(a)** Gain medium - a 20 cm long double-clad single-mode thulium-doped fiber (TDF: DCF-TM-6/128-22, CorActive, Canada) with numerical aperture (NA), core/cladding diameter and absorption at 1570 nm of 0.23, 5.3/125 μm, and 0.5 dB/m, respectively; **(b)** Pump source - The gain medium was pumped by an in-house designed ML fiber laser that produced 340 ps pulses with a repetition rate of 6.57 MHz and a maximum average power of 200 mW through a 1550/2000 nm wavelength division multiplexer (WDM, WD1520BB, Thorlabs). The pump laser was designed using a double-clad Erbium/Ytterbium co-doped fiber as the gain medium, pumped by a 976 nm multimode laser diode. The laser operated in a QS Self mode-locked regime when the pump power was below 695 mW and became purely ML at higher pump power. We described in detail the design and characteristics of the laser in Chapter 5; **(c)** Polarization Controller (PC): An all-fiber PC was used to optimize the polarization states of the circulating waves in the resonator, and **(d)** Output: The output of the laser resonator was extracted using a 20% fused fiber coupler (FFC, TW2000R2F2A, Thorlabs). The residual 1570 nm pump source was monitored using a power meter (FOT 90A, EXFO) at port 2, as shown in Figure 6.3. The laser output was analyzed using a 10 GHz Oscilloscope (MS068B, Tektronix), an Optical Spectrum Analyzer (OSA, 205C, 1 – 5 μm, Thorlabs), a 10 GHz photodetector (818-BB-51F, Newport), and a power meter (PM 160T, Thorlabs).

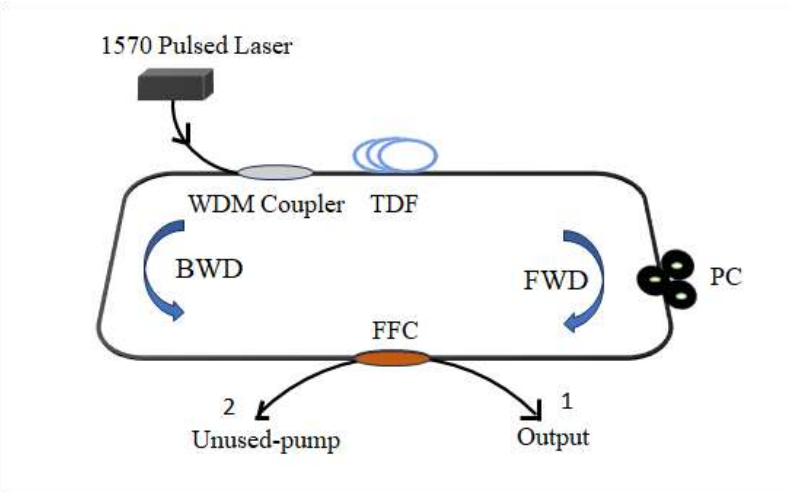

Figure 6.3: Schematic of experimental setup.

6.3 Results and Discussion

Initially, we measured the amplified spontaneous emission (ASE) spectrum of the TDF using a spectrometer (iHR 550 fitted with PbSe detector, HORIBA) in the forward and backward directions when pumped with a 1570 nm ML pulse laser. It was observed that the amount of ASE produced in the backward direction (BWD) was much higher than in the forward direction (FWD) due to the reabsorption of the ASE in the 2.0 μm band. Thus, the counter-propagating waves (BWD) dominate over the co-propagating waves (FWD), and the resonator operates in a ring cavity configuration without an optical isolator in the cavity, which is one of the unique contributions of the presented research work. Although an isolator-free unidirectional thulium-doped fiber laser has been reported based on a theta cavity configuration, the process requires a lot of simulation and optimization compared to our design [185]. Further, to verify that the resonator is operating in a ring cavity configuration, we used a fiber Bragg grating (FBG, peak

wavelength 1925 nm, and 95% reflection) at terminal 2, and output obtained at terminal 1, which produced ML pulses with the same repetition rate as without the FBG of 20 MHz.

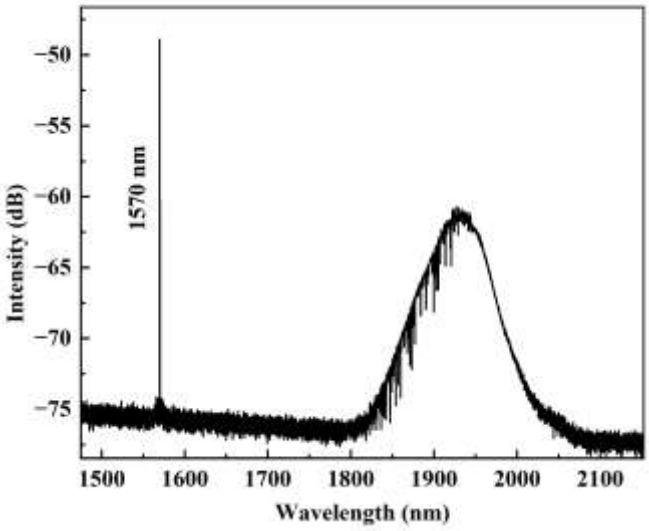

(a)

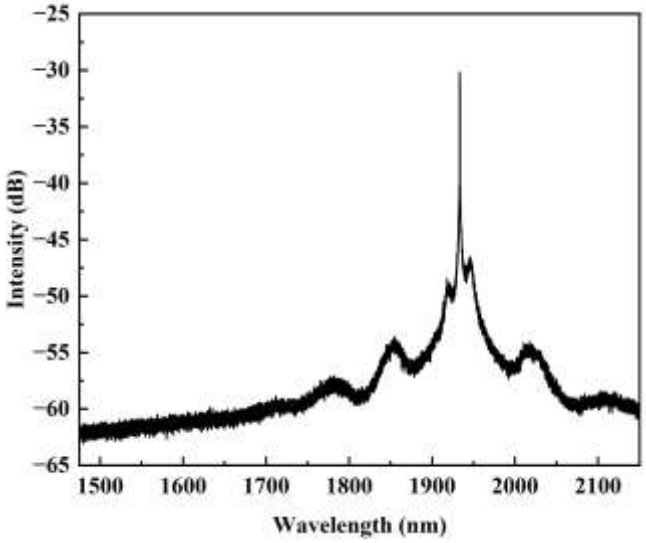

(b)

Figure 6.4: Output spectrum of GS-TDFL (a) below threshold, and (b) above threshold.

To find the efficiency of the laser, it is important to know the amount of pump power absorbed by the gain fiber (TDF). Figure 6.4 (a) shows the laser output obtained at terminal 2 using a spectrometer when the laser operated below threshold pump power. We observed that the ASE power increased linearly with the pump power, but a small portion of the pump laser remained unabsorbed in the FWD. However, the unabsorbed pump power becomes insignificant at higher pump power, as shown in Figure 6.4 (b).

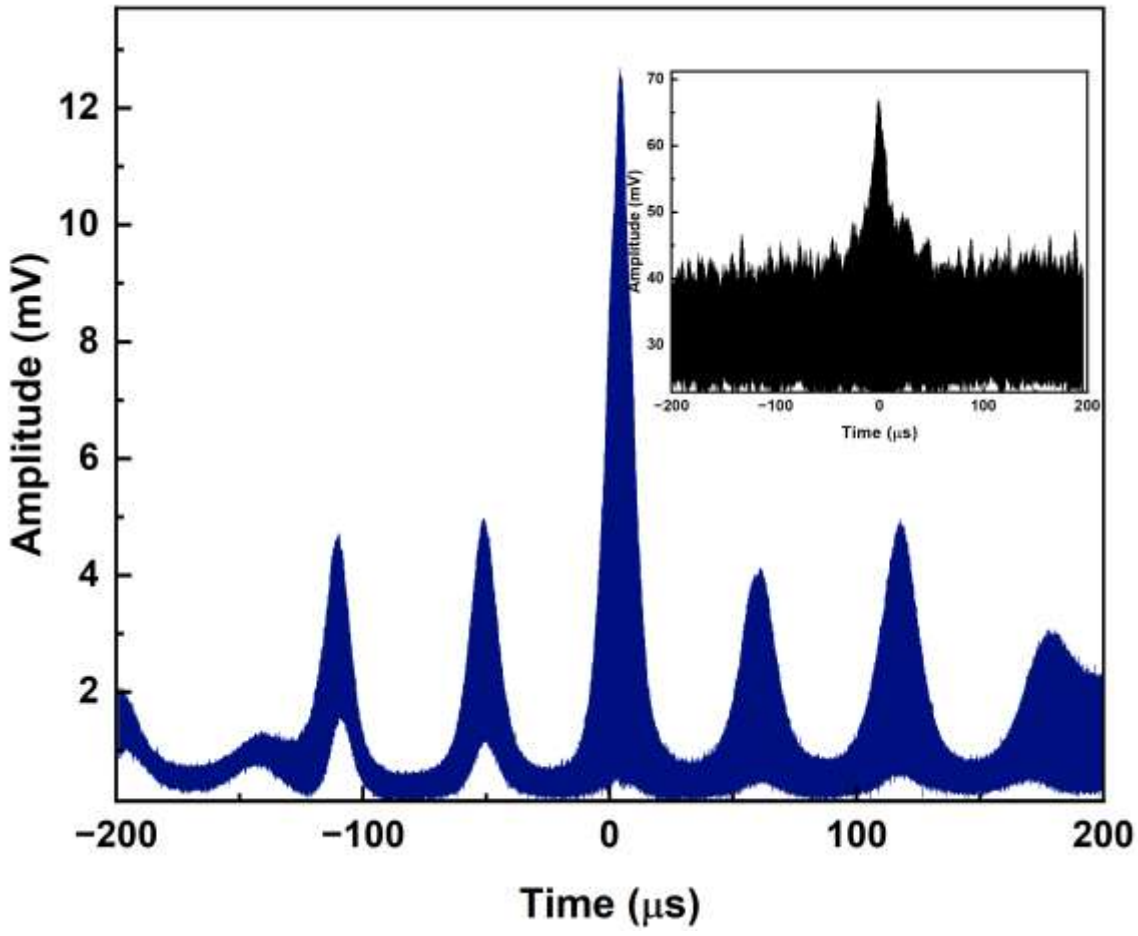

(a)

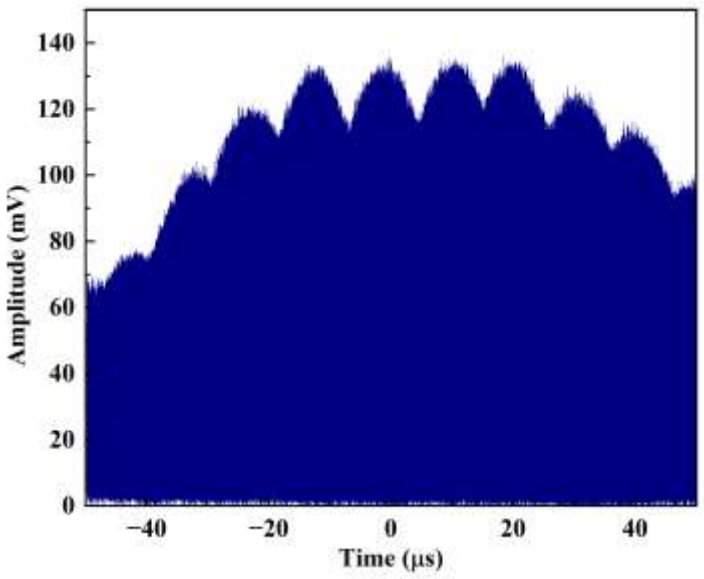

(b)

Figure 6.5: Temporal characteristics of GS pulses (a) at a pump power of 85 mW, (inset: pulse profile at pump power 160 mW), and (b) at a pump power of 126 mW.

Figure 6.5 shows the temporal characteristics of the GS-TDFL with a repetition rate of 17 kHz, obtained for a pump power of 85 mW. The threshold power was 67 mW. We obtained stable pulses at the repetition rate of 3.3 to 25.8 kHz. The repetition rate of the pulses increases with pump power, and at high power 160 mW, they collapse into a single giant pulse, as shown in the inset of Figure. 6.6 (a). Figure 6.6 (b) shows the gain-switched pulses at pump power 126 mW. We observed that with increasing pump power, the GS pulses came closer and at high power it was difficult to distinguish them, this indicates formation of GS pulses.

We studied the characteristics of the laser using a radio frequency (RF) spectrum analyzer at each pump power. We found a few peaks at lower pump power, and it becomes noisy with multiple peaks at higher power, which is attributed to the generation

of lasing peaks at multiple relaxation oscillation frequencies, as we did not optimize the pump pulse duration to allow only the first relaxation oscillation of the GS pulse to lase [186]. Also, it has been reported that pumping with a high peak power and short pulse width laser leads to fast relaxation oscillation and quick stabilization [187]. Further, a resonant pumping scheme, where the pump and emission transition levels are the same, with a high repetition rate of ML pulses, can produce a stable GS pulse [188].

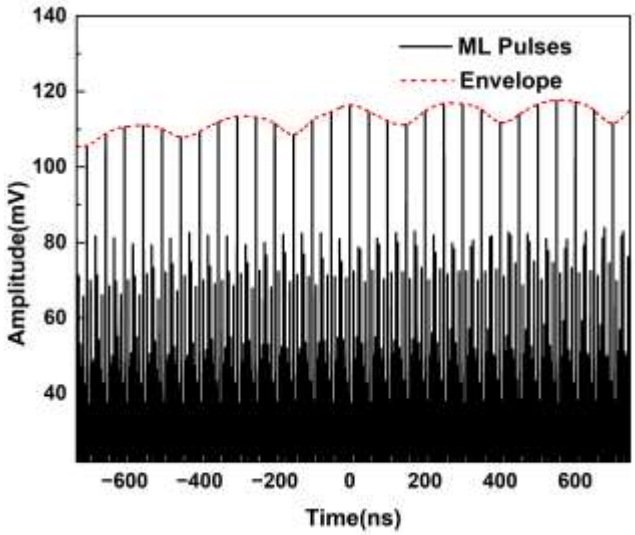

(a)

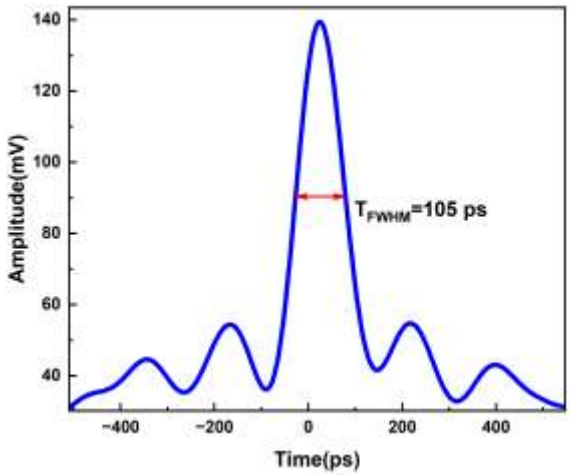

(b)

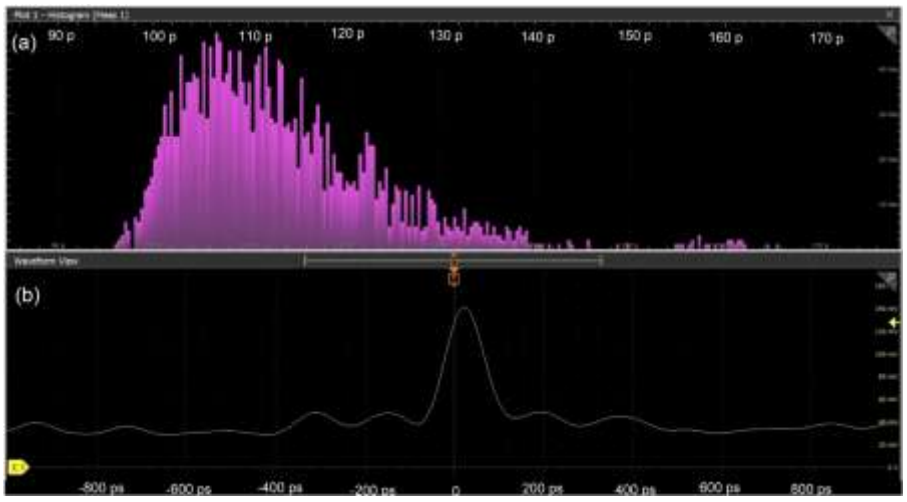

(c)

Figure 6.6: (a) ML pulses at pump power 160 mW pump power, (b) Single pulse profile of ML pulse, and (c) Single pulse profile of ML pulse and histogram.

After further investigation of the oscilloscope spectrum, we observed that the GS pulse (as well as the giant pulse at the higher power) envelope contains ML pulses with a repetition rate of 20 MHz. Figure 6.6 (a) shows ML pulses separated by 50 ns. The output shows modulation, which we attribute to the beating between longitudinal modes supported by the cavity. Figure 6.6 (b) shows the temporal profile of a single pulse with a pulse width of 105 ps at 160 mW obtained using ORIGIN software, and Figure 6.6 (c) shows the oscilloscope profile of the pulse, and the histogram of the pulse width obtained with the Histogram Option, that gives the pulse width in real-time, which varied between 90 to 120 ps. The histogram's peak confirms that most pulses had a width of 105 ps, similar to the single pulse duration calculated using ORIGIN software (Figure 6.6 (b)). The developed TDFL can produce gain-switched mode-locked (GS-ML) pulses at lower pump power and transform them into ML pulses at a pump power of more than 126 mW.

The ML pulses in the TDFL are produced due to SPM when high-intensity pulses propagate through a fiber with a small core diameter, and self-mode locking occurs due to un-pumped thulium ions. The high modulation depth in GS pulses indicates the presence of un-pumped ions, which act as a weak saturable absorber. [188]. One ML pump pulse at 1570 nm with an energy of 24 nJ produced three ML pulses with an energy of 0.24 nJ each. The repetition rate for the 1570 nm ML laser was 6.57 MHz, and the repetition rate for TDFL was approximately 20 MHz. In other words, one pump pulse produced three pulses at 1925 nm.

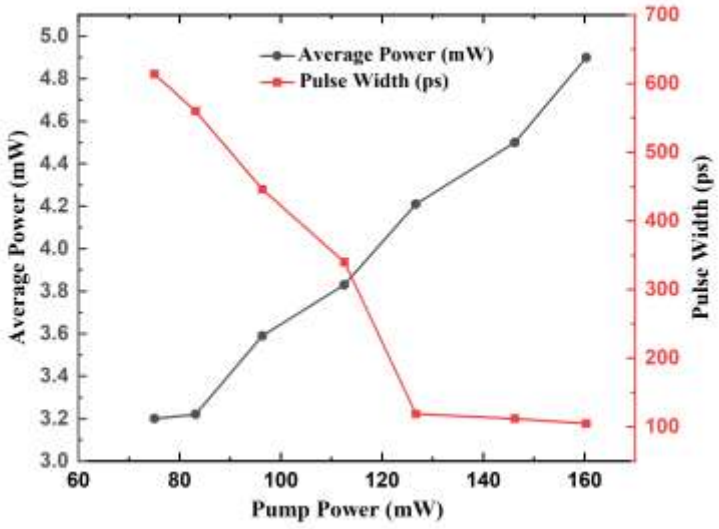

Figure 6.7: Average power and Pulse width variation with Pump power.

Figure 6.7 shows the average output power and pulse width variation with pump power. Average power increased with increasing pump power, but pulse width decreased linearly for low pump power. However, at high pump power, it decreased sharply and almost remained constant beyond a particular level, as seen in Figure 6.7. In general, the

pulse width of ML pulses is uniform, contrary to the ML pulses in the GS envelope, where the pulse width of ML pulses varies between the leading and trailing edges of the GS envelope. Once the GS pulse collapsed, the linewidth became stable. This is one of the characteristics of a GS-ML fiber laser [120;188]. Figure 6.8 shows the RF spectra of generated ML pulses in the 2 GHz range with a resolution bandwidth of 2 kHz. It was not uniform as in the case of a typical ML laser. The frequency difference between the two consecutive peaks was 20 MHz, which matched the data obtained using an oscilloscope. A maximum SNR of 70 dB was observed, which shows that the pulses were stable. To study the long-term stability of the pulses, we observed the output of the TDFL for four hours running without any interruption, and did not see any changes. We repeated the experiment after 48 hours, the laser's characteristics were unchanged at the same lab environmental condition. This shows that the generated pulses were highly stable.

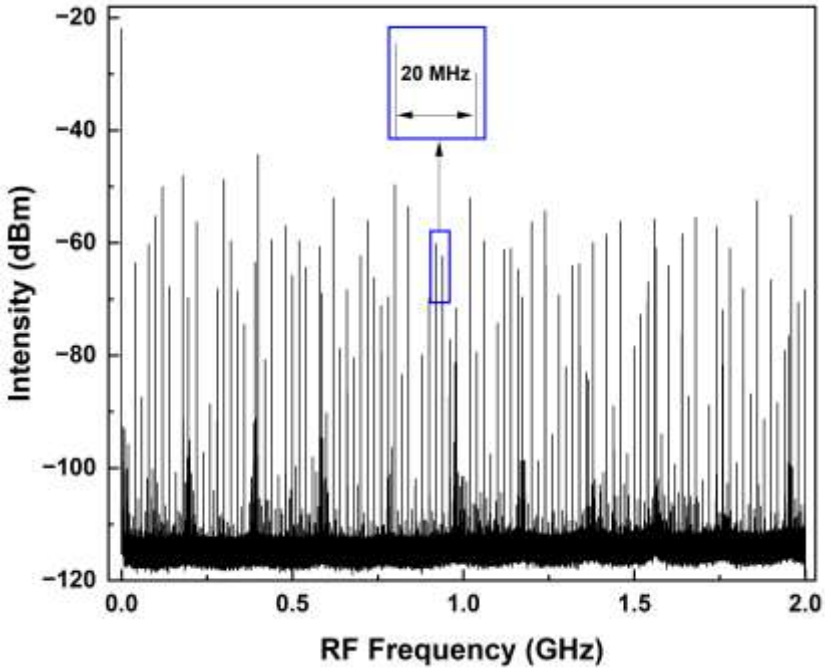

Figure 6.8: RF spectrum of ML Pulses.

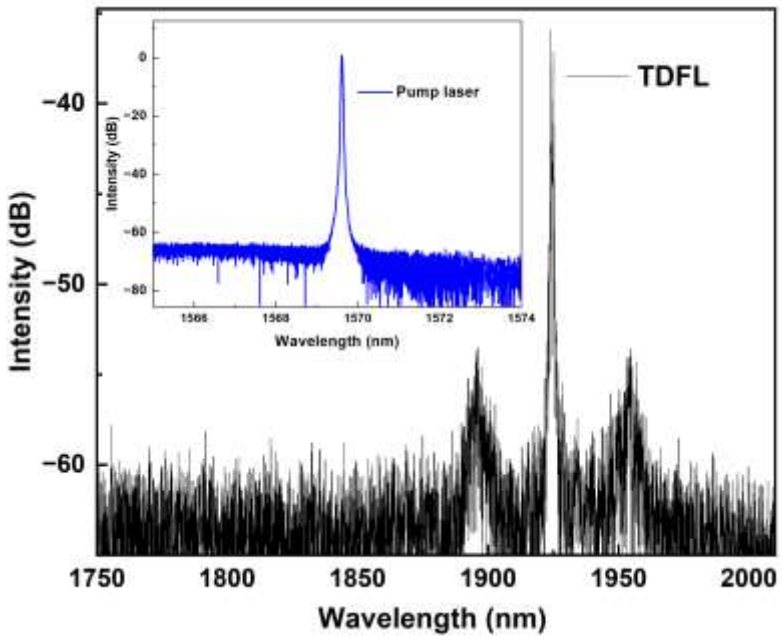

Figure 6.9: Spectrum of TDFL obtained using a spectrometer (Inset: Output spectrum of pump laser obtained using an OSA).

Figure 6.9 shows the optical spectra of the GS-ML TDFL emission centered at 1925 nm and in the inset, spectrum of the pump laser at 1570 nm. The output of the pump laser was obtained using an optical Spectrum Analyzer with a resolution of 0.03 nm (MS9740A, Anritsu).

6.4 Wavelength Tunability

The wavelength tunability of the laser can be obtained using two different methods: (a) compression and expansion of the FBG, (b) Using GNRs of AR 17.5 at various concentrations.

(a) The peak wavelength and bandwidth of the FBG was 1925 nm and 0.02 nm, respectively. It was connected at terminal 2 of Figure 6.4. The FBG reflected ASE exiting from terminal 2 and propagated in the BWD. The output of the laser was identical, with little power enhancement.

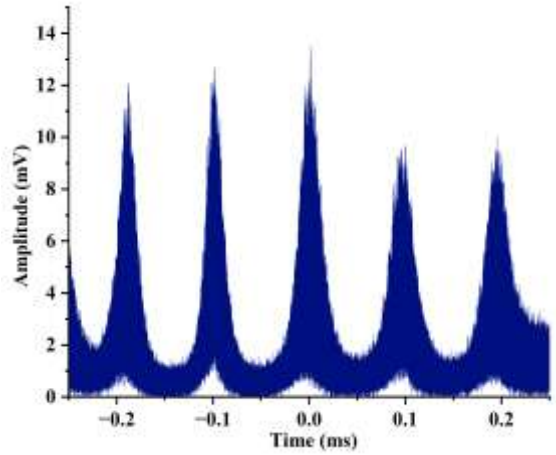

(a)

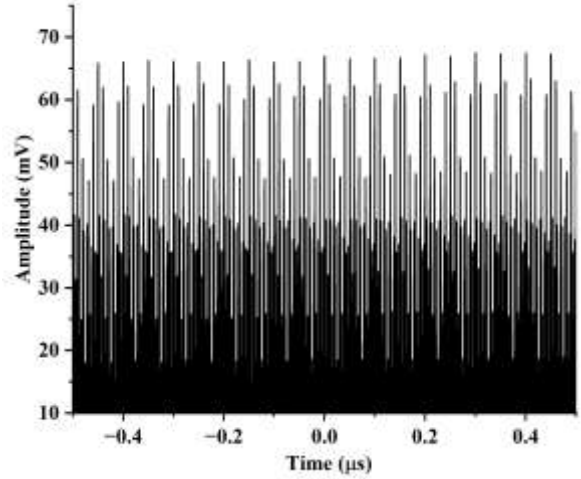

(b)

Figure 6.10: (a) GS pulses at pump power 130 mW, and (b) ML pulses at pump power 175 mW.

Figure 6.10 (a) shows the GS pulses at a pump power of 130 mW, and Figure 6.10 (b) shows the ML pulses at a pump power of 175 mW. One can tune the laser wavelength by compression or expansion as described in the reference [189].

(c) We used GNRs in the cavity for wavelength tuning. As described in Chapter 3, GNRs have wide absorption bands, and the peak absorption wavelength changes based on their AR. It can be used as a SA in a laser cavity to generate QS and ML pulses. We demonstrated that a mixture of GNRs and PVA can be used to tune the laser wavelength and as a SA. Different amounts of GNRs and PVA mixture at a particular concentration were used in the cavity to achieve tunability. The peak wavelength of the laser shifted towards shorter wavelengths (1896 nm to 1883 nm) as we increased the amount of mixture, which increased the absorption at the peak wavelength. The mixture also acted as a SA in the cavity.

To prepare the GNRs and PVA mixture, GNRs were purchased from Nanopartz Inc. USA with an AR of 17.5 (LSPR peak at 2100 nm) and PVA (Average molecular weight 85000-124000, 87-89% hydrolyzed) from Sigma Aldrich. The aqueous solution was prepared by mixing colloidal GNRs and PVA solution. PVA solution was prepared by mixing 2 g of PVA in 100 ml deionized water using a magnetic stirrer, keeping the temperature 70 – 80 degrees centigrade for an hour. To increase the concentration of GNRs, excess CTAB was removed from the standard GNRs solution, 500 µl of GNRs were centrifuged at 14500 rpm for 20 minutes, and 300 µl supernatant was taken out. The remaining 200 µl GNR solution was mixed with 100 µl PVA. It was mixed on the magnetic stirrer without heat for 40 minutes, and ultrasonication was used to ensure uniformity. The experiment was performed with different amounts of GNRs solution (40

µl and 80 µl). A drop of this solution was dried on the ferrule tip and connected to another ferrule using a sleeve, as described in **Chapter 3**.

Figure 6.11 shows the schematic for TDFL when GNRs and PVA mixture were incorporated in the cavity. A 25 cm long double-clad single-mode thulium-doped fiber was used as a gain medium (TDF: DCF-TM6/128-22, Coractive, Canada). We adopted bi-directional pumping using a 1570 nm ML pulse laser with maximum power of 200 mW (Chapter 5) and amplified spontaneous emission (ASE) at 1550 nm with maximum power of 100 mW with the help of two wavelength division multiplexing couplers (1550/2000 WD1520BB, Thorlabs). A 10% fused fiber coupler (FFC-TW2000R2F2A, Thorlabs) was used for measuring output. PC plates were used to increase the stability of the laser. A mixture of GNRs and PVA was used as a SA in the cavity following the method described in Chapter 3. The laser output was characterized by using instruments as described in Section 6.2 above.

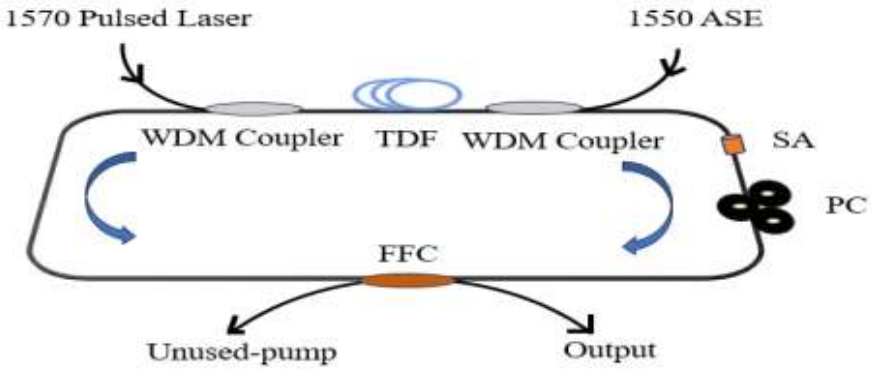

Figure 6.11: Schematic of the experimental setup with a bi-directional pumping scheme.

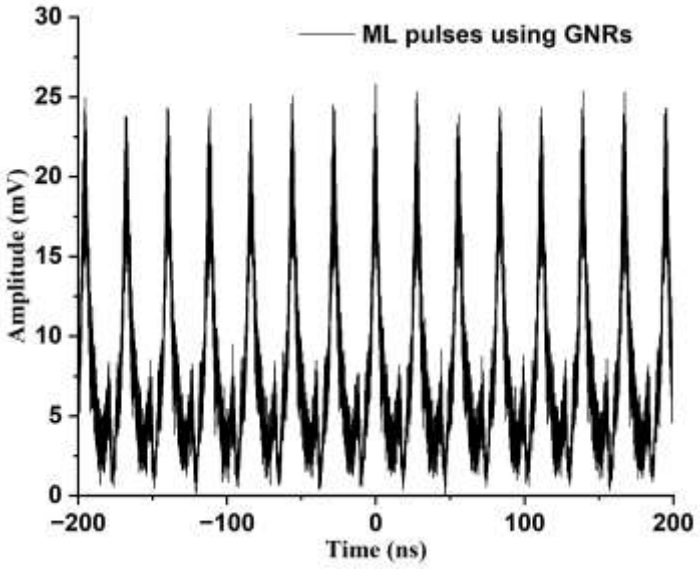

Figure 6.12: Mode-locked pulses obtained using GNRs in the cavity.

Figure 6.12 shows the ML pulses obtained when GNRs were present in the cavity. It can be seen that the pulse shape is different from gain-switched mode-locked pulses. The stability and pulse shape of the laser did not change with increasing amounts of GNRs and PVA mixture. However, the pulse duration variation was attributed to the presence of GNRs in the cavity, which gave a wider pulse width. The laser produced ML pulses with pulse width, repetition rate, average power, and energy of 8.7 ns, 35.80 MHz, 312 μW, and 8.715 pJ, respectively. Further, ML pulses were observed inside the QS envelope. The width and repetition rate of the QS pulses are 1.2 μs and 10 kHz at the pump power of 200 mW. The repetition rate of the ML pulses was larger than that described in Section 6.3, as the laser operated in harmonic ML regime, and the presence of the ferrule connector to hold the GNRs and PVA mixture made a Fabry-Perot cavity

configuration instead of a ring cavity. The total length of the resonator was approximately 9 m.

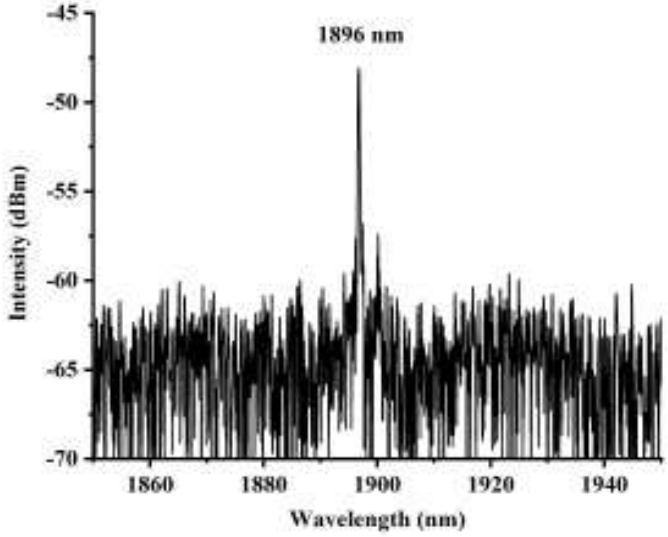

(a)

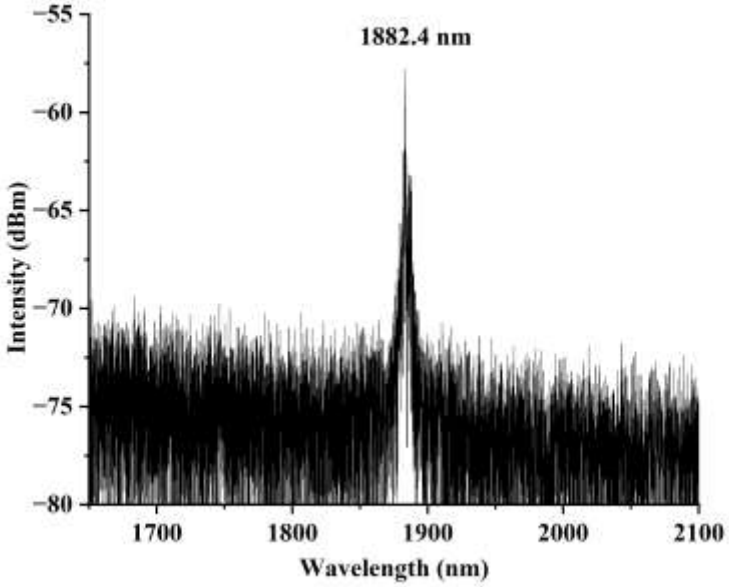

(b)

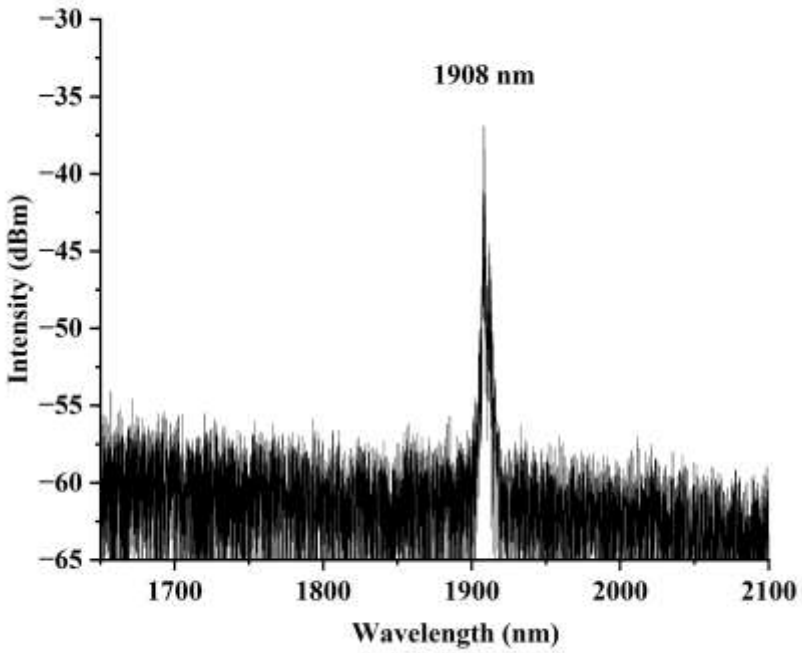

(c)

Figure 6.13: Output of the laser with (a) 40 µL GNRs and PVA mixture, and (b) 80 µL GNRs and PVA mixture in the cavity (c) Output of the laser without any GNRs in the cavity.

Figure 6.13 (a) shows the output of the laser with 40 µl GNRs and PVA mixture in the cavity. The peak wavelength was 1896 nm. Figure 6.13 (b) shows the output of the laser when the mixture amount was increased to 80 µl and the peak wavelength was shifted to 1883 nm. It was found that, by adjusting the amount of GNRs and PVA solution mixture in the cavity, we could tune the laser at wavelengths from 1896 nm to 1883 nm by adding 40 µL of GNRs and PVA mixture incrementally. In each case, we allowed the mixture to dry for 24 hours. Further, the laser produced QS-ML pulses at 1908 nm when the mixture of GNRs and PVA solution were absent in the cavity, as shown in Figure 6.13 (c).

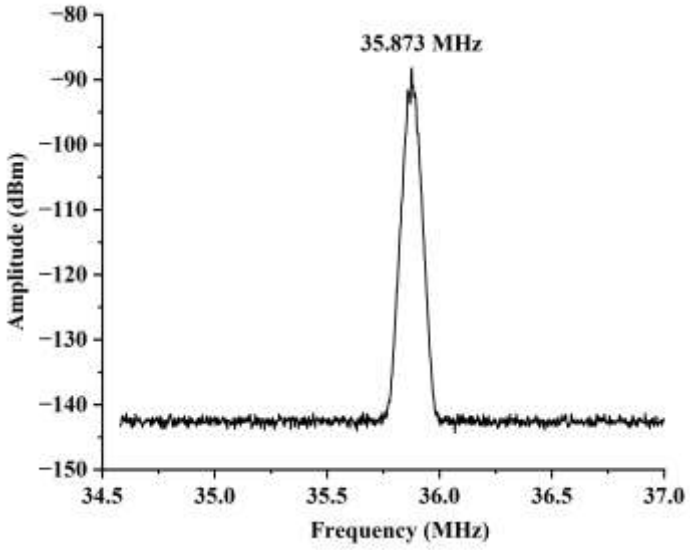

Figure 6.14: RF spectra of ML pulses obtained when GNRs were present in the cavity.

Figure 6.14 shows the RF spectrum of the ML pulses, with a frequency of 35.87 MHz, which matched the repetition rate of the laser obtained from the oscilloscope. The resolution bandwidth was 10 Hz. The RF spectrum shows a SNR of ~ 53.5 dB, which signifies the high stability of the pulses.

We experimentally demonstrated that GNRs mixed with PVA could be used as a SA and tuning laser peak wavelength over the 25 nm range for a TDF pulsed laser in the 1.9 μm region, which can replace the application of FBG in the cavity. It will be possible to increase the tuning range by adjusting the concentration of GNRs in PVA. The developed laser can detect gases (N_2O, CO_2, and NH_3) at a lower concentration.

6.5 Applications: Real-time gas sensing

The detection of gases from fertilized agricultural fields is becoming an in demand function worldwide, especially with the changing climate conditions. Detection of trace gases (e.g., nitrogen oxide, carbon dioxide, and ammonia) in real-time at sub-ppb (parts per billion by volume) levels is challenging and requires a complex system. Most of the gases emitted from fertilized agricultural fields have overtones of the characteristics absorption (fundamental) and the combinations of the overtones in the mid-infrared (mid-IR) region (1.8 – 2.6 μm) [24]. For example, NH_3 has four infrared active fundamental vibrational absorption bands: $\nu_1 = 3337\ cm^{-1}$. $\nu_2 = 950\ cm^{-1}$, $\nu_3 = 3444\ cm^{-1}$ and $\nu_4 = 1627\ cm^{-1}$, where ν_3 and ν_4 are doubly-degenerate. Figure 6.16 shows the overtones and combinations of the fundamental vibrational absorption bands in the 2.0 μm region of the electromagnetic spectrum for ammonia. The advantage of using these transition bands is that they are unique for a particular molecule and can be identified by their absorption spectrum. Further, an InGaAs detector can be used to detect the signal at room temperature.

It is to be noted that the absorption at the 2.0-micron band by gases (Ammonia and Carbon dioxide) is much higher than that at the 1.55-micron band (e.g., Figure 6.15 (a) & (b)), and thus, the system based on 2.0 μm ASE using an Intra Cavity Absorption Spectroscopy (ICAS), will be much more sensitive.

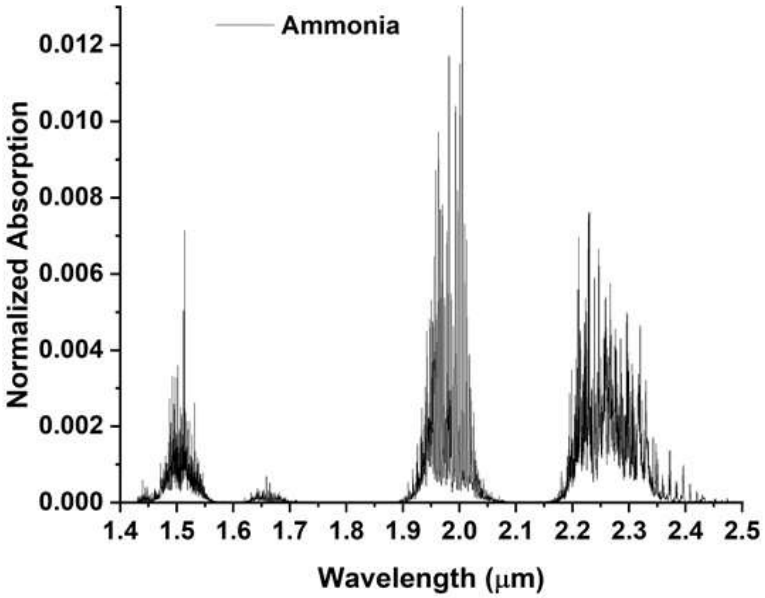

(a)

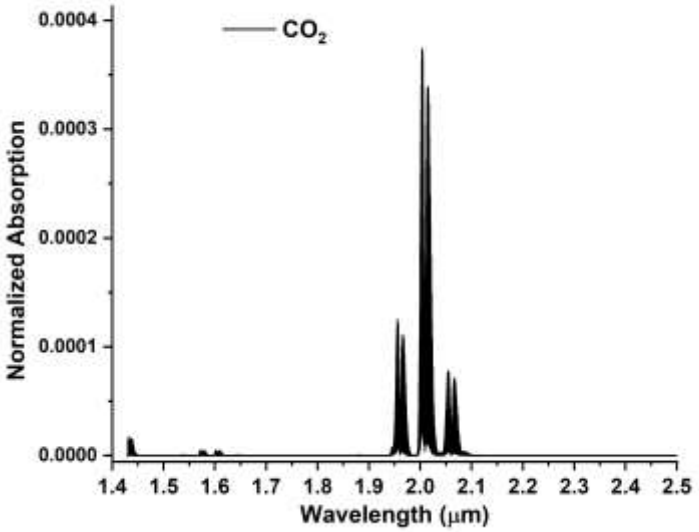

(b)

Figure 6.15: Absorption spectra of (a) Ammonia and (b) Carbon dioxide.

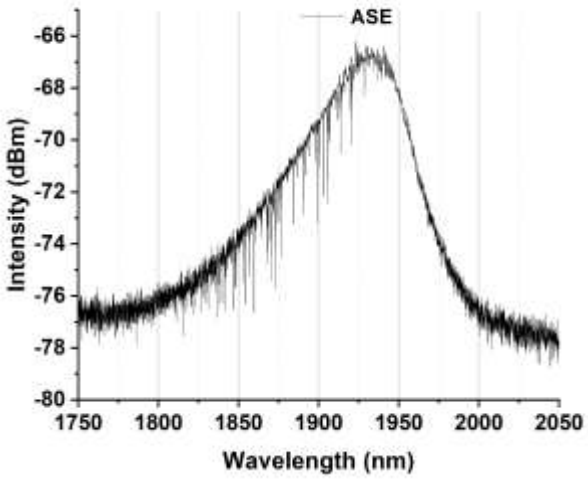

Figure 6.16: ASE Spectrum at threshold.

Figure 6.16 shows the output spectrum of the laser when it was operated at the threshold, so any small loss in the cavity will reflect at the output [190]. The output is noisy due to the detector sensitivity at room temperature. A detector cooled at - 40 degrees centigrade or lower will be the best option to reduce the noise.

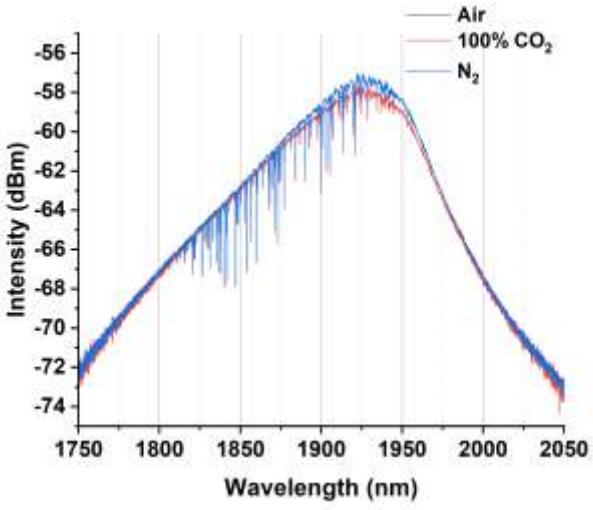

Figure 6.17: Absorption spectra of CO_2.

For this research work, we focussed on CO_2, but in the future it can be extended to other gases such as CO and NH_3. The experiment was performed using a gas cell formed by two ceramic ferrules connected by a sleeve and enclosed in a box fitted with a gas inlet and outlet, where the gap between the two ferrules (200 microns) allowed the gas to interact with the ASE spectrum [191]. The system was used at ambient gas concentration.

Figure 6.17 shows the spectra obtained with Air, Nitrogen (N_2) and 100% carbon dioxide (CO_2). It was observed that when the enclosure was flushed with nitrogen and lab air, spectra did not change (they coincide), but once flushed with carbon dioxide, the total spectral intensity was reduced, showing absorption of the gas over the spectral region. The absorption peaks are not prominent as the noise level for the detector is too high (Figure 6.16). However, overall sensitivity can be improved with reduced system noise such as using iHR 550 (Horiba, USA), which has a PbSe detector cooled at -40 degrees.

To the best of our knowledge, this is the first demonstration of gas sensing using the ASE spectrum at a 2.0-micron band when the laser cavity operates at the threshold condition. It is possible to increase the number of ceramic ferrule modules in the enclosure to increase sensitivity and responsivity. The newly developed technology based on the ASE spectrum is expected to open a new direction to detect gases at a lower concentration or molecular level, leading to more efficient devices based on vibrational transition, such as molecular lasers where gas pressure plays a significant role.

6.6 Conclusion

We have demonstrated the generation of a fast GS-ML laser at 1925 nm using an ML laser at 1570 nm as a pump source for the first time at a threshold value of 53 mW only.

The laser showed some improved intensity and reduced amplitude variation when a FBG was inserted at terminal 2 of the FFC. The laser can be operated at different wavelengths by tuning the FBG [189]. Also, GNRs were used for tuning the wavelength, which works as SA as well as a wavelength selector. With GNRs, the laser was operating between 1896 nm and 1883 nm. Further, one can change the repetition rate of the generated pulses by adjusting the TDFL's cavity parameters instead of changing the pump laser for a desired application. The developed laser was highly stable as pulses were observed continuously for more than four hours on an oscilloscope. Also, the experiments were repeated after 48 hours, and the laser output was the same.

The developed TDFL can detect carbon dioxide in real time by operating it at a threshold [184]. In the future, it can be used to detect other gases, e.g., Ammonia and carbon monoxide. Further, the laser can be used as a pump source to generate a mid-IR laser beyond the 2.0 μm band.

Chapter 7

Mid-IR laser based on gas-filled Hollow - Core Photonic Crystal Fiber

This chapter describes the preliminary work for developing a mid-infrared (mid-IR, 2.00 μm – 5 μm) laser using a gas-filled hollow-core photonic crystal fiber (HC-PCF). We will also discuss Kagome HC-PCF, a class of photonic crystal fibers (PCF) that holds gas in the laser resonator cavity. Our preliminary work shows the design of the resonating cavity and the process of optimizing the cavity parameters (e.g., pressure of the gas inside the HC-PCF) using acetylene gas, and later, it will be replaced with carbon monoxide gas. Both gases will act as a medium of gain for the mid-IR laser. We have developed two pump sources at 1533 nm and 1570 nm, which will be used as a pump with acetylene and carbon monoxide gases, respectively. The detailed development procedures and results are reported in ***Chapter 5.***

7.1 Introduction

In the last several years, fiber gas lasers have become a choice to generate a mid-IR laser, as the laser's output can be much higher than the laser based on solid-core fibers. For the development of mid-IR gas lasers, gases that have emissions in the mid-IR region can be used as a gain medium. The absorption band of the gases dictates the need for a pumping source. Many gases have absorption in the near-infrared region (NIR) and emission in the mid-infrared region, making them suitable as gain medium for developing mid-IR gas lasers. Thus, a laser in the NIR region can be used as a pump source. Such as acetylene has an absorption at 1.53 μm, and CO has an absorption at 1570 nm, as shown in Figure 7.1, and emission at 3.1 μm and 2.1 μm. Absorption and emission wavelengths can change based on different gases (e.g., HCN – Hydrogen Cyanide). So, with a NIR pump source at various wavelengths, mid-IR gas lasers can be obtained at any desired wavelength.

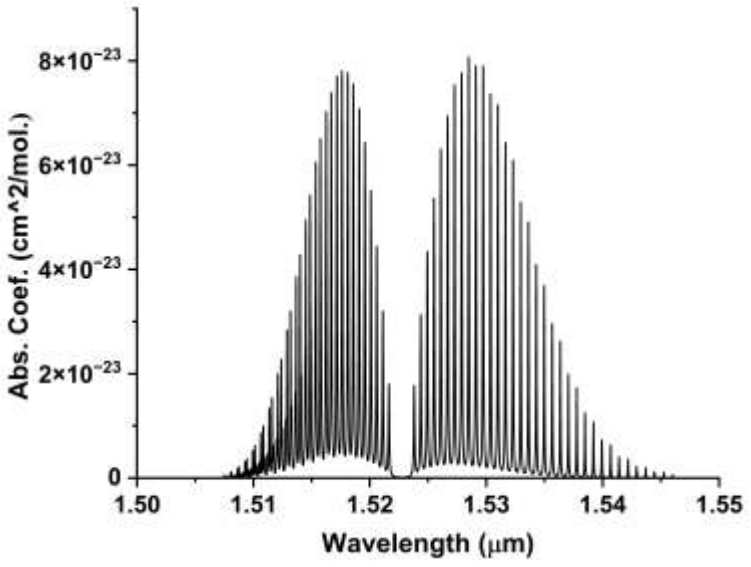

(a)

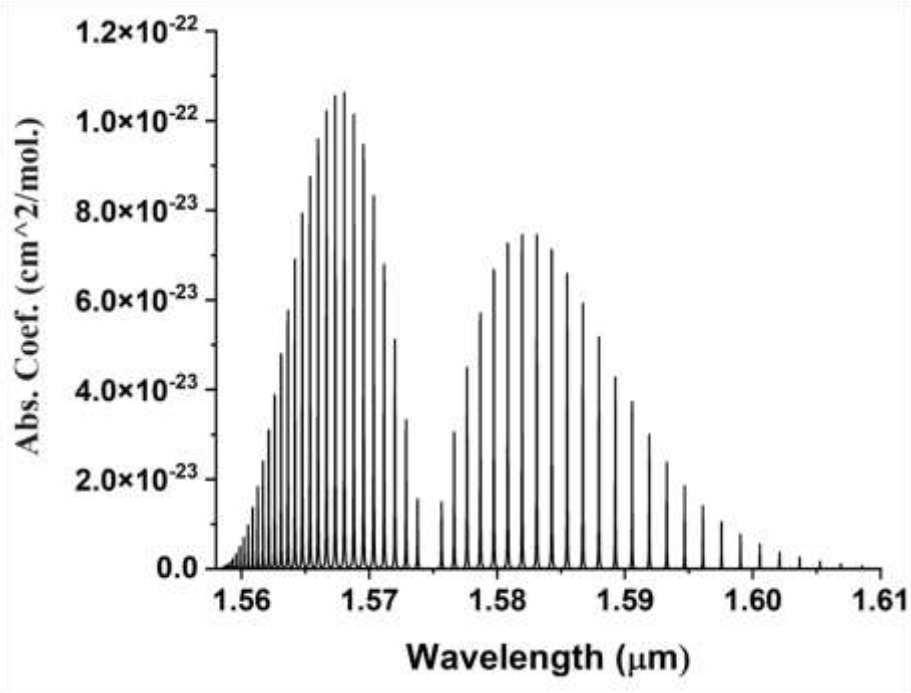

(b)

Figure 7.1: Absorption spectra of acetylene and CO gas [156].

Further, fiber gas lasers are gaining popularity because of their high damage threshold, large gain cross-section, and good heat dissipation capacity. Many optically pumped gas lasers have been reported in the past. For example, a CH_3F gas laser optically pumped by a Q-switched CO_2 laser was reported [192], and a CO_2 gas laser was developed at 10.6 μm using a gas discharge pulsed Hydrogen Bromide (HBR) chemical laser as a pump source [23]. Up to now, several gases have been used for developing gas lasers, such as carbon monoxide [193], nitrous oxide [194], and carbon dioxide [195]. In 2022, an HBr gas laser with tunability from 3.8 μm to 4.5 μm was reported [196], which motivated the development of other tunable gas lasers and increased their emission band. Recently, a mid-IR fiber gas amplifier based on acetylene-filled hollow-core fiber has

been reported [197]. In September 2024, a high-power hollow-core fiber gas laser at 3.1 μm was reported [198]. The advantages of gas lasers have been explored based on the broad absorption and emission cross-sections of gases. Although a lot of research work has been done in the field of gas lasers, there are still opportunities to develop more efficient and high power lasers based on CO, which still has much-undiscovered potential that needs attention, and acetylene is still the choice of research all over the world.

For the development of gas lasers, these gases need to be enclosed in gas cells. Initially, bulk gas cells and glass capillaries have been extensively used to develop the system, as shown in Figure 7.2. However, this type of configuration makes the system bulky and less efficient because it needs high power from the pump source because of the short interaction length of the gas cell, and the overlap of the pump beam and gas medium is not optimal [199]. The advent of hollow core fibers (HC - PCF) eliminated both limitations and decreased the threshold [200].

Figure 7.2: Herriot gas cell with 30 m effective path length.

In the past decade, different types of PCFs came into existence and gave a new direction to the field of fiber gas lasers [26]. Based on their structure or design, the core of the fiber can be hollow, which can hold gas inside and provide the perfect environment for the interaction of pump light and gaseous medium [201]. These PCFs have a different

light propagation mechanism, which will be discussed in section 7.3. The pump light and gas molecules can interact in the hollow region, creating population inversion. The transitions of molecules to the lower energy states produce lasers at different wavelengths when the HC-PCF filled gaseous gain medium is placed inside a resonator. An efficient laser resonator (e.g., Fabry-Perot) is required to increase the output power level.

The mid-IR fiber gas laser discussed in this chapter is based on population inversion in the molecular gases (C_2H_2 and CO) in Kagome fiber, a particular class of PCFs. Population inversion happens when light interacts with gas molecules and transitions from one vibrational energy level to another. The gas molecules absorb NIR radiation and are excited to higher energy levels (Figure 7.1), which have the same energy as their energy level difference. Most specifically, molecules transition from a lower to a higher energy level by absorbing pump energy after the interaction. The molecules at higher energy levels decay to relatively lower energy levels and emit photons at lower energy or longer wavelengths [202].

We have developed pump sources at 1533 nm and 1570 nm wavelengths, which match vibrational energy level transitions for C_2H_2 and CO to develop gas lasers at 3.1 μm and 2.1 μm wavelengths, respectively.

7.2 Fundamentals of Molecular gas lasers

This section will discuss the fundamentals of molecular gas lasers based on vibrational energy level transitions. We decided to use acetylene and carbon monoxide gas as the gain medium for the development of the gas laser, so it's essential to

understand their structure, fundamental vibrational modes, and energies associated with vibrational and rotational motion of molecules. Most gaseous media used as gain medium are diatomic, triatomic, or polyatomic. The number of atoms determines the number of fundamental vibrational modes. Further, in gaseous molecules, atoms are connected by covalent bonds [203]. A molecule initially occupying a particular vibrational and rotational energy level can make a transition to another energy level either by absorbing or emitting radiation or light (Figure 7.4) ,following the selection rules [202].

Acetylene is a linear and symmetric molecule comprised of two carbon atoms (yellow circle) attached to two hydrogen atoms (white circle) through covalent bonds. It has five fundamental vibration modes, combining three stretching modes and two bending modes, as shown in Figure 7.3. The fundamental modes ν_1 and ν_3 are symmetric and anti-symmetric C- H stretch, ν_2 mode corresponds to C - C symmetric stretch, ν_4 and ν_5 modes correspond to C-H symmetric and anti-symmetric bending stretch [203]. Acetylene has an absorption band in the near-infrared region and emission in the mid-IR region, as shown in Figure 7.4 [156].

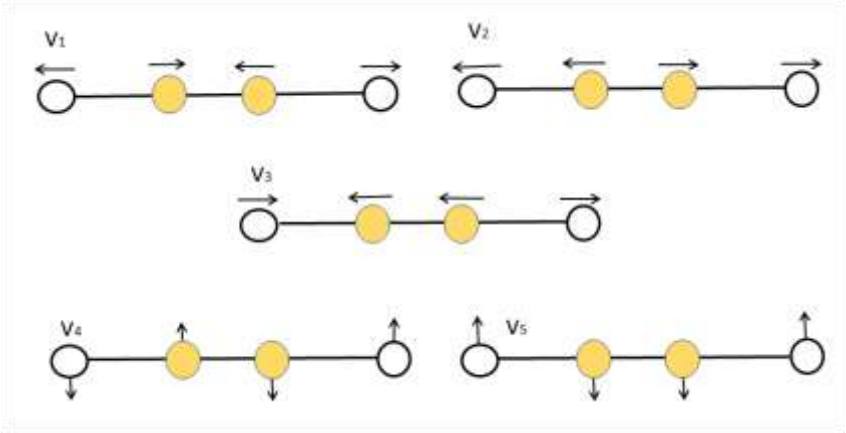

Figure 7.3: Fundamental vibration modes of acetylene.

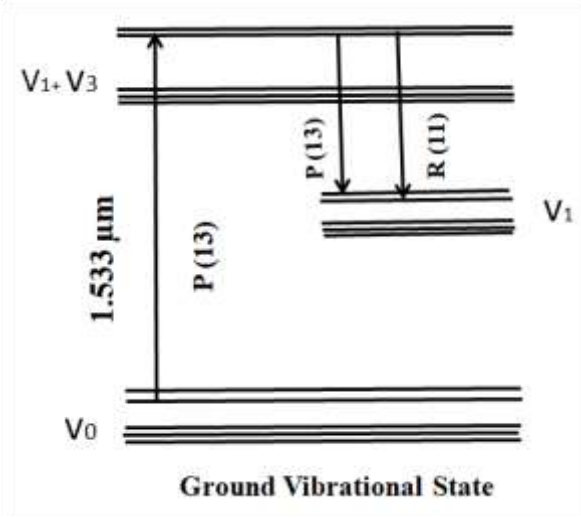

Figure 7.4: Energy transition for acetylene gas.

7.3 Photonic Crystal Fiber (PCF)

The research area of photonic crystals or PCF is not bound to one specific subject for the explanation. It is a field of broad interest and characterized by research groups with at least three different scientific backgrounds, mainly classical optics, solid-state physics, and quantum physics [204]. Adapting characteristics from these different subjects, PCF becomes very rich in the family of optical fibers. In PCF design, the important parameters are core diameter, pitch, and air-filling fraction. These parameters can be modulated which consequently changes the properties of fiber, such as the operation in the single-mode regime, dispersion, and nonlinearities. Thus, the choice of parameters makes the fiber unique and different from the conventional optical fiber [205].

Cregan et al. reported the proof of principle of fabricating hollow-core photonic crystal fiber (HC-PCF) for the first time in 1999 [206]. After that, different types of PCFs consisting of solid and hollow cores came into existence, such as photonic band gap fiber

and Kagome fiber. In the following section, we will discuss Kagome fiber, which will be used for the experiment.

7.4 Kagome Fiber

The first fiber consisted of a Kagome lattice, reported by Benabid et al. [202]. Kagome fiber comes under the umbrella of hollow-core photonic crystal fiber (HC-PCF). As its name differs from the rest of the fibers similarly, its guidance mechanism also differs from the conventional TIR in standard optical fibers. One might think this name originates from the name of some scientist, but this is not true. The word Kagome means a BAMBOO BASKET (kago) WOVEN PATTERN (me) composed of interlaced triangles where each lattice point has four neighbouring points [207;208]. The Kagome lattice is very rich in properties as it features both the hexagon from the honeycomb lattice and the equilateral triangles from the triangular one, and each node has four neighbours like the square lattice [209]. Kagome fiber shows wide optical transmission bands with relatively low loss without surface mode coupling [210]. Several suggestions have been proposed for the guidance mechanism in these fibers, such as low cladding density of states, less overlapping between core and cladding modes, and high-order bandgaps [211].

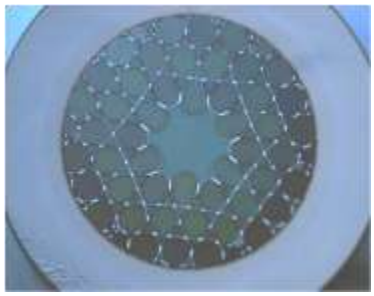

Figure 7.5: Kagome fiber structure (GLO photonics).

In 2007, a guidance mechanism named "inhibited coupling" was identified in HC-PCF for the first time [212]. It relies on designing a core and a cladding so that the cladding modal spectrum is populated with modes with minimal spatial overlap and symmetry matching. Core and cladding modes are confined to their specific region and cannot interact with each other. This has been called "Inhibited Coupling (IC)" as the coupling of core modes to cladding modes is suppressed. This guidance mechanism does not need a higher index core material or the photonic band gap effect. This works on the principle that core modes and continuum modes can coexist with the same frequency and effective refractive index without strongly hybridizing [26].

Initially, the exact mechanism of light propagation through the fiber was unknown as it was not dependent on TIR and photonic band gap (PBG) effects. Many researchers were working to unfold the theory behind the light guidance. Von Neuman and Weigner proposed the concept of bound states in continuum (BIC) in 1929 for the first time which was helpful in understanding the phenomenon of light guidance in Kagome fiber. BIC do not fall in the category of this traditional approach as these remain localized with lifetimes diverge to infinity while staying in the radiation continuum [213]. They constructed an artificial quantum potential to support a BIC - an electronic state with energy that falls above the continuum threshold. They proved that it's possible to embed the isolated eigenvalues of the single particle Schrodinger equation in the continuum of positive energy states [214]. The concept of BICs is extended beyond the quantum system, as it is based on interference. So, it can also be applied to any wave system [215]. The resemblance between the optical system and the general quantum system leads to the

concept that facilitated the explanation of the light guidance mechanism in Kagome fiber. This concept has gained a lot of attention in the last decade.

As Von Neuman-Weigner explained, the bound electronic states in a continuum. In the same way, Kagome HC-PCF can have guided modes in the core region in the cladding continuum without interacting with each other. Benabid and coworkers extended the concept of BIC and Quasi BIC (QBIC) to the field of fiber photonics in 2007 [212]. It is important to notice that the Kagome HC-PCF core mode is leaky, that is why it is known as QBIC instead of BIC. The research group worked on Kagome lattice fiber and emphasized that core modes and cladding modes can be longitudinally phase-matched, However, strong transverse phase mismatching inhibits the coupling of core and cladding modes. Because of incompatible symmetry there is a spatial separation between cladding glass modes and core air modes [216].

In conclusion, we can say that in Kagome fiber, guided core modes and cladding modes can accompany each other at the same frequency and effective index. Supporting the concept, where bound or quasi-bound states remain localized within a continuum (cladding modes). It follows the principle of inhibited coupling, which means core and cladding modes are not interacting with each other. A strong transverse-field mismatch between the modes is responsible for this weak interaction. Also, it has been reported that fast field oscillations of the cladding mode, leads to washing out of the overlap with the slowly varying core-field distribution and supports their coexistence without interacting with each other [212].

Kagome HC-PCF has several advantages over other PCFs as it has a large transmission bandwidth compared to PBG fiber. Losses are low as the guidance

mechanism is based on less overlapping of core and cladding modes, so light is well confined in the hollow core region. It has low dispersion, which can be achieved while designing the fiber [212;217]. Due to its structure, light-matter interaction can be enhanced by multiple times in this fiber compared to conventional fiber. All these properties make it advantageous over others, and losses can be decreased further by taking care of all the parameters, e.g., Hypocycloid curvature (negative curvature) of the core is one of the key parameters when talking about losses because by changing the core radius from circular to hypocycloidal, confined losses are strongly reduced as with this modification, optical overlap can be reduced [217]. Large pitch regime also controls the losses as in large pitch regime, the high index material mode is highly localized with very little optical power overlapping with low index material.

7.5 Experimental Setup

A Gas cell based on Kagome HC-PCF (GloPhotonics) will be used in the experiment. It has a core diameter of 48 μm and an outer diameter of 320 μm. Figure 7.6 shows the schematic of the gas cell [109]. It is a combination of two cells equipped with a gas inlet and gas outlet to facilitate gas samples inside the fiber and evacuate them out of it. The HC-PCF will be filled with gas, acting as a gain medium. We have completed the preliminary alignment of the gas cell, as shown in Figure 7.6, using a tunable laser at 1550 nm. A standard HC-PCF (Crystal Fiber) length of 1 m was used to couple the light from the laser, and maximum coupling was attained. The light was coupled to the HC-PCF fiber on the input of the gas cell through window 1, and the output of the HC-PCF was coupled through window 2 and the combination of lenses to a SMF, which will be connected to an OSA. The next step will be to optimize the gas fitting connected to the

gas cell to optimize the pressure. Most importantly, we need to keep the pressure at a certain value (~ 0.1 millibars). This optimization will be completed using acetylene gas.

To obtain the optimum pressure and alignment, a broadband source (1520 nm to 1560 nm) will be used, and the cell output will be monitored by observing the acetylene spectrum. Once the alignment and the cavity are optimized to hold the pressure, the HC-PCF will be replaced with the Kagome fiber. We will follow the same alignment procedure and optimization of the pressure multiple times to obtain the optimum coupling condition. A Fabry-Perot resonating cavity will be formed using mirrors of the desired reflectivity, and the gas cell will be used as the gain medium. A pulsed laser, as described in chapter 5, at 1533 nm and 1570 nm, will be used as a pump source.

Further, once the cavity is optimized using acetylene gas, the system will be ready for further experiments. C_2H_2 will be replaced with CO gas. CO has absorption in the 1.5 μm region, a transition at 1570 nm is selected to be used to achieve population inversion. We have developed a pulsed laser at 1570 nm as described in Chapter 5, which will be used as a pump laser for the gas laser based on CO gas. Other gases, such as nitrous oxide, can also be used as the gain medium, which has absorption in the 1.55 μm band [218].

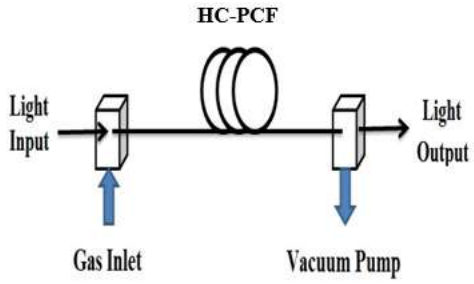

Figure 7.6: Setup for optimization of the cavity.

7.6 Conclusion

We have discussed the fundamentals of Kagome HC-PCF and the theory of its application in developing the mid-IR laser. We also discussed the molecular theory of laser. Once the resonator parameters are optimized, one can seal the Kagome HC-PCF so that no gas will leak, which is one of the advantages of the designed resonator. The gas cell can be filled with gases such as acetylene and carbon monoxide to generate lasers at 3.1 μm and 2.0 μm regions, respectively. The process will shift the paradigm in making lasers in the desired wavelength, like the one we described in **Chapter 5**, based on a doped fiber.

Chapter 8

Summary and future work

8.1 Summary

The main objective of the research project was to develop a mid-IR laser. One of the requirements to achieve this goal was to develop a high-power pulsed laser in the NIR region of the electromagnetic spectrum, which could be used as a pump source for developing a mid-IR laser. Most importantly, we were interested in developing a ML laser with high peak power at 1570 nm and 1533 nm. We completed the project and accomplished several important milestones, shaping the future research endeavour in developing mid-IR lasers. The following sections summarize our accomplishments:

i. Designing a high-power pulsed laser at 1570 nm

We used a double-clad erbium-ytterbium co-doped fiber as a gain medium, and a high-power multimode laser diode at 976 nm was used as the pump. The following sections show the chronology of the process of achieving the goal.

- **We proposed and demonstrated for the first time the application of an aqueous solution** of GNRs and PVA as a SA to develop a Q-Switched pulse laser in the NIR region of the electromagnetic spectrum, eliminating the complicated process of manufacturing SA. Further, the aqueous solution increased the damage threshold of the GNRs. The laser generated good-quality Q-switched pulses. However, the output power of the laser was not adequate to be applicable as a pump source for the mid-IR laser. *The research work was published in Optical Fiber Technology. Varsha and Gautam Das, "Q-switched Er-doped fiber laser using an aqueous solution of gold nanorods and polyvinyl alcohol," Optical Fiber Technology 83,103672, 2024.*
- After a thorough investigation, we concluded that the high intracavity losses were responsible for the low output power. The laser resonator was modified, which could generate Q-switched and Mode-Locked (ML) pulses at different pump power levels. By adjusting the intracavity losses, we could operate the laser in single-wavelength or dual-wavelength or switch between C and L band regimes. However, the output power levels were inadequate for use as a pump source for mid-IR laser. *We published our research work in the Results in Optics. Varsha and Gautam Das, "Generation of wavelength-switchable nanosecond mode-locked pulses in an Erbium/Ytterbium co-doped fiber laser cavity," Results in Optics, Volume 16,1000723, 2024.*
- Generally, a fiber laser based on a FBG can produce a laser at a desired wavelength with high output power. We modified the laser resonator by incorporating FBG and a tunable FBG (1570 nm to 1580 nm). The laser could

generate QS and ML pulses over the 1570 nm to 1580 nm range. However, as in the previous designs, the laser could not produce the desired high-output power. *Varsha and Gautam Das, "Tunable Mode-locked Erbium/Ytterbium co-doped fiber laser", Optical Fiber Technology, Volume 90, 104083, 2025.*

- Finally, we proposed and demonstrated the design of a high-power ML laser at 1570 nm. The laser produced QS and ML pulses simultaneously at lower pump power and ML pulses at high pump power. The laser was generated based on the self-Q-switching and mode-locking process. The ML pulses produced 72 W peak power, which was adequate for a pump source to generate a mid-IR laser. *Revised Manuscript under review (April 2025) Optical Fiber Technology.* Simultaneously, a pulsed laser at 1533 nm was also developed.

ii. Design of mid-IR lasers

We adopted two approaches in developing the mid-IR lasers as follows:

- The high peak power ML laser at 1570 nm was used as a pump source to develop a ML laser at 1925 nm wavelength. A double-clad thulium-doped fiber (DC-TDF) was used as a gain medium. The laser was developed based on a gain-switched mechanism. Further, the developed laser is unique in many aspects – **i.** The threshold power of the laser was very low compared to that reported in the literature, **ii.** The laser produced ~ 100 ps pulses and 2 W peak power, **iii.** The laser wavelength could be tuned over the TDF emission band using tunable FBG

or GNRs with longitudinal surface plasmon resonance (LSPR) wavelength of 2100 nm, and **iv.** It can be used to develop an **ICLAS** system.

Varsha and Gautam Das, "In-band pumped, high peak-power gain-switched mode-locked thulium-doped fiber laser at 1925 nm", Optics Continuum, Volume 4, Issue 1, pp. 30-36, 2025.

- We investigated the feasibility of developing mid-IR lasers based on gas-filled HC-PCF (Kagome Fiber) and completed the groundwork. The developed ML lasers in the 1533 nm and 1570 nm will be used as a pump source for acetylene (C_2H_2) and carbon monoxide (CO) filled HC-PCF, respectively. We have designed the laser cavity and developed the gas cell to hold the gas as a gain medium. Preliminary work on light coupling optics has been done. The advantages of this laser are that by changing the gas inside the HC-PCF, one can produce any desired wavelength, and it is possible to generate a high-power laser required in medicine.

8.2 Future Research

We have made significant progress in developing a mid-IR laser using gas filled HC-PCF. The laser based on CO will be able to produce high output power at a 2.0-micron band. Further, a laser based on C_2H_2 gas will produce ML pulses at a 3.0-micron band, which can be used in many applications, including Raman pump source. A PhD student joined the research group and will continue with the research.

The laser developed using TDF as the gain medium in a 2.0-micron band will be used to develop a CRDS system for trace gas sensing. A new PhD student will pursue this research work very shortly.

Our research group has already developed a prototype of a gas analyzer for detecting greenhouse gases, which operates on a laser at 1.5 μm band. In the future, the system will be modified based on a laser in the 2.0-micron band, which will enhance the efficiency of the gas analyzer.

The analyzer, based on a 2.0-micron band laser system, will be beneficial for developing a multi-component gas analyzer to monitor greenhouse gas (GHG) emissions from fertilized agricultural fields, which involves field trials at Lakehead University's agriculture research station (LUARS). The developed device will be cost-effective and compact. In the next section, we will show and analyze some of the data we collected from LUARS using a commercially available analyzer (Picarro G2508) (Figure7.1).

Figure 8.1: Setup to analyze greenhouse gases collected from LUARS.

Here is one example of the gas analysis data based on G2508 collected from LUARS after applying fertilizers in a canola field. The graph shows that the emission of ammonia is much higher initially than that of nitrous oxide for different fertilizers (Figure 8.2). A system based on a 2.0-micron band laser will be more efficient as absorption is higher in the 2.0-micron region as compared to the 1.5-micron region.

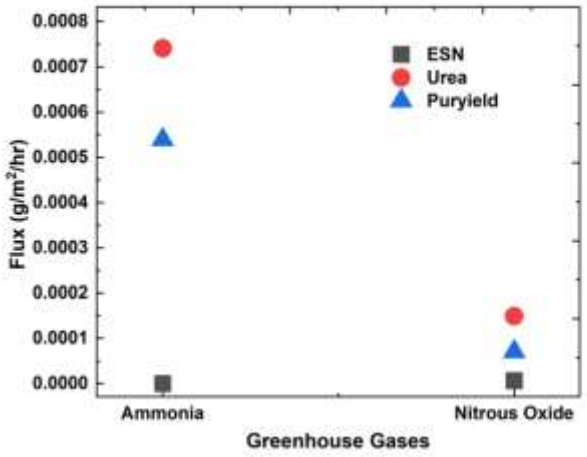

Figure 8.2: Greenhouse gas emission for different fertilizers (ESN, Urea, and Puryield).

References

[1] A. J. Gross and T. R. W. Herrmann, "History of Lasers," *World Journal of Urology*, vol. 25, pp. 217-220, 2007.

[2] T. H. Maiman, "Stimulated Optical Radiation in Ruby," *Nature*, vol. 187, pp. 493-494, 1960.

[3] R. W. Waynant, I. K. Ilev, and I. Gannot, "Mid-infrared laser applications in medicine and biology," Philosophical Transaction of the Royal Society of London. Series A: Mathematical, Physical and Engineering Sciences, Vol. 359, pp. 635-644, 2001.

[4] Y. C. Shin, B. Wu, S. Lei, et al., "Overview of Laser Applications in Manufacturing and Material Processing in Recent years," *Journal of Manufacturing Science and Engineering, Vol.* 142 (11), pp. 110818, 2020.

[5] N. P. Barnes, B. M. Walsh, D. J. Reichle, and R. J. DeYoung, "Tm:fiber lasers for remote sensing," *Optical materials,* 31(7), pp. 1061-1064, 2009.

[6] F. Klopf, R. Krebs, J. P. Reithmaier, and A. Forchel, "High-temperature operating 1.3 μm quantum-dot lasers for telecommunication applications," *IEEE Photonics Technology Letters, Vol.* 13(8), pp. 764-766, 2001.

[7] A. G. Berezin, O. V. Ershov, and A. I. Nadezhdinskii, "Trace complex-molecule detection using near-IR diode lasers," *Applied Physics B, Vol* 75(2), pp. 203-214, 2002.

[8] M. Kong, Z. Luo, Y. Lu, and W. J. Fan, "Inspection of Car's Emission Using Infrared Spectrum Technique," *Journal of Physics: Conference Series, Vol.* 48(1), pp. 1186-1189, 2006.

[9] A. I. Lopez-Lorente and B. Mizaikoff, "Mid-infrared spectroscopy for protein analysis: potential and challanges," *Analytical and bioanalytical chemistry, Vol.* 408, pp. 2875-2889, 2016.

[10] M. Razeghi, Q. Y. Lu, N. Bandyopadhyay, et al., "Quantum cascade lasers: from tool to product," *Optical express, Vol.* 23(7), pp. 8462-8475, 2015.

[11] C. Barnard, P. Myslinski, J. Chrostowski, and M. Kavehrad, "Analytical Model for rare-earth-doped fiber amplifiers and lasers," *IEEE Journal of Quantum Electronics, Vol.* 30(8), pp. 1817-1830, 1994.

[12] A. M. Jones, A.V. Vasudevan Nampoothiri, R. Kadel, et al., "Mid-IR fiber lasers based on molecular gas-filled hollow-core photonic crystal fiber," CLEO: 2011-Laser Sciences to Photonic Applications. IEEE, 2011.

[13] J. Faist, F. Capasso, D. L. Sivco, C. Sirtori, A. L. Hutchinson, and A. Y. Cho, "Quantum cascade laser," *Science*, Vol. 264(5158), pp. 553-556, 1994.

[14] O. Cathabard, R. Teissier, J. Devenson, J. C. Moreno, and A. N. Baranov, "Quantum cascade lasers emitting near 2.6 μm," *Applied Physics Letters*, Vol. 96(14), 2010.

[15] R. F. Curl, F. Capasso, C. Gmachl, et al., "Quantum cascade lasers in chemical physics," *Chemical Physics Letters*, Vol. 487(1-3), pp. 1-18, 2010.

[16] S. Takagi, H. Tanimura, T. Kakuno, R. Hashimoto, and S. Saito, "Thermal analysis and heat dissipation improvement for quantum cascade lasers through

experiments, simulations, and structure function," *Japanese Journal of Applied Physics*, Vol. 58(9), 2019.
[17] A. Bellemare, "Continuous-wave silica-based erbium-doped fibre lasers," *Progress in Quantum Electronics*, Vol. 27(4), pp. 211-266, 2003.
[18] G. Das, Z. J. Chaboyer, J. E. Navratil, and R. A. Drainville, "Passively Q-switched Yb- and Sm-doped fiber laser at 1064 nm," *Optics Communications*, Vol. 334, pp. 258-264, 2015.
[19] S. W. Harun, M. R. A. Moghaddam, K. Dimyati, and H. Ahmad, "The performance of double-clad ytterbium-doped fiber laser with different pumping wavelengths," *Laser Physics Letters*, vol. 6(6), pp. 458-460, 2009.
[20] E. A. Thoroh De Souza, D. Steinberg, L. A. M. Saito, et al., "Ultrashort pulse generation in erbium-doped fiber lasers in South America: a historical review," *Journal of the Optical Society of America B, Vol.* 40(4), pp. C148-C176, 2023.
[21] L. C. B. Silva and M. E. V. Segatto, "Recent advances in thulium-doped fiber lasers based on saturable absorber materials at 2000 nm," *Optical Fiber Technology, Vol.* 78, pp. 103310, 2023.
[22] J. Wang, X. Zhu, R. A. Norwood, and N. Peyghambarian, "Beyond 3 μm Dy3+/Er3+ co-doped ZBLAN fiber lasers pumped by 976 nanometer laser diode," *Applied Physics Letters*, Vol. 118(15), 2021.
[23] T. Y. Chang and O. R. Wood, "Optically pumped atmospheric-pressure CO_2 laser," *Applied Physics Letters, Vol.* 21(7), pp. 19-21, 1972.
[24] L. S. Rothman, I. E. Gordon, Y. Babikov, et al., "The HITRAN 2012 molecular spectroscopic database," *Journal of Quantitative Spectroscopy & Radiative Transfer*, vol. 130, pp. 4-50., 2013
[25] A. V. V. Nampoothiri, A. M. Jones, C. Fourcade-Dutin, et al., "Hollow-core optical fiber gas lasers (HOFGLAS): a review [Invited]," *Optical Materials Express*, vol. 2(7), pp. 948-961, 2012.
[26] B. Debord, F. Amrani, L. Vincetti, et al., "Hollow-Core Fiber Technology: The Rising of " Gas Photonics"," *Fibers*, vol. 7(2), 16, pp 16, 2019.
[27] G. Thomas and R. Isaacs, "Basic principles of lasers," *Anaesthesia & Intensive Care Medicine*, Vol.12(12), pp. 574-577, 2011.
[28] A. Yariv, *Optical Electronics in Modern Communications*, New York: Oxford University Press, 1997.
[29] A. E. Siegman, *Lasers* University Science Books, 1986.
[30] L. V. Tarasov, "LASER AGE IN OPTICS," *Book*, 1981.
[31] G. Keiser, "*Optical Fiber Communications,"* 3 ed. Boston, MA: McGraw Hill, 2000.
[32] S. Addanki, I. S. Amiri, and P. Yupapin, "Review of optical fibers-introduction and applications in fiber lasers," *Results in Physics*, Vol. 10, pp. 743-750, 2018.
[33] N. I. Zanoon, "The Phenomenon of total internal reflection and acceleration of light in fiber optics," *Journal of Computer Applications, Vol. 975,* pp. 8887, 2014.
[34] M. Arumugam, "Optical fiber communication - An overview," *Pramana,* 57 ed, pp. 849-869, 2001.
[35] M. J. Digonnet, "Optical and electronic properties of rare earth ions in glasses," *Rare-earth-doped fiber lasers and amplifiers*, Vol. 2nd edition 2001.

[36] K. R. Tamura, "Additive Pulse Mode-Locked Erbium-Doped Fiber Lasers," 1994.
[37] M. Hamada, M. Shimizu, M. Okayasu, T. Takeshita, et al., "Noise Characteristics of Er^{3+} - Doped Fiber Amplifiers Pumped by 0.98 and 1.48 μm Laser Diodes," *IEEE Photonics Technology Letters*, Vol. 2(3), pp. 205-207, 1990.
[38] Lynn Elizabeth Nelson, "Mode-locking of Thulium-doped and Erbium-doped Fiber Lasers," *Thesis*, 1997.
[39] W. L. Barnes, S. B. Poole, J. E. Townsend, et al., "Er $^{3+}$ - Yb $^{3+}$ and Er $^{3+}$ Doped Fiber Lasers," *IEEE Journal of Lightwave Technology, Vol.* 7(10), pp. 1461-1465, 1989.
[40] K. Aiso, Y. Tashiro, T. Suzuki, and T. Yagi, "Development of Er/Yb Co-doped Fiber for High-Power Optical Amplifiers," *Furukawa Electric Review*, pp. 35-39, 2001.
[41] M. Kamradek, J. Aubrecht, P. Varak, et al., "Energy transfer coefficients in thulium-doped silica fibers," *Optical Material Express,* 11(6), pp. 1805-1814, 2021.
[42] D. J. Richardson, J. Nilsson, and W. A. Clarkson, "High power fiber lasers: current status and future perspectives," *Journal of the Optical Society of America B-Optical Physics*, vol. 27(11), pp. B63-B92, 2010.
[43] D. Kouznetsov, J. V. Moloney, and E. M. Wright, "Efficiency of pump absorption in double-clad fiber amplifiers. I. Fiber with circular symmetry," *JOSA B,* Vol. 18(6), pp. 743-749, 2001.
[44] D. Kouznetsov and J. V. Moloney, "Efficiency of pump absorption in double-clad fiber amplifiers. II. Broken circular symmetry," *Journal of the Optical Society of America B-Optical Physics*, Vol. 19(6), pp. 1259-1263, 2002.
[45] A. Liu and K. Ueda, "The absorption characteristics of circular, offset, and rectangular double-clad fibers," *Optical Communications, Vol.* 132(5-6), pp. 511-518, 1996.
[46] Y. Li, S. D. Jackson, and S. Fleming, "High absorption and low splice loss properties of Hexagonal double-clad fiber," *IEEE Photonics and Technology Letters*, Vol. 16(11), pp. 2502-2504, 2004.
[47] W. T. Silfvast, "*Laser Fundamentals"*, Second ed 2004.
[48] R. Scheps and J. F. Myers, "Performance of a diode-pumped laser repetitively Q-switched with a mechanical shutter," *Applied Optics,* Vol. 33(6), pp. 969-978, 1994.
[49] S. Chen, D. Zhang, W. Zhang, et al., "Single-Frequency Linearly-Polarization Q-Switched Nanosecond Fiber Ring-Cavity Laser Enabled by an Electro-optic Modulator," *IEEE Photonics Journal, Vol.* 15(4), pp. 1-6, 2023.
[50] R. I. Woodward and J. R. Kelleher, "2D Saturable Absorbers for Fibre Lasers," Applied Sciences*,* Vol. 5(4), pp. 1440-1456, 2015.
[51] K. Y. Lau and D. Hou, "Recent Research and Advances of Material-Based Saturable Absorber in Mode-Locked Fiber Laser," *Optics and Laser Technology*, Vol. 137, pp. 106826, 2021.
[52] S. M. Kobtsev, "Artificial saturable absorbers for ultrafast fibre lasers," *Optical Fiber Technology, Vol.* 68, pp. 102764, 2022.

[53] G. Wang, A. A. Baker-Murray, and W. J. Blau, "Saturable Absorption in 2D Nanomaterials and Related Photonic Devices," *Laser and Photonics Reviews, Vol.* 13(7), pp. 1800282, 2019.
[54] S. Zhang, F. Lu, and J. Wang, "Self-Q-switching and mode-locking in an all-fiber Er/Yb co-doped fiber ring laser," *Optics Communications*, Vol. 263(1), pp. 47-51, 2006.
[55] H. A. Haus, "Mode-Locking of Lasers," *IEEE Journal of Selected Topics in Quantum Electronics*, Vol. 6(6), pp. 1173-1185, 2000.
[56] O. M. Asirim, R. Huber, and C. Jirauschek, "Impact of self-phase modulation on the operation of Fourier domain mode locked lasers," *Optical and Quantum Electronics*, Vol. 55(7), pp. 621, 2023.
[57] G. P. Agrawal, *Nonlinear Fiber Optics*, 3rd ed Academic Press, 2000.
[58] M. E. Fermann, F. Haberl, M. Hofer, and H. Hochreiter, "Nonlinear amplifying loop mirror," *Optics Letters*, Vol. 15(13), pp. 752-754, 1990.
[59] J. Szczepanek, T. M. Kardas, M. Michalska, C. Raszewicz, and Y. Stepanenko, "Simple all-PM-fiber laser mode-locked with a nonlinear loop mirror," *Optics Letters*, Vol. 40(15), pp. 3500-3503, 2015.
[60] J. WANG, "Tunable Mode-Locked Fiber Lasers With Optical Fiber Grating Devices," *Thesis*, 2017.
[61] M. Hofer, M. E. Fermann, F. Haberl, M. H. Ober, and A. J. Schmidt, "Mode-Locking with Cross-Phase and Self-Phase Modulation," *Optics Letters*, Vol. 16(7), pp. 502-504, 1991.
[62] U. Keller, K. J. Weingarten, F. X. Kartner, D. Kopf, B. Braun, I. D. Jung, R. Fluck, C. Honninger, N. Matuschek, and J. A. DerAu, "Semiconductor saturable absorber mirrors (SESAM's) for femtosecond to nanosecond pulse generation in solid-state lasers," *IEEE Journal of Selected Topics in Quantum Electronics*, Vol. 2(3), pp. 435-453, 1996.
[63] J. Li, S. D. Jackson, Y. Liu, and D. D. Hudson, "Efficient 2.87 μm fiber laser passively switched using a semiconductor saturable absorber mirror," *Optics Letters*, Vol. 37(18), pp. 3747-3749, 2012.
[64] J. He, L. Tao, H. Zhang, and B. Zhou, and L. Jingbo, "Emerging 2D materials beyond graphene for ultrashort pulse generation in fibre lasers," *Nanoscale*, Vol. 11(6), pp. 2577-2593, 2019.
[65] S. A. Hussain, "Ultrashort Dual Colour Laser at 1.55 and 1.88 μm by using a Carbon Nanotube Saturable Absorber," *IEEE Phot. Tech. Lett.*, Vol. 31(12), pp. 990-993, 2019.
[66] Z. Qin, T. Hai, G. Xie, et al., "Black phosphorous Q-switched and mode-locked mid-infrared Er: ZBLAN fiber laser at 3.5 μm wavelength," *Optics Express*, Vol. 26(7), pp. 8224-8231, 2018.
[67] X. Wang, Z. Luo, M. Liu, et al., "Wavelength-switchable femtosecond pulse fiber laser mode-locked by silica-encased gold nanorods," *Laser Physics Letters*, Vol. 13(4), pp. 045101, 2016.
[68] D. Zhao, Y. Liu, J. Qiu, and X. Liu, "Plasmonic Saturable Absorbers," Advanced Photonics Research, Vol. 2(8), pp. 2100003, 2021.

[69] L. Cui, J. Liu, N. Li, et al., "Passively mode-locked Er^{3+} and Tm^{3+} -doped fiber lasers by using a common gold nanorods/D-shaped fiber as saturable absorber," *Laser Physics Letters*, Vol. 17(11), pp. 115104, 2020.
[70] J. Olesiak-Banska, M. Gordel, R. Kolkowski, et al., "Third-Order Nonlinear Optical Properties of Colloidal Gold Nanorods," The Journal of Physical Chemistry C, Vol. 116(25), pp. 13731-13737, 2012.
[71] Y. W. Lee, C. M. Chen, W.H. Chuang, et al., "Highly efficient mode-locked and Q-switched Er^{3+} doped fiber lasers using a gold nanorod saturable absorber," *Scientific Reports*, Vol. 11(1), pp. 20079, 2021.
[72] Z. Kang, Y. Xu, L. Zhang, et al., "Passively mode-locking induced by gold nanorods in erbium-doped fiber lasers," *Applied Physics Letters*, Vol. 103(4), 2013.
[73] S. Lu, L. Du, Z. Kang, et al., "Stable Dissipative Soliton Generation from Yb-Doped Fiber Laser Modulated via Evanescent Field Interaction with Gold Nanorods," *IEEE Photonics Journal*, Vol. 10(5), pp. 1-8, 2018.
[74] X. D. Wang, Z. C. Luo, et al., "Microfiber-based gold nanorods as saturable absorber for femtosecond pulse generation in a fiber laser," *Applied Physics Letters*, Vol. 105(16), 2014.
[75] Varsha and G. Das, "Q-switched Er-doped fiber laser using an aqueous solution of gold nanorods and polyvinyl alcohol," Optical Fiber Technology, 83, pp. 103672, 2024.
[76] T. Jiang, Y. Xu, Q. Tian, L. Liu, Z. Kang, R. Yang, G. Qin, and W. Qin, "Passively Q-switching induced by gold nanocrystals," *Applied Physics Letters*, Vol. 101(15), 2012.
[77] H. Chen, L. Shao, Q. Li, and J. Wang, "Gold nanorods and their plasmonic properties," *Chemical Society Reviews*, Vol. 42(7), pp. 2679-2724, 2013.
[78] Z. Kang, X. Guo, Z. Jia, et al., "Gold nanorods as saturable absorbers for all-fiber passively Q-switched erbium-doped fiber laser," *Optical Materials Express, Vol.* 3(11), pp. 1986-1991, 2013.
[79] G. Jiang, Y. Jin, et al., "Tunable Gold Nanorods Q-Switcher for Pulsed Er-Doped Fiber Laser," *IEEE Photonics Journal*, Vol. 9(5), pp. 1-9, 2017.
[80] H. Luo, Z. Kang, Y. Gao, et al, "Large aspect ratio gold nanorods (LAR-GNRs) for mid-infrared pulse generation with a tunable wavelength near 3 μm," *Optics Express*, Vol. 27(4), pp. 4886-4896, 2019.
[81] C. Shi, H. Huang, M. Li, Y. Bao, and Z. Li, "Passively Q-switched 3 μm erbium-doped solid state lasers using gold nanorods as broadband saturable absorber," *Optics and Laser Technology*, Vol. 160, pp. 109095, 2023.
[82] W. U. Schroder, J. R. Birkelund, J. R. Huizenga, and W. W. Wilcke, "Effect of Pauli Blocking on Exchange and Dissipation Mechanisms Operating in Heavy-Ion Reactions," *Physical Review Letters, Vol.* 44(5), pp. 308-312, 1980.
[83] Y. Wang, S. Liu, J. Yuan, et al., "Ultra-broadband Nonlinear Saturable Absorption of Two-dimensional Bi2TexSe3-x Nanosheets," Scientific Reports, Vol. 6(1), pp. 33070, 2016.
[84] Z. Kang, X. Gao, L. Zhang, et al., "Passively mode-locked fiber lasers at 1039 and 1560 nm based on a common gold nanorod saturable absorber," *Optical Material Express*, Vol. 5(4), pp. 794-801, 2015.

[85] J. Jeon, J. Lee, and J. H. Lee, "Numerical study on the minimum modulation depth of a saturable absorber for stable fiber laser mode locking," *Optical Society of America B*, Vol. 32(1), pp. 31-37, 2014.
[86] P. Kumar and I. Roy, "Applications of Gold Nanoparticles in Clinical Medicine," *International Journal of Pharmacy and Pharmaceutical Sciences*, Vol. 8(7), pp. 11-16, 2016.
[87] J. Perez-Juste, I. Pastoriza-Santos, L. M. Liz-Marzan, and P. Mulvaney, "Gold nanorods: Synthesis, characterization and applications," *Coordination Chemistry Reviews*, Vol. 249(17-18), pp. 1870-1901, 2005.
[88] M. R. K. Ali, B. Snyder, and M. A. El-Sayed, "Synthesis and Optical Properties of Small Au Nanorods Using a Seedless Growth Technique," *Langmuir*, Vol. 28(25), pp. 9807-9815, 2012.
[89] L. Zhu, Z. Lu, L. Zhang, and N. He, "Seedless synthesis of gold nanorods with tunable plasmonic peaks beyond 1300 nm," *Chinese Chemical Letters*, Vol. 33(5), pp. 2491-2495, 2022.
[90] N. R. Jana, L. Gearheart, and C. J. Murphy, "Wet Chemical Synthesis of High Aspect Ratio Cylindrical Gold Nanorods," *J. Phys. Chem. B*, Vol. 105(19), pp. 4065-4067, 2001.
[91] H. M. Chen, H. C. Peng, R. S. Liu, et al., "Controlling the length and shape of gold nanorods," *The Journal of Physical Chemistry B Letters*, Vol. 109(42), pp. 19553-19555, 2005.
[92] R. S. Liu, H. M. Chao, and S. F. Hu, "Synthesis and Characterization of Long Gold Nanorods," *IEEJ Transaction on Electrical and Electronics Engineering*, Vol. 2(4), pp. 468-472, 2007.
[93] M. Hu, J. Chen, Z. Li, L. Au, G. Hartland, X. Li, M. Marquez, and Y. Xia, "Gold nanostructures: engineering their plasmonic properties for biomedical applications," *Chemical Society Reviews*, Vol. 35(11), pp. 1084-1094, 2006.
[94] B. Nikoobakht and M. A. El-Sayed, "Preparation and Growth Mechanism of Gold nanorods (NRs) Using Seed-Mediated Growth Method," *Chemistry of Material.*, Vol. 15(10), pp. 1957-1962, 2003.
[95] B. D. Busbee, O. Obare, and C. J. Murphy, "An Improved Synthesis of High-Aspect-Ratio Gold Nanorods," *Advanced Materials*, Vol. 15(5), pp. 414-416, 2003.
[96] N. R. Jana, "Gram-Scale Synthesis of Soluble, Near-Monodisperse Gold Nanorods and Other Anisotropic Nanoparticles," *Small*, Vol. 1(8-9), pp. 875-882, 2005.
[97] T. K. Sau and C. J. Murphy, "Room Temperature, High-yield Synthesis of Multiple Shapes of Gold Nanoparticles in Aqueous Solution," *J. Am. Chem. Soc.*, Vol. 126(28), pp. 8648-8649, 2004.
[98] X. Wu, Y. Ni, J. Zhu, et al., "Thermal Transport across Surfactant Layers on Gold Nanorods in Aqueous Solution," *Applied Materials & Interfaces*, Vol. 8(16), pp. 10581-10589, 2016.
[99] Y. Horiguchi, K. Honda, Y. Kato, et al., "Photothermal Reshaping of Gold Nanorods Depends on the Passivating layers of the Nanorod Surfaces," *Langmuir*, Vol. 24(20), pp. 12026-12031, 2008.

[100] A. S. Rao, "Saturation effects in nonlinear absorption, refraction, and frequency conversion: a review," *Optik, Vol.* 267, pp. 169638, 2022.
[101] B. Gu, Y. X. Fan, J. Wang, et al., "Characterization of saturable absorbers using an open-aperture Gaussian-beam Z scan," *Atomic, Molecular, and Optical Physics, Vol.* 73(6), pp. 065803, 2006.
[102] K. Zhang, M. Feng, G. Sun, et al., "Q-Switched and noise-like mode-locked fiber laser based on ternary transition-metal carbide Nb2AlC saturable absorber," *Optics and Laser Technology, Vol.* 162, pp. 109237, 2023.
[103] Z. Hu, X. Hu, P. He, J. Chen, J. Huang, Z. Xie, Y. Zhao, L. Tao, M. Hao, and J. He, "NbS2-nanosheet-based saturable absorber for 1.5 μm and 2 μm ultrafast fiber lasers," *Photonics and Nanostructures - Fundamentals and Applications*, Vol. 54, pp. 101117, 2023.
[104] B. Braun, F.X. Kartner, G. Zhang, M. Moser, and U. Keller, "56-ps passively Q-switched diode-pumped microchip laser," *Optics Letters,* Vol. 22(6), pp. 381-383, 1997.
[105] X. Hao, Z. Tong, W. Zhang, and Y. Cao, "A fiber laser temperature sensor based on SMF core-offset structure," *Optics Communications,* Vol. 335, pp. 78-81, 2015.
[106] Z. Li, A. M. Heidt, N. Simakov, et al., "Diode-pumped wideband thulium-doped fiber amplifiers for optical communications in the 1800-2050 nm window," *Optics Express, Vol.* 21(22), pp. 26450-26455, 2013.
[107] S. Taccheo, "Fiber lasers for medical diagnostics and treatments: state of the art, challanges and future perspectives," *Optical* Fibers and Sensors for Medical Diagnostics and Treatment Applications XVII, 10058, pp. 37-42, 2017.
[108] J. K. Valiunas, G. Stewart, and G. Das, "Detection of Nitrous Oxide (N2O) at Sub-ppmv Using Intracavity Absorption Spectroscopy," *IEEE Photonics Technology Letters*, Vol. 28(3), pp. 359-362, 2016.
[109] J. K. Valiunas, M. Tenuta, and G. Das, "A Gas Cell Based on Hollow-Core Photonic Crystal Fiber (PCF) and Its Application for the Detection of Greenhouse Gas (GHG): Nitrous Oxide (N2O)," *Journal of Sensors 2016*, Vol. (1), pp. 7678315, 2016.
[110] W. Huang, Z. Zhou, Y. Cui, et al., "4.5 W mid-infrared light source based on acetylene-filled hollow-core fibers," *Optics and Laser Technology*, Vol. 151, pp. 108090, 2022.
[111] W. Huang, Z. Wang, Z. Zhou, et al., "Fiber laser source of 8 W at 3.1 μm based on acetylene-filled hollow-core silica fibers," *Optics Letters*, Vol. 47(9), pp. 2354-2357, 2022.
[112] G. R. Lin, H. H. Lu, and J. Y. Chang, "Wavelength Tunability of a Coupler and Air-Gap Etalon Controlled High-Efficiency L-Band Mode-Locked Erbium-Doped Fiber Laser," *IEEE Photonics Technology Letters, Vol.*18(21), pp. 2233-2235, 2006.
[113] K. Guesmi, Y. Meng, A. Niang, et al., "1.6 μm emission based on linear loss control in a Er: Yb doped double-clad fiber laser," *Optics Letters, Vol.*39(22), pp. 6383-6386, 2014.

[114] M. Wang, M. Liu, Y. Chen, et al., "Stable noise-like pulse generation in all-PM mode-locked Tm-doped fiber laser based on NOLM," *Chinese Optics Letters, Vol.* 19(9), pp. 091402, 2021.
[115] M. Duran-Sanchez, E. A. Espinosa-De-La-Cruz, O. Pottiez, et al., "Passively Q-switched mode-locked thulium-doped fiber laser using nonlinear polarization rotation technique," Ceramics International, Vol. 49(24), pp. 41230-41237, 2023.
[116] A. Anjum and M. Rochette, "All-fiber nonlinear multimode interference saturable absorber in reflection mode," Optical Fiber Technology, Vol.74, pp. 103092, 2022.
[117] X. Ma, D. Chen, Q. Shi, et al., "Widely Tunable Thulium-Doped Fiber Laser Based On Multimode Interference With a Large No-Core Fiber," *Journal of Lightwave Technology, Vol.* 32(19), pp. 3234-3238, 2014.
[118] N. Li, W. Y. Zhang, J. Zhang, M. Guo, and Z. X. Guo, "Mode-locked Er-doped fiber laser based on nonlinear multimode interference," *Laser Phys. Lett.*, vol. 17(8), pp. 085105, 2020.
[119] M. Duran-Sanchez, B. Posada-Ramirez, R. I. Alvarez-Tamayo, H. Santiago-Hernandez, et al., "Soliton Molecules in Self-Mode-Locked Ring-Cavity Er/Yb Double-Clad Fiber Laser," *IEEE Photonics Journal, Vol.* 11(5), pp. 1-8, 2019.
[120] J. Swiderski, M. Michalska, and P. Grzes, "Mode-locking and self-mode-locking-like operation in a resonantly pumped gain-switched Tm-doped fiber laser," *Optics Communications, Vol.* 453, pp. 124406, 2019.
[121] H. Zhang, J. Zhang, et al., "Self-mode-locking and Self-phase modulation in Tm^{3+}-doped double clad fiber laser for pulse peak power enhancement and multi-wavelength generation," Optics and Laser Technology, Vol. 141, pp. 107128, 2021.
[122] N. F. Zulkipli, A. A. A. Jafry, R. Apsari, et al., "Generation of Q-Switched and mode-locked pulses with Eu2O3 saturable absorber," *Optics and Laser Technology, Vol.* 127, pp. 106163, 2020.
[123] M. M. Najm, S. W. Harun, S. Salam, et al., "8-Hydroxyquinolino cadmium chloride hydrate for generating nanosecond and picosecond pulses in erbium-doped fiber laser cavity," *Optical Fiber Technology, Vol.* 61, pp. 102439, 2021.
[124] Y. S. Jang, J. Park, and J. Jin, "Full C-band wavelength-tunable, 250 MHz repetition rate mode-locked polarization-maintaining fiber laser," *Scientific Reports, Vol.* 13(1), pp. 3623, 2023.
[125] M. Bartnick, G. Bharathan, T. A. Goebel, et al., "Wavelength-stabilized tunable mode-locked thulium-doped fiber laser beyond 2 μm," *Optics Letters, Vol.* 47(8), pp. 2085-2088, 2022.
[126] J. Jiang, Y. Ma, M. Wang, et al., "L-band filter-less wavelength tunable mode-locked fiber laser incorporating a long-period fiber grating," *Results in Optics, Vol.* 10, pp. 100360, 2023.
[127] Y. Peng, J. Peng, H. Pan, et al., "Switchable multi-wavelength actively Q-switched erbium-doped fiber laser based on nonlinear polarization rotation and Sagnac filter," *Optik, Vol.* 284, pp. 170955, 2023.

[128] F. Huang, J. Si, T. Chen, L. Hou, and X. Hou, "Wide-Range Wavelength-Tunable Mode-Locked Fiber Laser Based on Fiber Bragg Grating," *IEEE Photonics Technology Letters, Vol.* 32(17), pp. 1025-1028, 2020.
[129] M. Olivier, M. D. Gagnon, and M. Piche, "Automated mode locking in nonlinear polarization rotation fiber lasers by detection of a discontinuous jump in the polarization state," *Optics Express, Vol.* 23(5), pp. 6738-6746, 2015.
[130] M. M. Najm, P. Zhang, A. A. Al-Azzawi, et al., "Sodium carbonate modulated ultrashort mode-locked stretched pulses in an erbium-doped fiber laser," *Applied Optics, Vol.* 62(26), pp. 7008-7016, 2023.
[131] M. M. Najm, H. Arof, B. Nizamani, A. S. Al-Hiti, et al., "Ultra-short pulse generating in erbium-doped fiber laser cavity with 8-Hydroxyquinolino cadmium chloride hydrate (8-HQCdCl2H2O) saturable absorber," *Journal of Modern Optics, Vol.* 68(5), pp. 237-245, 2021.
[132] K. Tamura, J. Jacobson, E. P. Ippen, et al, "Unidirectional ring resonators for self-starting passively mode-locked lasers," *Optics Letters*, vol. 18(3), pp. 220-222, 1993.
[133] H. A. Haus, E. P. Ippen, and K. Tamura, "Additive-Pulse Mode locking in Fiber Lasers," *IEEE Journal of Quantum Electronics*, vol. 30(1), pp. 200-208, 1994.
[134] B. Posada-Ramírez, M. Duran-Sanchez, R. I. Alvarez-Tamayo, J. Alaniz-Baylon, et al., "Compact narrow linewidth actively Q-switched Er-Yb double-clad fiber laser," *Fibers*, Vol. 5(2), pp. 21, 2017.
[135] F. Z. Qamar and T. A. King, "Self-mode-locking effects in heavily doped single-clad Tm^{3+}-doped silica fiber lasers," *Journal of Modern Optics, Vol.* 52(8), pp. 1053-1063, 2005.
[136] B. Ibarra-Escamilla, M. Duran-Sanchez, R. I. Alvarez-Tamayo, et al., "Switchable and dual-wavelength self-Q-switched fiber laser based on a homemade Er/Yb double clad fiber and polarization maintaining fiber Bragg grating," *Laser Physics*, vol. 29(1), pp. 015102, 2018.
[137] D. Wu, C. Quan, Z. Guo, Z. Cai, and H. Xu, "Self Q-switched mode-locking in compact red Pr3+-doped ZBLAN fiber laser," Journal of Optics, Vol. 20(8), pp. 085501, 2018.
[138] S. Colin, E. Contesse, P. L. Boudec, G. Stephan, and F. Sanchez, "Evidence of a saturable-absorption effect in heavily erbium-doped fibers," *Optics Letters*, Vol. 21(24), pp. 1987-1989, 1996.
[139] J. L. Xu, Y. X. Ji, Y. Q. Wang, et al.,, "Self-Q-switched, orthogonally polarized, dual-wavelength laser using long-lifetime Yb3+ crystal as both gain medium and saturable absorber," *Optics Express*, Vol. 22(6), pp. 6577-6585, 2014.
[140] Y. Tang and J. Xu, "Effects of excited-state absorption on self-pulsing in Tm 3+ -doped fiber lasers," *JOSA B*, Vol. 27(2), pp. 179-186, 2010.
[141] P. Myslinski, J. Chrostowski, J. A. K. Koningstein, and J. R. Simpson, "Self-mode-locking in a Q-switched erbium-doped fiber laser," *Applied Optics*, Vol. 32(3), pp. 286-290, 1993.
[142] S. G. C. Vicente, M. A. M. Gamez, A. V. Kiryanov, Y. O. Barmenkov, and M. V. Andres, "Diode-pumped self-Q-switched erbium-doped all-fibre laser," *Quantum Electronics*, Vol. 34(4), pp. 310-314, 2004.

[143] B. N. Upadhyaya, A. Kuruvilla, U. Chakravarty, M. R. Shenoy, K. Thyagarajan, and S. M. Oak, "Effect of laser linewidth and fiber length on self-pulsing dynamics and output stabilization of single-mode Yb-doped double-clad fiber laser," *Applied Optics, Vol.* 49(12), pp. 2316-2325, 2010.
[144] C. Liu, Z. Luo, Y. Huang, B. Qu, H. Cheng, Y. Wang, et al., "Self-mode-locked 2 μm Tm^{3+}-doped double-clad fiber laser with a simple linear cavity," *Applied Optics*, Vol. 53(5), pp. 892-897, 2014.
[145] B. Ibarra-Escamilla, M. Duran-Sanchez, B. Posada-Ramirez, P. Prieto-Cortes, R. I. Alavarez-Tamayo, and E. A. Kuzin, "Self-Q-switch and CW Operation of a Tunable Dual-Wavelength Er/Yb Double-Clad Fiber Laser," *Applied Sciences*, Vol. 8(2), pp. 171, 2017.
[146] Z. Hu, D. Wu, W. Lin, Z. Li, and S. Dai, "Simulation of the generation conditions and influence parameters of a self-mode-locked erbium-doped fiber laser," *Optics Express*, Vol. 31(4), pp. 5882-5892, 2023.
[147] H. Ahmad, N. H. Mansor, M. Z. Samion, and S. A. Reduan, "High power mode-locked erbium-ytterbium doped fiber laser using GIMF-SIMF-GIMF fiber structure as saturable absorber," *Optical and Quantum Electronics, Vol.* 55(3), pp. 213, 2003.
[148] J. Nilsson, S. U. Alam, J. A. Alavarez-Chavez, P. W. Turner, A. Clarkson, and A. B. Grudinin, "High-Power and Tunable Operation of Erbium-Ytterbium Co-Doped Cladding-Pumped Fiber Lasers," *IEEE Journal of Quantum Electronics*, Vol. 39(8), pp. 987-994, 2003.
[149] K. Bremer, A. Pal, S. Yao, et al., "Sensitive detection of CO_2 implementing tunable thulium-doped all-fiber laser," *Applied. Optics*, Vol. 52(17), pp. 3957-3963, 2013.
[150] N. M. Fried, K. E. Murray, "High-Power Thulium Fiber Laser Ablation of Urinary Tissues at 1.94 μm," *Journal of Endourology*, Vol. 19(1), pp. 25-31, 2005.
[151] I. Mingareev, F. Weirauch, A. Olowinsky, et al., "Welding of polymers using a 2 μm thulium fiber laser," *Optics and Laser Technology*, Vol. 44(7), pp. 2095-2099, 2012.
[152] X. Li, X. Huang, X. Hu, et al., "Recent progress on mid-infrared pulsed fiber lasers and the applications," *Optics and Laser Technology, Vol. (*158), pp. 108898, 2023.
[153] G. Liu and B. Jacquier, "Spectroscopic properties of Rare Earth in Optical Material," *Springer Sciences and Business Media*, Vol. 83, 2006.
[154] P. Peterka, B. Faure, W. Blanc, et al., "Theoretical modelling of S-band thulium-doped silica fiber amplifiers," *Optical and Quantum Electronics*, Vol. 36, pp. 201-212, 2004.
[155] M. J. Digonnet, "Optical and electronic properties of rare earth ions in glasses," *Rare-earth-doped fiber lasers and amplifiers*, Vol. 2nd edition 2001.
[156] L. S. Rothman, "HITRAN 2012," 2012.
[157] Y. Lin, Q. Gu, Y. Chen, et al., "Realizing enhanced lithotripsy efficiency using 700 W peak power thulium-doped fiber laser," *Optics and Laser Technology*, Vol. 179, pp. 112267, 2024.

[158] J. Cook, P. Roumayah, D. J. Shin, et al., "Narrow linewidth 80 W tunable thulium-doped fiber laser," Optics and Laser Technology, Vol. 146, pp. 107568, 2022.
[159] N. Simakov, A. Hemming, W. A. Clarkson, J. Haub, and A. Carter, "A cladding-pumped, tunable holmium doped fiber laser," *Optics Express*, Vol. 21(23), pp. 28415-28422, 2013.
[160] R. Lopez-Estopier, A. Camarillo-Aviles, M. Bello-Jimenez, et al., "Q-switched mode locking noise-like pulse generation from a thulium-doped all-fiber laser based on nonlinear polarization rotation," *Results in Optics, Vol.* 5, pp. 100115, 2021.
[161] B. Ren, C. Li, T. Wang, K. Guo, and P. Zhou, "Stable noise-like pulse generation from a NALM-based all-PM Tm-doped fiber laser," *Optics Express*, vol. 30(15), pp. 26464-26471, 2022.
[162] Y. Zhang, Y. Zheng, X. Su, J. Peng, H. Yu, T. Sun, and H. Zhang, "All-Polarization Maintaining Noise-Like Pulse from Mode-Locked Thulium-Doped Fiber Laser Based on Nonlinear Loop Mirror," *IEEE Photonics Journal*, Vol. 14(1), pp. 1-5, 2022.
[163] K.Y. Lau and D. Hou, "Recent research and advances of materials-based saturable absorber in mode-locked fiber laser," *Optics and Laser Technology*, Vol. 137, pp. 106-826, 2021.
[164] L. A. Sanchez, C. Cuadrado-Laborde, A. Carrascosa, A. Diez, J. L. Cruz, and M. V. Andres, "Low-repetition-rate all-polarization maintaining thulium-doped passively mode-locked fiber laser," *Optics and Laser Technology*, Vol. 149, pp. 107856, 2022.
[165] Z. Kang, M. Y. Liu, X. J. Gao, N. Li, S. Y. Yin, G. S. Qin, and W. P. Qin, "Mode-locked thulium-doped fiber laser at 1982 nm by using a gold nanorods saturable absorber," *Laser Physics Letters, Vol.* 12(4), pp. 045105, 2015.
[166] S. Chu, D. Sun, J. Chen, L. Sun, W. Shi, J. Lu, and X. Xu, "Passively mode-locked thulium-doped fiber laser based on a SWCNTs@AFI saturable absorber," *Infrared Physics and Technology*, Vol. 128, pp. 104479, 2023.
[167] K. Y. Lau and M. Z. Zulkifii, "1.56 μm and 1.93 μm synchronized mode-locked fiber laser with graphene saturable absorber," *Infrared Physics & Technology*, Vol. 112, pp. 103606, 2021.
[168] P. Myslinski, X. Pan, C. W. Barnard, J. Chrostowski, B. T. Sullivan, and J. F. Bayon, "Q-switched thulium-doped fiber laser," *Optical Engineering*, Vol. 32(9), pp. 2025-2030, 1993.
[169] S. D. Jackson and T. A. King, "Efficient Gain-Switched Operation of a Tm-Doped Silica Fiber Laser," *IEEE Journal of Quantum Electronics*, Vol. 34(5), pp. 779-789, 1998.
[170] Y.J. Zhang, B.Q. Yao, Y.L. Ju, and Y.Z. Wang, "Gain-switched Tm^{3+}-doped double-clad silica fiber laser," *Optics Express*, Vol. 13(4), pp. 1085-1089, 2005.
[171] M. Jiang and P. Tayebati, "Stable 10 ns, kilowatt peak-power pulse generation from a gain-switched Tm-doped fiber laser," *Optics Letters, Vol.* 32(13) pp. 1797-1799, 2007.

[172] N. Simakov, A. Hemming, S. Bennetts, and J. Haub, "Efficient, polarised, gain-switched operation of a Tm-doped fibre laser," *Optics Express*, Vol. 19(16), pp. 14949-14954, 2011.
[173] Z. Ren-Lai, Z. Jie, Yuang-Chi., C. Zhao-Yu, J. You-Lun, and W. Yue-Zhu, "All-Fiber Gain-Switched Thulium-Doped Fiber Laser Pumped by 1.558 μm Laser," *Chinese Physics Letters, Vol.* 29(6), pp. 064201, 2012.
[174] Z. Jiao, B. Zhang, and B. Wang, "Linearly polarized and narrow-linewidth pulse generation at high repetition rate from an all-fiber gain-switched Thulium-doped fiber laser," *Optics and Laser Technology, Vol.* 55, pp. 58-61, 2014.
[175] D. S. Chowdhary, A. Pal, D. Pal, S. Chatterjee, M. C. Paul, R. Sen, and M. Pal, "High repetition rate gain-switched 1.94 μm fiber laser pumped by 1.56 μm dissipative soliton resonance fiber laser," *Optics Letters*, Vol. 42(13), pp. 2471-2474, 2017.
[176] M. Duran-Sanchez, B. Posada-Ramirez, R. I. Alvarez-Tamayo, J. Alaniz-Baylon, M. Bello-Jimenez, I. Armas-Rivera, J. L. Cruz, M. V. Andres, and B. Ibarra-Escamilla, "Low repetition rate gain-switched double-clad thulium-doped fiber laser operating in the 2 μm wavelength region," *Optics Fiber Technology, Vol.* 66, pp. 102660, 2021.
[177] X. Ma, T. Feng, S. Zhao, et al., "Dissipative soliton resonance and noise-like pulse in a self-pulsing fiber laser," *Optics and Laser Technology*, Vol. 157, pp. 108754, 2023.
[178] J. Shang, T. Feng, S. Zhao, J. Zhao, Y. Zhao, Y. Song, and T. Li, "An investigation into self-pulsing behavior in an Er-doped ring laser," *Applied Physics Express*, Vol. 13(11), pp. 112006, 2020.
[179] X. Ma, W. Huang, S. Zhao, et al., "Gain-switched 2 μm fiber laser pumped by a Q-switching and mode-locking self-pulsing Er-doped fiber laser," *Optical Fiber Technology, Vol.* 83, pp. 103681, 2024.
[180] B. C. Dickinson, S. D. Jackson, and T. A. King, "10 mJ total output from a gain-switched Tm-doped fiber laser," *Optics Communications, Vol.* 182(1-3), pp. 199-203, 2000.
[181] S. Kivisto, R. Koskinen, J. Paajaste, S. D. Jackson, M. Guina, and O. Okhotnikov, "Passively Q-switched Tm^{3+}, Ho^{3+} -doped silica fiber laser using a highly nonlinear saturable absorber and dynamic gain pulse compression," *Optics Express, Vol.* 16(26), pp. 22058-22063, 2008.
[182] K. Yin, W. Yang, B. Zhang, S. Zeng, and J. Hou, "Temporal characteristics of gain-switched thulium-doped fiber laser near threshold," JOSA B, Vol. 30(11), pp. 2864-2868, 2013.
[183] J. Yang, Y. Tang, and J. Xu, "Development and applications of gain-switched fiber lasers," *Photonics Research, Vol.* 1(1), pp. 52-57, 2013.
[184] Varsha, J. O. Trevisanutto, and G. Das, "Detection of Gases at the Molecular Level," LAOP MEXICO 2024.
[185] S. Kharitonov and C. S. Bres, "Isolator-free unidirectional thulium-doped fiber laser," *Light: Science and Applications, Vol.* 4(10), pp. e340-e340, 2015.
[186] F. Wang, D. Shen, H. Chen, D. Fan, and Q. Lu, "Modelling and Optimization of Stable Gain-Switched Tm-Doped Fiber Lasers," *Optical review, Vol.* 18, pp. 360-364, 2011.

[187] J. Yang, H. Li, Y. Tang, and J. Xu, "Temporal characteristics of in-band-pumped gain-switched thulium-doped fiber lasers," *JOSA B, Vol.* 31(1), pp. 80-86, 2013.
[188] J. Swiderski and M. Michalska, "Generation of self-mode-locked resembling pulses in a fast gain-switched thulium-doped fiber laser," *Optics Letters, Vol.* 38(10), pp. 1624-1626, 2013.
[189] R. A. Drainville and G. Das, "Widely Tunable Fiber Bragg Grating and Its Application in Fiber Lasers," *Microwave and Optical Technology Letters*, vol. 55(12), pp. 2824-2826, 2013.
[190] N. Arsad, M. Li, G. Stewart, and W. Johnstone, "Intra-Cavity Spectroscopy Using Amplified Spontaneous Emission in Fiber Lasers," *Journal of Lightwave Technology*, Vol. 29(5), pp. 782-788, 2011.
[191] J. O. Trevisanutto, J. K. Valiunas, and G.. Das, " Detection of C2H2 using a segmented HC-PCF gas cell," *Measurement: Sensors*, Vol. 27, pp. 100773, 2023.
[192] T. Y. Chang and T. J. Bridges, "Laser action at 452, 496, and 541 μm in optically pumped CH3F," *Optics Communications*, Vol. 1(9), pp. 423-426, 1970.
[193] J. E. McCord, H. C. Miller, G. Hager, et al., "Experimental Investigation of an Optically Pumped mid-Infrared Carbon Monoxide Laser," *IEEE Journal of Quantum Electronics*, Vol. 35(11), pp. 1602-1612, 1999.
[194] F. B. A. Aghbolagh, V. Nampoothiri, B. Debord, F. Gerome, L. Vincetti, F. Benabid, and W. Rudolph, "Mid IR hollow core fiber gas laser emitting at 4.6 μm," *Optics Letters.*, Vol. 44(2), pp. 383-386, 2019.
[195] Y. Cui, W. Huang, Z. Wang, M. Wang, Z. Zhou, Z. Li, et al., "4.3 μm fiber laser in CO_2-filled hollow-core silica fibers," *Optica*, Vol. 6(8), pp. 951-954, 2019.
[196] Z. Zhou, Z. Wang, W. Huang, et al, "Towards high-power mid-IR light source tunable from 3.8 to 4.5 μm by HBr-filled hollow-core silica fibres," *Light: Science & Applications*, Vol. 11(1), pp. 15, 2015.
[197] W. Huang, Z. Zhou, Y. Cui, Z. Wang, and J. Chen, "Mid-infrared fiber gas amplifier in acetylene-filled hollow-core fiber," *Optics Letters*, Vol. 47(18), pp. 4676-4679, 2022.
[198] W. Song, Q. Zhang, X. Zhang, Y. Hou, and P. Wang, "High-power hollow-core fiber gas laser at 3.1 μm with a linear-cavity structure," *Optics Letters*, Vol. 49(17), pp. 4922-4925, 2024.
[199] W. Huang, Z. Wang, Z. Zhou, W. Pei, Y. Cui, X. Li, Z. Li, and J. Chen, "Tunable Fiber Gas Raman Laser of 6 W at 2.9 μm by Deuterium-Filled Hollow-Core Fiber," *IEEE Journal of Selected Topics in Quantum Electronics*, Vol. 30(6), pp. 1-7, 2023.
[200] F. Benabid, J. C. Knight, G. Antonopoulos, and P. S. J. Russell, "Stimulated Raman scattering in hydrogen-filled hollow-core photonic crystal fiber," *Science*, Vol. 298(5592), pp. 399-402, 2002.
[201] F. Benabid and P. J. Roberts, "Linear and nonlinear optical properties of hollow core photonic crystal fiber," *Journal of Modern Optics*, Vol. 58(2), pp. 87-124, 2011.
[202] B. R. Puri, L. R. Sharma, and M. S. Pathania, "Principles of physical chemistry," *Book*, 1998.

[203] A. M. Jones, "Realizing a mid-infrared optically pumped molecular gas laser inside hollow-core photonic crystal fiber," 2012.
[204] A. Bjarklev, J. Broeng, and A. S. Bjarklev, "Photonics Crystal Fibers," *Book*, 2003.
[205] S. Singla. and P. Singal, "Photonic crystal fiber: construction, properties, developments and applications," *IJEE*, Vol. 9(1), pp. 1-8, 2017.
[206] R. F. Cregan, B. J. Mangan, J. C. Knight, T. A. Birks, P. S. Russell, P. J. Roberts, and D. C. Allan, "Single-mode photonic band gap guidance of light in air," *Science*, Vol. 285(5433), pp. 1537-1539, 1999.
[207] M. Mekata, "Kagome: The Story of the Basketweave lattice," *Physics Today*, Vol. 56(2), pp. 12-13, 2003.
[208] I. Syozi, "Statistics of Kagome Lattice," *Progress of Theoretical Physics*, Vol. 6(3), pp. 306-308, 1951.
[209] K. J. H. Law, A. Saxena, A. R. Bishop, "Localized Structures in Kagome Lattices," *Physical Review A- Atomic, Molecular and Optical Physics,* Vol. 79(5), pp. 053818, 2009.
[210] F. Couny, F. Benabid, and P. S. Light, "Large-pitch kagome-structured hollow-core photonic crystal fiber," *Optics Letters*, Vol. 31(24), pp. 3574-3576, 2006.
[211] G. J. Pearce, G. S. Wiederhecker, C. G. Poulton, S. Burger, and P. S. J. Russel, "Models for Guidance in Kagome-Structured Hollow-core Photonic Crystal Fibers," *Optics Express*, Vol. 15(20), pp. 12680-12685, 2007.
[212] F. Couny, F. Benabid, P. J. Roberts, et al, "Generation and Photonic Guidance of Multi-Octave Optical-Frequency Combs," *Science*, Vol. 318(5853), pp. 1118-1121, 2007.
[213] S. I. Azzam and A. V. Kildishev, "Photonic Bound States in the Continuum: From Basics to Applications," *Advanced Optical Materials*, Vol. 9(1), pp. 2001469, 2021.
[214] F. H. Stillinger, D. R. Herrick, "Bound States in the Continuum," *Physical Review A*, Vol. 11(2), pp. 446, 1975.
[215] Y. Plotnik, O. Peleg, et al., "Experimental Observation of Optical Bound States in the Continuum," *Physical Review Letters*, Vol. 107(18), pp. 183901, 2011.
[216] B. Debord, F. Amrani, L. Vincetti, et al., "Hollow-core Fiber Technology: The Rising of "Gas Photonics"," *Fibers*, Vol. 7(2), pp. 16, 2019.
[217] Y. Y. Wang, N. V. Wheeler, F. Couny, et al., "Low loss broadband transmission in hypocycloid-core Kagome Hollow-core photonic crystal fiber," *optics letters*, Vol. 36(5), pp. 669-671, 2011.
[218] A. A. Ionin, M. V. Ionin, I. O. Kinyaevskiy, et al., "R&D of carbon monoxide lasers at the Lebedev physical institute of the Russian academy of sciences," *Optical and Quantum Electronics*, Vol. 55(9), pp. 763, 2023.